HIGH-SPECTRUM-EFFICIENCY TRANSMISSION TECHNIQUE BASED ON FULL-DUPLEX COOPERATIVE NON-ORTHOGONAL MULTIPLE ACCESS

XINYU WANG

PhD

The Hong Kong Polytechnic University

This programme is jointly offered by The Hong Kong Polytechnic University and Harbin Institute of Technology

2023

The Hong Kong Polytechnic University

Department of Electronic and Information Engineering

Harbin Institute of Technology

School of Electronics and Information Engineering

High-Spectrum-Efficiency Transmission Technique Based on Full-Duplex Cooperative Non-Orthogonal Multiple Access

XINYU WANG

A thesis submitted in partial fulfilment of

the requirements for the degree of

Doctor of Philosophy

September 2022

Certificate of Originality

I hereby declare that this thesis is my own work and that, to the best of my knowledge and belief, it reproduces no material previously published or written, nor material that has been accepted for the award of any other degree or diploma, except where due acknowledgement has been made in the text.

_____(Signed)

Xinyu Wang (Name of student)

Abstract

To meet the increasing demand and the requirements for low latency and massive connectivity, non-orthogonal multiple access (NOMA) has recently received significant attention due to its potential of achieving enhanced user fairness, enlarged connections, reduced access latency, and facilitated diverse quality of service. In the meanwhile, cooperative communication has obtained a lot of attention because of its ability to provide spatial diversity gain to mitigate fading, to extend coverage and to improve the communication reliability. Therefore, cooperative non-orthogonal multiple access (CNOMA) has attracted a great deal of attention since it is promising to further improve the system efficiency and to achieve an ideal win-win situation for NOMA users. This thesis investigates and proposes the CNOMA scheme from four perspectives for high spectrum efficiency.

Firstly, we propose a half-duplex (HD) CNOMA scheme based on spectrum sensing. In this scheme, a primary user (PU), i.e., a weak user, intends to communicate with the base station with the assistance of a secondary user (SU), i.e., a strong user, which works as a HD relay. In the meanwhile, the SU obtains an additional opportunity to share the same spectrum band originally belonging to the PU by NOMA. This scheme adopts spectrum sensing technique to identify spectrum holes, accordingly, to choose an appropriate form of transmitted signals, avoid useless transmission, and eventually obtain superior system capacity. We take the practical assumption of imperfect spectrum sensing into consideration and characterize the performance of our proposed scheme. Closed-form expressions for outage probability, system through-

put in delay-limited transmission mode, ergodic rate, and system throughput in delay-tolerant transmission mode are derived, with or without the direct link between the base station and the PU. Simulation results are presented to further validate these closed-form derivation expressions, verify the effectiveness of employing the spectrum sensing technique, and illustrate the superior performance of the proposed HD CNOMA scheme compared with two cooperative benchmarks.

Secondly, we investigate a full-duplex (FD) CNOMA scheme based on spectrum sensing. In this scheme, PU communicates with the base station with the assistance of SU which works as a FD relay. The proposed collaboration scheme adopts spectrum sensing to identify spectrum holes and accordingly avoid the waste of spectrum hole resources. It enables PU and SU to share the licensed spectrum band of PU by NOMA, which further increases the spectrum efficiency. By adopting FD mode, the proposed FD CNOMA scheme not only achieves better system performance than HD mode by receiving and transmitting simultaneously, but also overcomes inherent issues of a conventional cognitive radio network. To characterize the performance of the proposed scheme, expressions of exact and asymptotic ergodic rates and system throughput are worked out. Accordingly, the high signal-to-noise ratio slopes for these ergodic rates are further derived. Simulation results are presented to verify the correctness of all these derivation results and to illustrate the performance superiority of FD CNOMA compared with other cooperative benchmarks in real-world scenarios in terms of both ergodic rates and system throughput.

Thirdly, we present a three-stage relay selection strategy with dynamic power allocation (TRSPA) for the above-proposed FD CNOMA scheme based on spectrum sensing. Considering the higher priority of PU than SU, the relay selection objective is to maximize the transmission data rate of the selected relay, i.e., SU, on the condition that PU's signal is successfully uploaded to the base station by precisely narrowing down relay candidates step-by-step and dynamically allocating optimal power coefficients. Exact and asymptotic outage probabilities and ergodic rates are worked out.

Accordingly, diversity orders and spatial multiplexing gains are derived. We further exploit the impact of self-interference (SI) on TRSPA for FD CNOMA and then compare its performance with TRSPA applied in other relaying modes, that is half-duplex and orthogonal multiple access. Finally, simulation results are presented to reveal that: (i) theoretical derivation results are correct; (ii) TRSPA always outperforms other relay selection strategies in terms of outage probability and ergodic rate; and (iii) TRSPA for FD CNOMA in a real-world scenario achieves better performance than other relaying modes in spite of the adverse effect of SI in FD mode.

Fourthly, we exploit a two-way relaying FD CNOMA scheme, where NOMA users intend to exchange messages via a two-way FD relay. To characterize the potential performance gain brought by this proposed FD CNOMA scheme, the outage probability and ergodic rate are analyzed. Specifically, the closed-form expressions for the outage probabilities, diversity orders, ergodic rates, and system throughputs in delay-limited and delay-tolerant transmission modes are derived under the realistic assumption of imperfect self-interference cancellation. Furthermore, to present the comprehensive performance evaluation, both perfect and imperfect successive interference cancellations (SICs) are taken into consideration. Simulations are performed to validate the accuracy of the derivation results and to illustrate the outstanding performance of the proposed scheme in low signal-to-noise ratio region compared with HD CNOMA system and cooperative orthogonal multiple access system. Our results show that under the conditions of both perfect and imperfect SICs, outage probability floors and ergodic rate ceilings exist for the proposed FD CNOMA scheme due to the inter-user interference among superimposed NOMA signals and the residual self-interference caused by the imperfect self-interference cancellation.

Publications

Journal papers

- **Xinyu Wang**, Min Jia, Qing Guo, Ivan Wang-Hei Ho, and Francis Chung-Ming Lau. "Full-Duplex Relaying Cognitive Radio Network with Cooperative Nonorthogonal Multiple Access". *IEEE Systems Journal*, 2019, 13(4): 3897-3908.

- **Xinyu Wang**, Min Jia, Ivan Wang-Hei Ho, Qing Guo, and Francis Chung-Ming Lau. "Exploiting Full-Duplex Two-Way Relay Cooperative Non-Orthogonal Multiple Access". *IEEE Transactions on Communications*, 2019, 67(4): 2716-2729.

- **Xinyu Wang**, Min Jia, Qing Guo, Ivan Wang-Hei Ho, and Jinsong Wu. "Joint Power, Original Bandwidth, and Detected Hole Bandwidth Allocation for Multi-Homing Heterogeneous Networks Based on Cognitive Radio". *IEEE Transactions on Vehicular Technology*, 2019, 68(3): 2777-2790.

- **Xinyu Wang**, Min Jia, Ivan Wang-Hei Ho, Qing Guo, and Francis Chung-Ming Lau. "Relay Selection for Spatially Random Full-Duplex Cooperative Non-Orthogonal Multiple Access Networks". *IET Communications*, 2021, 15(8): 1060-1075.

- Min Jia, **Xinyu Wang**, Qing Guo, Ivan Wang-Hei Ho, Xuemai Gu, and Fran-

cis Chung-Ming Lau. “Performance Analysis of Cooperative Non-Orthogonal Multiple Access Based on Spectrum Sensing”. *IEEE Transactions on Vehicular Technology*, 2019, 68(7): 6855-6866.

Conference papers

- **Xinyu Wang**, Min Jia and Qing Guo. “Full-Duplex Cooperative Non- Orthogonal Multiple Access with Spectrum Sensing”. in *IEEE International Conference on Signal Processing (ICSP)*, Beijing, China, 2020: 411-416.

Acknowledgments

I would like to express my sincere gratitude to supervisors, colleagues and my family who have ever offered me help on the verge of the completion of my Ph.D. study.

First and foremost, I would like to give heartfelt thanks to my supervisor Prof. Francis Chung-Ming Lau and co-supervisor Dr. Ivan Wang-Hei Ho at The Hong Kong Polytechnic University for offering me an opportunity to study and exchange ideas as a joint PhD student. With their support, I broaden my scientific research horizons and improve my English speaking and writing skills. Owning to their help, I keep up with the studying pace at The Hong Kong Polytechnic University easily and put myself into course learning, scientific research and academic paper writing tasks quickly.

I am also deeply grateful to my supervisor Prof. Qing Guo and co-supervisor Dr. Min Jia at Harbin Institute of Technology. They not only impart knowledge and resolve doubts for me academically, but also lead by example and teach me how to behave in life. I am so glad to meet these two great professors who always consider their students first. I genuinely appreciate Prof. Guo and Dr. Jia for their unselfish generous dedication.

I also own thanks to my colleagues in both universities. They are Zhenhui Situ, Yuhao Wang, Josyl Mariela Rocamora, Xue Wang, Shuo Zhang, Wanmai Yuan, Zhisheng Yin, Dongbo Li, Ximu Zhang and Jian Yang. I will always remember these days that we study and support one another together. With their company, I am not alone but full of power when conducting scientific research. I sincerely wish all of us having a bright future.

Finally, and most importantly, I must thank my family. For all these years, their unremitting encouragement, generous understanding and unwavering love are the driving forces behind my PhD study and helping to push me forward. I wish them good health and happiness.

Contents

List of Figures

List of Tables

Chapter 1

Introduction

1.1 Background

The massive growth in mobile data traffic has become a significant concern for the development of future wireless networks. In the year of 2017, there were about 8.4 billion device connections all over the world. According to [1], it has been predicted that by the year of 2025, this number will exceed 75.4 billion. As forecasted in [2], a simple incremental enhancement of the fourth-generation (4G) mobile networks will not be able to satisfy such user demands in the near future. Therefore, a new generation of mobile networks, i.e., the fifth-generation (5G), is emerging [3]. The vision of 5G wireless communications lies in providing very high data transmission rates, low latency, manifold increase in base station (BS) capacity, significant improvement in users' perceived quality of service (QoS), enormous number of connected devices and so on, compared to current 4G networks [3].

In order to achieve the above targets, non-orthogonal multiple access (NOMA) has emerged as an innovative technology for larger data rates, higher BS capacity and more connected devices [4] [5] [6]. NOMA utilizes superposition coding at the transmitters and successive interference cancellation (SIC) at the receivers. According to [7], NOMA is able to provide a significant performance gain compared with conventional

orthogonal multiple access (OMA). The core of NOMA is to allow multiple users to share the same time, frequency and code resource elements via different power levels. At the transmitter side, signals from various users are superposed and the resulting signal is then transmitted over the same channels in the same time slot. At the receiver sides, SIC is utilized to detect the required signals. The basic idea of SIC [8] is that user signals are successively decoded. After one user's signal is decoded, it is subtracted from the combined signal before the next user's signal is decoded. So far, NOMA has been studied extensively in the following references [9] [10] [11]. In [9], an uplink power control scheme has been proposed in order to achieve diverse arrived power in a NOMA system. Reference [10] has investigated the performance of NOMA in a cellular downlink scenario with randomly deployed users. Reference [11] has investigated the application of simultaneous wireless information and power transfer (SWIPT) to cooperative NOMA. A new cooperative multiple-input single-output SWIPT NOMA protocol has been proposed, where a user with a strong channel condition acts as an energy-harvesting relay by adopting power splitting scheme to help a user with a poor channel condition.

In wireless networks, cooperative communication has gained a lot of attention because of its ability to provide spatial diversity to mitigate fading [12], to extend coverage and to improve the communication reliability [13]. Therefore, cooperative nonorthogonal multiple access (CNOMA) has attracted a great deal of attention [14] [15] [16] [17] [18] since it is promising to further improve the system efficiency in terms of capacity [19] and it is capable of ensuring NOMA users to achieve their QoS requirements [20] [21]. CNOMA has been first proposed in [17], where a near user with strong channel conditions acts as a relay to help a far user which is suffering from weak channel conditions. Such cooperation is particularly preferred by the weak user when its QoS cannot be met by itself [20]. As to the near user, it obtains an additional opportunity [19] [20] to access the spectrum band which originally belongs to the weak user. In a word, the collaboration scheme achieves an ideal win-win situation.

There are three types of CNOMA schemes which are respectively based on different relaying protocols, including decode-and-forward (DF) relaying, amplify-and-forward (AF) relaying, and compress-and-forward (CF) relaying. In a DF relaying system, the relay completely decodes its received signal, re-encode it and then send it to the terminal equipment. In an AF relaying system, the relay directly amplifies its received signal along with the embedded noise and then forwards them together to the terminal receiver. In a CF relaying system, the relay compresses its overheard signal and then transmits the resultant signal to the intended terminal receiver [22]. Authors have introduced a multi-antenna AF relay to a CNOMA system to assist transmissions from the BS to NOMA users in [23]. Performances of AF relaying CNOMA systems under Nakagami-*m* fading channels with the consideration of perfect and imperfect evaluation of channel state information have been investigated in [24] and [25], respectively. Authors of [26] has studied and proposed the relay selection strategy for a AF relaying CNOMA system with multiple relays assisting the transmissions from BS to users. Moreover, [27] has also investigated the relay selection problem and proposed a two-stage relay selection strategy for a AF relaying CNOMA system. The achieved diversity order is the same with the number of AF relays. As to DF relaying CNOMA systems, authors of [27] and [28] have studied the two-stage relay selection strategy as well, in order to obtain spatial diversity and thus better outage performance. Reference [29] has employed multiple antennas at the DF relay and users in a CNOMA scheme in order to increase the cell edge coverage. Full-duplex relaying is definitely a significant topic for DF relaying CNOMA systems and researchers have already achieved relevant achievements including [30] [31] [32] and [33]. Additionally, simultaneous wireless information and power transfer has been introduced by DF relaying CNOMA transmissions in [34] and [35]. While CF relaying CNOMA is still far from being well studied. It has only been explored in [36] with relay broadcasting channels and in [37] for a cognitive radio network. After comparison AF with DF, we conclude that AF and DF have their distinct pros and cons. AF has relatively low

complexity and is easy to implement, since it directly amplifies and forwards signals. However, such simple linear processing only extends transmission scope in terms of energy. While the relay is amplifying signals, noise level gets larger as well. Partial transmit power of relay must be wasted, and the noise and distortion of signals are proportionally amplified as well. DF overcomes the above drawbacks of AF. DF reduces effects brought by noise during the second hop by completely decoding and then forwarding signals. Transmission reliability is improved but computational complexity is also increased. It is noted that when it comes to CNOMA systems with untrusted relays, DF is not an advisable choice, since the untrusted relay must be prevented from decoding and obtaining signal [38]. We then compare AF with CF. According to [39], it is indicated that the achieved secrecy sum rate by AF is larger than CF. The implementation complexity of AF is lower. Furthermore, the theoretical secrecy analysis for CF is too complex to hardly make any insightful conclusions.

It needs to be pointed out that we aim to improve the system efficiency in this thesis, without regard to untrusted relays. Therefore, we employ DF for our considered CNOMA systems since it focuses more on system performance. To be specific, 'CNOMA' refers to DF relaying CNOMA in subsequent chapters.

1.2 Literature Review

1.2.1 CNOMA Inspired by Cognitive Radio

Cognitive radio (CR) has also become one of the promising key technologies in 5G wireless communications to increase the spectrum efficiency [40]. The main ideas of CR are (i) to allow the secondary user (SU) to share the licensed spectrum band with the primary user (PU) on the condition that the QoS of PU is guaranteed, and (ii) to utilize the spectrum resources more efficiently. The combination technique of CR and CNOMA has recently attracted the researchers' attention [20] [21] for higher capacity

and better reliability. In fact, the treatises for investigating the potential benefits by integrating the two promising technologies CR and CNOMA are still in their infancy. Reference [20] has investigated the application of CNOMA to multicast cognitive radio networks. A dynamic CNOMA scheme has been proposed, where the multicast secondary users serve as relays to improve the performance of both primary and secondary networks. As to [21], the authors focus on the scenario where the PU locates far from the BS and the SUs seat closely to the BS. In such case, the QoS requirement of PU may not be met by the primary network itself due to PU's poor channel conditions or its limited transmission capability. The PU-SU collaboration achieves a win-win situation since the PU grants the SUs an access to the licensed spectrum, in exchange for the SUs improving PU's performance by working as relays to help reach the PU's QoS requirement. It is noted that just like conventional CR networks, the PU has higher priority than SUs.

In this thesis, we consider the weak and the strong users as a primary user and a secondary user, respectively.

1.2.2 CNOMA and its Relay Selection Strategies

CNOMA research contributions mainly include two categories, namely, half-duplex (HD) [20] [17] and full duplex (FD) [41] [42] [43] [44] [45] [46].

In a HD CNOMA system, the far user transmits its signals to the near user and the BS in the first phase. And the near user decodes and forwards the message of the far user in the second phase. In this way, the BS obtains two copies of signals, one is from the far user and the other is from the near user. By combining these two copies and leveraging the spatial diversity gains, the BS may improve the reliability of the received signals. In particular, authors of [16] have investigated the application of SWIPT to HD CNOMA. A new cooperative SWIPT HD NOMA protocol has been proposed, where near NOMA users which are close to the source act as energy

harvesting relays to help far NOMA users. A HD CNOMA transmission scheme has been also proposed in [17]. It has assumed that users with better channel conditions has prior information about the messages of other users. System performance is then analyzed and an approach based on user pairing is proposed to reduce system complexity. Reference [18] has proposed a two-stage relay selection strategy for HD CNOMA networks with different QoS requirements at the users. In fact, relay selection (RS) is one of the main focuses of a CNOMA scheme. To be specific, Ding et al. have proposed a RS strategy for a HD CNOMA system to achieve the minimal overall outage probability [47]. Yang et al. have considered the unicast traffic where one BS communicates with two mobile users with the aid of multiple dedicated relays [48]. Two kinds of RS strategies for HD CNOMA networks with decode-and-forward and amplify-and-forward relaying protocols have been proposed, respectively. For a multicast cognitive HD CNOMA system, Lv et al. have presented three different secondary user scheduling strategies based on the available channel state information (CSI) to exploit the inherent spatial diversity [49]. Xu et al. have investigated optimal RS schemes for HD CNOMA networks with multiple dedicated relays by adaptively ordering users based on instantaneous CSI rather than quality of service requirements [50]. The related works [47] [48] [49] [50] have laid a solid foundation for the understanding of RS strategies for HD CNOMA. But the improvement of reliability and capacity comes at the price of resource utilization efficiency reduction due to the additional time resource cost during HD cooperation, which may offset the capacity gain promised by cooperation communication.

On the other hand, FD mode [3] [51] is capable of overcoming the capacity loss in HD CNOMA systems since FD wireless device transmits and receives simultaneously. It is also noted that when a FD device is receiving signals, its transmitted signal is regarded as self-interference (SI). Thanks to rapidly developing self-interference suppression techniques [52] [53], they provide a strong possibility for the realization of the advantages brought by the FD mode. Accordingly, researchers begin to focus on FD

CNOMA schemes recently. A CNOMA scheme with FD relaying in multiuser single-input single-output downlink systems is investigated in [41]. It assumes perfect SI cancellation, and theoretically obtains the achievable rate region. A FD device-to-device (D2D)-aided CNOMA scheme is proposed in [42] to improve the performance of the NOMA weak user in a NOMA user pair, where the NOMA weak user is helped by the NOMA strong user with the capability of FD D2D communications. A FD CNOMA system with dual users has been proposed in [43], where a dedicated FD relay assists the information transmission to the user with weak channel condition. In [44], authors have studied a NOMA system with cooperative FD relaying. They analytically obtain the optimal power allocations with closed-form expressions at the BS and relay to minimize the outage probability. Furthermore, authors of [45] and [46] have proposed a CNOMA scheme where the user-relay selects different operation modes between FD and HD so that the proposed scheme always achieves better performance than cooperative orthogonal multiple access (COMA). We have learnt that there are considerable research findings about RS strategies for HD CNOMA. But RS for FD relaying CNOMA is far from being well studied. The only relevant finding is presented in [54]. Yue et al. have investigated the impact of RS on the performance of CNOMA, where relays are capable of working in either FD or HD mode [54]. In their proposed RS scheme, on the condition of ensuring the data rate of distant user, they serve the nearby user with data rate as large as possible for selecting a relay.

1.2.3 Two-Way Relay CNOMA

All of the above existing works on CNOMA are based on the one-way relay scheme, where the messages are delivered in only one direction. As a further advance, the two-way relay (TWR) technique introduced in [55] has attracted remarkable interest since it is capable of boosting the spectral efficiency. The basic idea of TWR systems is to exchange information between two nodes with the help of a relay.

Generally speaking, in a bi-directional communication scenario, network coding and multi-user detection (MUD) are two types of non-orthogonal technologies which are used to increase spectrum efficiency. The primary purpose of the former technology is to decode network-coded signals while the latter aims to recover individual signals. This thesis mainly studies the non-orthogonal technology of MUD, which means 'NOMA' in this thesis refers to MUD. As to network coding, [56] and [57] have first proposed physical-layer network coding (PNC), which is a sub-field of network coding, to enhance the relay transmission performance by exploiting networking. Similar to the DF protocol, PNC decodes signals from the overlapped signal by messages from multiple transmitters and then generates the network-coded signal. In contrast, analog network coding (ANC) has been first proposed by [58]. Similar to the AF protocol, ANC simplifies the weighted sum signal from multiple transmitters and then directly forwards it.

We next explain the concept of PNC in a typical two-way relay channel (TWRC). Two vehicles A and B move towards a intersection. A road side unit R lies in the intersection and works as a relay to assist them to exchange information X_A and X_B. Buildings or other physical obstacles at the corner lead to severe shadowing effects, creating a non-line-of-sight scenario. There are two phases during PNC, namely uplink and downlink transmissions. During the former phase, A and B send their signals X_A and X_B, respectively, to R simultaneously. Their signals then overlap at R. Relay R decodes X_A and X_B from the overlapped signal and generates the output signal by $X_R = X_A \oplus X_B$, where $\oplus$ refers to exclusive or (XOR). Afterwards, R broadcasts X_R during the downlink phase. Finally, A and B obtains their own intended signal, namely X_B and X_A, with the help of their self information. For example, A recovers its intended signal by $X_B = X_A \oplus X_R$. The scheduling problem has been investigated and a medium access control protocol named VPNC-MAC has been proposed by [59] and [60] in a PNC-based vehicular ad-hoc network (VANET). The proposed scheme includes two phases, namely the setup phase and the packet exchange phase, in order to guarantee

the reliability and efficiency of periodic beacon broadcasting. Authors of [61] have first considered the feasibility of PNC. According to [61], in a vehicle-to-everything communication system, PNC undergoes at most a signal to interference and noise ratio penalty of 3 dB even in the worst situation, compared with a traditional point-to-point communication system. Orthogonal frequency division multiplexing (OFDM) is commonly employed in the physical layer of IEEE 802.11 standard family. There have already been many research works on OFDM-modulated PNC such as [62] [63] and [64]. The synchronization problem has been carefully studied in [62] and [64]. Authors of [63] has analyzed the performance of PNC with effects of frequency-selective channels.

After comparing network coding and NOMA, we learn that both of them are used to increase spectrum efficiency in a bi-communicational scenario. But according to [56], the former is exploited in a TWRC where power levels of users are balanced. While in a NOMA scheme, multiple users are served by the same time, frequency and code resource element. Different power levels are allocated to these users to realize multiple access. According to [65], the superiority of NOMA even becomes more significant as channel state difference between different users gets larger. Therefore, the application scenarios distinguish from each other. Network coding is more suitable to users with balanced power levels while NOMA is applicable to a scenario with obvious power difference. We focus on the latter in this thesis, where one user is farther away from the relay than the other one.

According to [66], the application of TWR to FD CNOMA is a possible approach to improve the spectral efficiency of systems. Although the researches have already laid a solid foundation for the understanding of TWR technique [67] [68], the two-way relay FD CNOMA systems where NOMA users want to exchange messages via a FD relay are still far from being well understood. To the best of our knowledge, only Zheng et al. [69] [70] have investigated two-way relay FD CNOMA systems. Zheng et al. [69] have developed a two-way relay FD CNOMA network, in which

a rate splitting scheme and a successive group decoding strategy are employed. But the authors have not carried out any performance evaluation theoretically. Zheng et al. [70] have focused on the secrecy considerations in a two-way relay FD CNOMA network, in which two users exchange their NOMA signals via a trusted relay in the presence of single and multiple eavesdroppers. However, in the performance evaluation part, only the achievable ergodic rate has been analyzed. Zheng et al. [70] have also lacked systematic performance evaluation metrics, i.e., outage probability, system throughput and so on. Moreover, the above existing contributions about two-way relay FD CNOMA systems are studied on the condition of perfect SIC (pSIC). In practical scenarios, there still exist several potential implementation issues with the use of SIC (i.e., complexity scaling and error propagation) [66]. More precisely, these unfavorable factors will lead to errors in decoding. Once an error occurs when carrying out SIC, the NOMA systems will suffer from the residual interference signal (IS). Hence, it is significant to examine the detrimental impacts of imperfect SIC (ipSIC) for FD CNOMA systems. However, Zheng et al. [69] [70] fail to consider the situation of ipSIC.

1.3 Research Motivation and Contribution

1.3.1 HD CNOMA Based on Spectrum Sensing

All relevant papers about HD CNOMA inspired by CR neglect the objectively existing spectrum holes [71] [72], which means that the SUs will transmit the superimposed NOMA signals made up of their received signals and their own signals even when the PU does not exist and the received signals are nothing but noise. According to [71], instead of keeping occupying the licensed spectrum band, the PU only requires to transmit signals when it needs, and the licensed band will turn unoccupied if the PU finishes transmission. Considering such fact, this thesis proposes a HD CNOMA

scheme based on spectrum sensing [73] [74] [75], which adopts spectrum sensing to identify the spectrum holes and thus it is capable of avoiding useless transmission for better system performance. In brief, once the spectrum sensing results claim the existence of the PU, SUs will transmit the superimposed NOMA signals consisting of PU signals and their own signals. Otherwise, they will only transmit their own signals. In this way, the system resources are adequately utilized for user signals but not noise and thus useless transmission is avoided. To the best of our knowledge, in HD CNOMA systems inspired by CR, this thesis is the first to consider spectrum holes, the first to adopt spectrum sensing technique, and the first to present performance analysis under imperfect spectrum sensing assumption.

In this thesis, we propose and investigate a user relaying HD CNOMA scheme, which adopts spectrum sensing technique to identify spectrum holes, accordingly choose an appropriate form of transmitted signals, avoid useless transmission, and eventually obtain superior system performance. To characterize the performance of the proposed HD CNOMA scheme, closed-form expressions of outage probability, system throughput in delay-limited transmission mode, ergodic rate and system throughput in delay-tolerant transmission mode are worked out. It is noted that the above derivation is carried out under the practical assumption of imperfect spectrum sensing in real-world networks. Finally, simulation results are presented to validate these derived closed-form expressions and illustrate the superior performance of the proposed HD CNOMA scheme to two cooperative benchmarks, in terms of system throughput.

The contributions of this part are summarized as follows.

(1) We propose a HD CNOMA scheme based on spectrum sensing, where the user relay, i.e., the strong user, executes spectrum sensing to avoid useless transmission and efficiently utilize the system resources for larger system throughput.

(2) Closed-form expressions of outage probability, ergodic rate and system throughput in delay-limited and delay-tolerant transmission modes are derived under the practical assumption of imperfect spectrum sensing. Note that this thesis is the first to con-

cern spectrum holes, to adopt spectrum sensing technique, and to present performance analysis under imperfect spectrum sensing assumption in a HD CNOMA system.

(3) Simulation results are provided to verify the correctness of our derived expressions and the effectiveness of adopting spectrum sensing technique in the proposed scheme for better system performance. They also illustrate the following facts. The proposed HD CNOMA scheme is always superior to the cooperative benchmarks, in terms of system throughput both in delay-limited and in delay-tolerant transmission modes under scenarios with or without direct link between the primary user and the base station. Moreover, we learn that all of the involved cooperative access schemes, including the proposed HD CNOMA and two other benchmarks, obtain larger throughputs with direct link than without direct link. It is because the direct link offers additional possibility for signal transmission and thus provides spatial diversity gain.

1.3.2 FD CNOMA Based on Spectrum Sensing

The above-mentioned papers [41] [42] [43] [44] [45] [46] about FD CNOMA have failed to notice the fact that the weak user can finish transmission at any moment. Instead of keeping the spectrum bands occupied all the time, many practical wireless devices, such as Internet of Things (IoT) sensors, only transmit when they need to, and the spectrum bands will turn to be unoccupied and idle when they finish transmission [76]. These idle spectrum bands are defined as spectrum holes in [71] and [72]. The existing FD schemes neglect the spectrum holes which means that strong users, i.e., SUs, will forward their received signals even when weak users do not exist and the received signals are nothing but interference and noise signals. In such cases, the idle spectrum bands and the strong users' transmit power are wasted. To solve this problem, we adopt spectrum sensing to identify these spectrum holes. To be specific, once a spectrum sensing result claims the existence of the weak user (i.e., PU), the strong user (i.e., SU) will transmit a superimposed NOMA signal consisting of the two

NOMA users' signals. Otherwise, SU will transmit its own signal. In this way, spectrum holes are used for SU signal transmission but not for interference or noise signals. Moreover, by sharing the same spectrum band in a NOMA way, PU and SU are capable of increasing the spectrum efficiency compared with PU completely occupying the licensed spectrum band itself [77]. That is to say both idle and underutilized spectrum bands can be sufficiently utilized by the proposed FD CNOMA scheme based on spectrum sensing.

We want to point out one more thing about the adopted FD mode; it not only provides better system performance than HD as mentioned above, but also overcomes the following inherent drawbacks of conventional cognitive radio networks (CRNs). Traditionally, SUs adopt HD communication mode. Each time slot is divided into two mini-slots, i.e., a sensing slot and a transmission slot. This conventional scheme has the following critical drawbacks [78]. First, SUs cannot simultaneously sense spectrum bands and transmit data. They have to sense the bands only in sensing slots and transmit signals merely in transmission slots. That is to say, SUs need to sacrifice a great proportion of time resource for robust spectrum detection performance. Only a modest part of time is left for signal transmission, decreasing the transmission capacity. Second, SUs cannot find out any changes about PUs' statuses during data transmission slots. Therefore, collision and interference may happen when PUs appear, and spectrum holes are wasted when PUs disappear. On the other hand, the FD mode enables SUs to sense and transmit signals at the same time. So the above conflict no longer exists. Time slots in our FD-CR scheme are not divided into separate sensing and transmission slots. SU keeps sensing the licensed spectrum band all the time to make sure that the presence and absence of PU can be identified immediately, without worrying about transmission-time loss. Accordingly, problems such as spectrum hole resource waste and collision between PU and SU are overcome. So our FD-CR scheme improves the spectrum utilization efficiency and increases the system reliability.

In this thesis, we propose and investigate a FD CNOMA scheme based on spec-

trum sensing, where a PU communicates with the BS under the assistance of an SU which has the capability of spectrum sensing. Besides the win–win situation between PU and SU, the proposed collaboration scheme provides the following benefits. First of all, it adopts spectrum sensing to identify spectrum holes and accordingly avoid the waste of spectrum hole resources. Second, it enables PU and SU to share the licensed spectrum band by NOMA, which further increases the spectrum efficiency. Third, the employed FD mode helps obtain better system performance, such as larger capacity, and it also helps overcome the above-mentioned problems of conventional CRNs. To characterize the performance of the proposed scheme, expressions of exact and asymptotic ergodic rates are worked out. Corresponding high signal-to-noise ratio (SNR) slopes for ergodic rates are further derived. We then analyze the system throughput based on these obtained ergodic rates. It is noted that performance evaluation in this thesis is analyzed under practical assumptions of imperfect SI cancellation and imperfect spectrum sensing. Finally, simulation results are presented to validate these derived expressions. They also illustrate that in practical scenarios, the proposed FD CNOMA scheme achieves better performance than other cooperative benchmarks in terms of both ergodic rates and system throughput.

The contributions of this part are summarized as follows.

(1) We propose a FD CNOMA scheme based on spectrum sensing, where the user-relay (i.e., SU) helps the weak user (i.e., PU) to communicate with the BS. By adopting the cooperative scheme, the spectrum sensing technology, the NOMA strategy, and the FD transmission mode, the proposed FD CNOMA scheme not only sufficiently utilizes both idle and underutilized spectrum resources, but also overcomes the commonly existing issues of conventional CRNs. This is the first time that NOMA is applied to a FD-CR system.

(2) Expressions of exact and asymptotic ergodic rates are derived under practical assumptions of imperfect spectrum sensing and imperfect SI cancellation. For more insights, we further work out their corresponding high-SNR slopes. In short, the high-

SNR slope of SU is one while the high-SNR slope of PU is equal to the miss detection probability which is much smaller than SU. Furthermore, we obtain the system throughput according to the derived ergodic rates.

(3) Simulation results are presented to verify the correctness of our derived expressions and the effectiveness of adopting spectrum sensing in the proposed scheme. They also illustrate the following facts. FD CNOMA always provides the largest ergodic rate for the SU, compared with other cooperative benchmarks. It also offers the largest ergodic rate to the PU in a real-world scenario where the residual SI has the same level with the noise floor. As to the system throughput, the proposed FD CNOMA scheme always outperforms other benchmarks.

1.3.3 Three-Stage Relay Selection Strategy With Dynamic Power Allocation

By recalling existing RS strategies introduced in Section 1.2.2, we conclude that these achievements have laid a solid foundation for the understanding of RS strategies for HD CNOMA. In contrast, RS for FD relaying CNOMA is far from being well studied. The only relevant finding is presented in [54], which, however, has the following two drawbacks. Firstly, a fixed power allocation is used by [54]. Optimizing the power allocation coefficients based on CSI will further improve the performance of CNOMA [49]. To the best of our knowledge, there are no existing works investigating a dynamic power-allocation-based RS scheme for CNOMA networks with FD relays. Secondly, the RS scheme presented in [54] is a centralized system. Channel estimation, relay selection and relevant data processing are controlled and completed by the BS itself, leading to a large demand of control signaling and system overhead.

Additionally, a general conclusion of research findings about CNOMA, such as [54] [79] [80] and [81], is that FD relaying CNOMA is superior to HD-based CNOMA in the low SNR region but not in the high SNR region due to effects of residual SI.

However, this conclusion still lacks a clear and explicit guidance to choose which relaying mode in practice. This is another focus of this part.

Motivated by the above consideration, we take a further step and propose a three-stage RS strategy with dynamic power allocation (TRSPA) for the proposed FD CNOMA scheme to overcome the two drawbacks of [54]. Due to the limited transmission capability [82] and the possible severe fading effect caused by physical obstacles or remote cell-edge location, a PU can be regarded as the weak user and it needs the assistance from other user relays, i.e., SUs. Many PUs such as real-time machine type communication devices are sensitive to time delay and they have the priority to access spectrum bands [83] to satisfy their QoS requirements first. In contrast, SUs such as cellular user relays are not sensitive to time delay, which makes them suitable to access a spectrum band opportunistically when the QoS requirements of PUs are met. The purpose of our proposed relay selection strategy TRSPA is to find out the best user relay to maximize the ergodic rate of that selected relay, i.e., SU, on the condition of guaranteeing successful transmissions of the PU's signal.

Different from [54] with fixed power allocations, power allocation coefficients adopted by our proposed TRSPA scheme are dynamically adjusted to optimal values all the time, in order to maximize the ergodic rate of the selected user relay and to realize successful transmissions of the PU's signal. Furthermore, different from [54], the system considered in our thesis is in fact a distributed system. Signal detection and decoding, power allocation, and relay selection are entirely completed by relays, instead of the BS. The role of the BS in our considered system model is merely a receiver, but not a controller. This kind of distributed system is more flexible and efficient with less control signaling and system overhead compared with the centralized system presented by [54]. Finally, we also reveal the practical impact of SI on TRSPA for FD CNOMA in terms of outage probability and ergodic rate.

The major contributions of this part are summarized as follows.

(1) We investigate a three-stage RS strategy for the proposed FD CNOMA scheme

based on spectrum sensing. With a dynamic power allocation method, TRSPA is proved to achieve the optimal outage probability and on this basis, the largest ergodic rate, among all possible RS strategies.

(2) We characterize the performance of TRSPA for FD CNOMA with imperfect SI cancellation. We derive the closed-form expressions of outage probability and ergodic rate. From the standpoint of practicality, relays are modelled as uniformly distributed. Also, we confirm that the diversity order of the weak user is worked out to be zero due to the effects of residual SI. The spatial multiplexing gain of strong user relay is worked out to be one, which is its achievable maximum value.

(3) Different from the inexplicit conclusion of other works, we straightforwardly reveal that even with the adverse effects of SI, FD CNOMA with reasonable SI suppression capabilities still achieves superior performance over HD CNOMA and COMA. We confirm that FD is the most sensible choice when designing a TRSPA strategy in reality.

1.3.4 Two-Way Relay FD CNOMA Scheme

Different from the existing works on one-way relay FD CNOMA schemes, a FD CNOMA scheme is proposed in this thesis where NOMA users under FD mode need to exchange messages with the assistance of a FD relaying node under decode-and-forward protocol. The considered system model can be applied to relay-assisted bi-directional transmission scenarios. Take the vehicular network inside an urban intersection area as an example, where vehicles move towards the intersection from different directions. Road intersections are always the traffic accident-prone locations. Vehicles need to exchange their up-to-date safety information such as locations and velocities to provide original data for the follow-up processing by particular vehicular techniques to avoid traffic accidents. The severe shadowing effects caused by buildings or other physical obstacles at the road corner create a non-line-of-sight situation

for such information exchange process. Therefore, a relay-assisted scheme is adopted. Message exchange is executed under the assistance of a roadside unit which is located at the road intersection. After proposing our two-way relay FD CNOMA scheme, we present the comprehensive investigation with both pSIC and ipSIC under the realistic assumption of imperfect self-interference cancellation, in terms of outage probability, system throughput in delay-limited transmission mode, ergodic rate and system throughput in delay-tolerant transmission mode.

The main contributions of this part are outlined as follows.

(1) We propose a CNOMA scheme where the relay and users operate in FD mode. The users intend to exchange information via the relay. The realistic assumption of imperfect self-interference cancellation and the situations of both pSIC and ipSIC are considered.

(2) We derive the closed-form expressions of the analytical and asymptotic outage probabilities in the proposed two-way relay FD CNOMA system with both pSIC and ipSIC. Based on these results, we work out corresponding diversity orders. The system throughput in delay-limited transmission mode is then accordingly derived. Due to the impact of inter-user interference among superimposed NOMA signals and the residual self-interference caused from imperfect self-interference cancellation, the outage probabilities for FD CNOMA converge to outage probability floors in the high SNR regime. That is to say the diversity orders for outage probabilities are equal to zero. We also learn that pSIC is incapable of overcoming the zero diversity order issue since the inter-user interference is unavoidable.

(3) We derive the closed-form expressions for analytical and asymptotic ergodic rates with pSIC and ipSIC. Accordingly, we obtain that the high SNR slopes for ergodic rates of FD CNOMA are equal to zero. That is to say these ergodic rates converge to their upper limits in high SNR region. We also derive the system throughput in the delay-tolerant transmission mode. However, the use of pSIC is still incapable of overcoming the zero slope issue of FD CNOMA in high SNR region due to the

existence of residual self-interference.

(4) By presenting simulation results, we validate the derived closed-form expressions and compare the performance of the proposed FD CNOMA system with the benchmarks, i.e., the HD CNOMA system and the COMA system for bi-directional communication. We conclude that FD CNOMA outperforms the benchmarks in terms of outage probability, ergodic achievable rate and system throughput in low SNR region. The pSIC scheme is capable of improving the performance of FD CNOMA compared to ipSIC.

1.4 Thesis Organization

The remainder of the thesis is organized as follows.

Chapter 2 proposes a HD CNOMA scheme based on spectrum sensing, where the primary user intends to communicate with the base station by the assistance of the secondary user. On the other hand, the secondary user can obtain an additional opportunity to access the spectrum band originally belonging to the primary user. Therefore, a win–win situation is achieved by our collaboration scheme. When employing the proposed scheme, the secondary user, i.e., the user relay, adopts the spectrum sensing technique to perceive the surrounding wireless environment by identifying the spectrum holes. According to the sensing results, the secondary user will intelligently determine its transmission signal form, eventually improving the overall system capacity.

Chapter 3 presents a FD CNOMA scheme based on spectrum sensing, where a primary user communicates with the base station under the assistance of a secondary user, in order to sufficiently utilize both idle and underutilized spectrum resources. When the PU does not exist, the SU identifies this idle licensed spectrum band by spectrum sensing and occupies it so that the waste of spectrum hole resource is avoided. When the PU exists, it allows the SU to share its spectrum band by NOMA to further increase the spectrum efficiency. By adopting FD mode, the proposed FD CNOMA scheme

not only achieves better system performance than half-duplex mode by receiving and transmitting simultaneously, but also overcomes inherent issues of conventional CRNs.

Chapter 4 investigates the relay selection problem and proposes a three-stage relay selection strategy with power allocation for the FD CNOMA scheme based on spectrum sensing which is proposed in Chapter 3. Uniformly-distributed strong user relays in the investigated scheme help a weak user communicates with the BS in an efficient and reliable way. The proposed TRSPA strategy maximizes the transmission data rate of the selected relay while ensuring successful transmissions for the weak user by precisely narrowing down relay candidates step-by-step and dynamically allocating optimal power coefficients. We further exploit the impact of SI on TRSPA for FD CNOMA and then compare its performance with TRSPA applied in other relaying modes, that is half-duplex and orthogonal multiple access.

Chapter 5 exploits a novel two-way relay FD CNOMA system, where users intend to exchange messages with the assistance of a decode-and-forward relay. To characterize the potential performance gain brought by the proposed FD CNOMA scheme based on a two-way relay, the outage probability and ergodic rate are analyzed. Moreover, to present the comprehensive performance evaluation, both perfect and imperfect SICs are taken into consideration.

Chapter 6 summarizes our work and provides some future research directions.

Chapter 2

Half-Duplex Cooperative NOMA Based on Spectrum Sensing

2.1 Introduction

In this chapter, we propose a HD CNOMA scheme based on spectrum sensing and then further evaluate its performance. To be specific, we first introduce the system model of the considered HD relaying CNOMA scheme and then explain the signal transmission process of our proposed HD CNOMA scheme. Afterwards, the closed-form expressions for outage probability, ergodic rate and system throughput of this scheme are derived. Finally, simulation results are presented to verify the correctness of these derived expressions and to validate the superiority of our proposed scheme in terms of system throughput both in delay-limited and in delay-tolerant transmission modes under scenarios with or without direct link between the PU and the BS. Note that for the sake of simplicity, "CNOMA" in this chapter specifically refer to HD CNOMA.

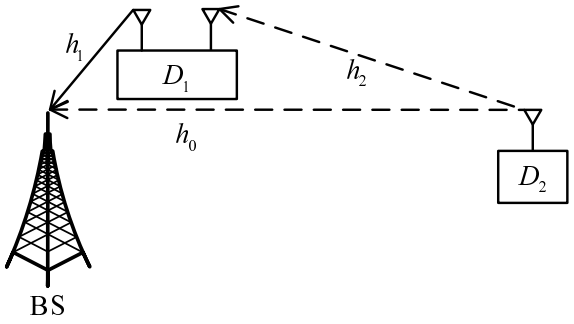

Figure 2.1: System model.

2.2 System Model

We consider an uplink CNOMA system in Fig. 2.1, consisting of two users D_1 and D_2, and one BS. The far user D_2, i.e., PU, communicates with the BS with the assistance of the near user D_1, i.e., SU. The proposed scheme operates in a half-duplex mode, as also assumed in [20, 21]. h_1, h_2 and h_0 represent the channel coefficients of $D_1 \rightarrow BS$, $D_2 \rightarrow D_1$ and $D_2 \rightarrow BS$ links. These wireless links are assumed to be independent non-selective block Rayleigh fading channels and they are disturbed by additive white Gaussian noise with the mean power of N_0. Ω_i ($i \in \{0, 1, 2\}$) denote the mean values of exponentially distributed random variables (RVs) $|h_1|^2$, $|h_2|^2$ and $|h_0|^2$. x_1 and x_2 denote the messages of the user-relay D_1 and the far user D_2, and they are assumed to be normalized unity power signals.

Under the hypothesis of the existence of PU, i.e., H_1, D_2 transmits x_2 during the first time slot. The SU D_1 executes spectrum sensing on its received signal. The observation at D_1 is

$$y^r_{D_1} = \sqrt{P_s} h_2 x_2 + n_{D_1}, \tag{2.1}$$

where n_{D_1} denotes the noise signal and P_s is the normalized transmission power of D_2. Therefore, the received signal to noise ratio (SNR) at D_1 to decode x_2 is

$$\gamma_{D_2 \rightarrow D_1} = |h_2|^2 \rho, \tag{2.2}$$

where $\rho = \frac{P_s}{N_0}$ is the transmit SNR. Specific spectrum sensing algorithm is not our main focus, so the widely-used energy detection (ED) method is adopted. Note that we consider the practical assumption of imperfect spectrum sensing, so even if the PU exists, the sensing result may still mistakenly claim the inexistence of the PU. If the sensing result precisely claims the existence of D_2 under H_1 which is defined as situation E_1 in this chapter, D_1 will decode its received D_2's signal and transmit the superimposed NOMA signal consisting of x_1 and x_2 to the BS in the second time slot. The NOMA signal is

$$y_{D_1}^t = \sqrt{P_r a_1} x_1 + \sqrt{P_r a_2} x_2, \tag{2.3}$$

where P_r is the normalized transmission powers of D_1. We assume that $P_r = P_s$ to simplify the derivation. a_1 and a_2 [1] denote the power allocation coefficients of x_1 and x_2. $a_1 + a_2 = 1$. Then the received signal by the BS for the relaying link is

$$y_{BS} = h_1 y_{D_1}^t + n_{BS}, \tag{2.4}$$

where n_{BS} is the noise signal at the BS. According to the NOMA principle, SIC is adopted at the BS. The received signal to interference and noise ratio (SINR) at the BS to decode x_2 for the relaying link is

$$\gamma_{D_2 \to BS, rel} = \frac{a_2 |h_1|^2 \rho}{a_1 |h_1|^2 \rho + 1}. \tag{2.5}$$

After decoding and then subtracting x_2 from the NOMA signal, the received SNR at the BS to decode x_1 is

$$\gamma_{D_1 \to BS} = a_1 |h_1|^2 \rho. \tag{2.6}$$

Otherwise, if miss detection happens and the sensing result claims the inexistence of D_2 under H_1 which is defined as situation E_2 in this chapter, D_1 will spend its entire

[1] In CRNs, PU signal always has high priority to satisfy its QoS requirement. Therefore, we assume that $a_2 > a_1$, which is also adopted in [46, 84].

power on its own message x_1. Then the received SNR at the BS is

$$\gamma'_{D_1 \to BS} = |h_1|^2 \rho. \tag{2.7}$$

The above illustration is analyzed without the direct link. For the scenario with direct link, the received SNR at the BS to decode x_2 for the direct link is

$$\gamma_{D_2 \to BS,dir} = |h_0|^2 \rho. \tag{2.8}$$

Upon maximal ratio combining (MRC) [42] over the two links during contiguous time slots, the resulting SINR at the BS is

$$\gamma_{D_2}^{MRC} = \gamma_{D_2 \to BS,dir} + \gamma_{D_2 \to BS,rel}. \tag{2.9}$$

Note that SINR values can be worked out in the same way, under the hypothesis of the inexistence of PU, i.e., H_0. To keep things simple, no more detailed similar statements under H_0 are presented here. As above-mentioned, H_1 is divided into situations E_1 and E_2. Moreover, considering the imperfect spectrum sensing, H_0 is divided into E_3 and E_4. E_3 is the situation when false alarm happens while E_4 means the sensing results precisely claim the inexistence of D_2.

Our proposed scheme can be applied to many practical application scenarios. For example, D_2 can be a medical health sensor with low data transmission rate [85] which immediately uploads its detected abnormal body-status-related data to the data fusion center for instant responses. An Internet of Things sensor is usually sensitive to time delay. It usually has un-rechargeable batteries [7] and thus limited transmission capability. Therefore, it needs the transmission assistance from other users. D_1 can be a video user [85] with relatively large data transmission rate so additional spectrum access opportunities are needed by them. A video user is not sensitive to time delay so opportunistic spectrum access is suitable to D_1. In a word, our win-win cooperative

scheme is a smart choice for them. On the one hand, if D_2 is claimed to be absent after spectrum sensing, the idle spectrum band will be used to transmit the broadband user D_1's signal [77]. On the other hand, as mentioned above, the sensor D_2 usually has low data transmission rate and thus the spectrum efficiency is quite low if it completely occupies the licensed spectrum band as in traditional OMA schemes. When D_2 exists, it shares the licensed spectrum band with D_1 by NOMA in our proposed scheme. Therefore, besides the signal transmission of D_2, D_1 also transmits signals by this spectrum band, increasing the overall system throughput and thus the system efficiency [77]. That is why our proposed CNOMA scheme based on spectrum sensing is capable of sufficiently utilizing both idle and underutilized spectrum bands.

2.3 Performance Analysis

In this performance analysis section, we respectively consider two types of transmission modes. They are the delay-limited transmission mode and the delay-tolerant transmission mode [86]. Under the delay-limited transmission mode, each user has a targeted data rate which is determined by its QoS requirement. The information of each user is transmitted at a fixed data rate. Outage probability is an important metric for performance evaluation when delay is limited. Delay-tolerant transmission refers to the situation without any time delay constraints. Users' targeted rates are allocated opportunistically. In fact, the transmission data rates are determined according to these users' specific channel conditions. The codeword can be designed arbitrarily long, which means it can span over all the fading states. It will be decoded when received in its full length. Therefore, the user is capable of decoding messages correctly during SIC. The performance metric for performance evaluation in this mode is ergodic rate. So the ergodic rate should be calculated on the condition of successfully decoding [87] during SIC.

2.3.1 Scenario without Direct Link

2.3.1.1 Outage Probability

Outage Probability of D_1 under H_1: First, for the situation E_1, the complementary event of communication outage for D_1 is that the BS can decode the messages of both D_2 and D_1, so the outage probability is

$$\begin{aligned} &P_{D_1}\left| H_1, P_d\left(|h_2|^2\right)\right. = 1- \\ &\Pr\left(\gamma_{D_2\to BS,rel} > \phi_2, \gamma_{D_1\to BS} > \phi_1\right) = 1 - e^{-\frac{1}{\Omega_1}\theta_{H_1,P_d}}, \end{aligned} \tag{2.10}$$

where $\phi_1 = 2^{2R_1} - 1$ and $\phi_2 = 2^{2R_2} - 1$. R_1 and R_2 are the targeted data rates for x_1 and x_2. $\theta_{H_1,P_d} = \max\left(\frac{\phi_2}{\rho(a_2 - a_1\phi_2)}, \frac{\phi_1}{\rho a_1}\right)$. $P_d\left(|h_2|^2\right)$ refers to the detection probability at D_1 to detect x_2 and it is a function of $|h_2|^2$. Note that (2.10) is derived under the assumption that $a_2 > a_1\phi_2$ [2]. For miss detection situation E_2, transmission outage will happen as long as the BS fails to decode x_1. $P_m\left(|h_2|^2\right) = 1 - P_d\left(|h_2|^2\right)$ represents the miss detection probability. Therefore, the outage probability under E_2 is

$$\begin{aligned} &P_{D_1}\left| H_1, P_m\left(|h_2|^2\right)\right. \\ &\quad = \Pr\left(\gamma'_{D_1\to BS} < \phi_1\right) = 1 - e^{-\frac{1}{\Omega_1}\frac{\phi_1}{\rho}}. \end{aligned} \tag{2.11}$$

Based on (2.10) and (2.11), the outage probability of D_1 under the hypothesis of H_1 is given by

$$\begin{aligned} &P_{D_1}\left| H_1 = \int_0^\infty \left(\left[P_{D_1}\left| H_1, P_d\left(|h_2|^2\right)\right.\right] P_d\left(|h_2|^2\right)\right. \\ &+ \left[P_{D_1}\left| H_1, P_m\left(|h_2|^2\right)\right.\right] P_m\left(|h_2|^2\right)\Big) f_{|h_2|^2}\left(|h_2|^2\right) d|h_2|^2 \\ &= \left(1 - e^{-\frac{1}{\Omega_1}\theta_{H_1,P_d}}\right)\int_0^\infty P_d(x) f_X(x)\, dx \\ &+ \left(1 - e^{-\frac{1}{\Omega_1}\frac{\phi_1}{\rho}}\right)\left(1 - \int_0^\infty P_d(x) f_X(x)\, dx\right), \end{aligned} \tag{2.12}$$

where x denotes $|h_2|^2$. $f_X(x) = f_{|h_2|^2}\left(|h_2|^2\right)$ represents the PDF of $|h_2|^2$. Now the key of

[2] Otherwise, $P_{D_1}\left| H_1, P_d\left(|h_2|^2\right)\right. = 1$.

(2.12) is to calculate $\int_0^\infty P_d(x) f_X(x) dx$. For the ease of the subsequent derivation, we focus on a more general form, i.e., $\int_{\frac{\phi_2}{\rho}}^\infty P_d(x) f_X(x) dx$. According to the central limit theorem, the detection probability for ED is given by

$$P_d(x) = Q\left(\frac{Q^{-1}\left(P_f^{pre}\right)\sqrt{2/K} - \rho x}{\sqrt{2/K}(1+\rho x)}\right), \tag{2.13}$$

where K is the sampling number and P_f^{pre} is the preset false alarm probability. $Q(\cdot)$ denotes the Marqum Q-function. Furthermore, we expand the Q-function according to the expansion formula (3.321.1) in [88], and then obtain the analytical result of $\int_{\frac{\phi_2}{\rho}}^\infty P_d(x) f_X(x) dx$ in (2.14), based on binomial expansion and the integral formula (3.351.4) in [88], where $A = pe^p$, $B = \frac{Q^{-1}\left(P_f^{pre}\right)\sqrt{2/K}+1}{\sqrt{2/K}}$, $u = \phi_2 + 1$, $p = \frac{1}{\Omega_2}\frac{1}{\rho}$ and $C_m^i = \frac{m!}{i!(m-i)!}$. $\mathrm{Ei}(\cdot)$ denotes Exponential integral function.

$$\begin{aligned}\int_{\frac{\phi_2}{\rho}}^\infty P_d(x) f_X(x) dx = {} & \frac{1}{2}e^{-\phi_2 p} - \frac{A}{\sqrt{\pi}}\sum_{m=0}^{\infty}\frac{(-1)^m\left(\frac{1}{\sqrt{2}}\right)^{2m+1}}{(m!)(2m+1)}\left(\left(-\sqrt{\frac{K}{2}}\right)^{2m+1}\frac{e^{-up}}{p}\right. \\ & \left. + \sum_{i=1}^{2m+1} C_{2m+1}^i\left(-\sqrt{\frac{K}{2}}\right)^{2m+1-i} B^i\left((-1)^i\frac{p^{i-1}\mathrm{Ei}(-pu)}{(i-1)!} + \frac{e^{-pu}}{u^{i-1}}\sum_{j=0}^{i-2}\frac{(-1)^j p^j u^j}{(i-1)(i-2)\cdots(i-j-1)}\right)\right)\end{aligned} \tag{2.14}$$

Note that numerically, $\int_0^\infty P_d(x) f_X(x) dx$ can be worked out by substituting $\phi_2 = 0$ into (2.14).

Outage Probability of D_1 under H_0: Similar with the above subsection, outage probabilities under E_3 and E_4 are $1-e^{-\frac{1}{\Omega_1}\theta_{H_0,P_f}}$ and $1-e^{-\frac{1}{\Omega_1}\frac{\phi_1}{\rho}}$. $\theta_{H_0,P_f} = \max\left(\frac{\phi_2}{\rho(a_2-a_1\phi_2)}, \frac{\phi_1}{\rho a_1}\right)$. Then the outage probability under H_0 is

$$\begin{aligned}& P_{D_1}\big|H_0 \\ & = \left(1-e^{-\frac{1}{\Omega_1}\theta_{H_0,P_f}}\right)P_f^{pre} + \left(1-e^{-\frac{1}{\Omega_1}\frac{\phi_1}{\rho}}\right)\left(1-P_f^{pre}\right).\end{aligned} \tag{2.15}$$

Outage Probability of D_2 under H_1: The complementary event of outage at D_2 under E_1 is that both D_1 and BS can decode x_2. So the communication outage probability

of D_2 under E_1 is

$$\begin{aligned} & P_{D_2}\big|\, H_1, P_d\left(|h_2|^2\right) \\ &= 1 - \Pr\left(\gamma_{D_2\to D_1} > \phi_2, \gamma_{D_2\to BS,rel} > \phi_2\right) \\ &= 1 - e^{-\left(\frac{1}{\Omega_1}\frac{\phi_2}{a_2\rho - a_1\rho\phi_2}\right)} \Pr\left(|h_2|^2 > \frac{\phi_2}{\rho}\right). \end{aligned} \tag{2.16}$$

Under E_2, D_1 only transmits its own message so the outage probability of D_2 is $P_{D_2}\big|\, H_1, P_m\left(|h_2|^2\right) = 1$. Accordingly, the outage probability of D_2 under H_1 is given by

$$P_{D_2}\big|\, H_1 = 1 - e^{-\left(\frac{1}{\Omega_1}\frac{\phi_2}{a_2\rho - a_1\rho\phi_2}\right)} \int_{\frac{\phi_2}{\rho}}^{\infty} P_d\left(x\right) f_X\left(x\right) dx, \tag{2.17}$$

where $\int_{\frac{\phi_2}{\rho}}^{\infty} P_d\left(x\right) f_X\left(x\right) dx$ is obtained according to (2.14).

Outage Probability of D_2 under H_0: D_2 does not exist under the hypothesis of H_0.

2.3.1.2 Throughput in Delay-Limited Transmission Mode

Next, the delay-limited transmission mode is considered under the hypothesis of $\mathcal{H}$, which is in fact the combination hypothesis of H_1 and H_0. Under $\mathcal{H}$, like the real-world systems, no one knows for sure whether D_2 is present or absent at the current time slot and D_2 can transmit its signals at any moment. We assume that D_2 randomly occupies the licensed spectrum or not with constant probabilities $P\left(H_1\right)$ and $P\left(H_0\right)$, as described in [89]. Then the system throughput without direct link is

$$\begin{aligned} R_l|\mathcal{H} &= \left(1 - P_{D_1}\big|\, H_0\right) R_1 P\left(H_0\right) \\ &+ \left(\left(1 - P_{D_1}\big|\, H_1\right) R_1 + \left(1 - P_{D_2}\big|\, H_1\right) R_2\right) P\left(H_1\right), \end{aligned} \tag{2.18}$$

where $P_{D_1}\big|\, H_0$, $P_{D_1}\big|\, H_1$ and $P_{D_2}\big|\, H_1$ are obtained from (2.15), (2.12) and (2.17).

2.3.1.3 Ergodic Rate

Ergodic Rate of D_1 under H_1: When user's rates are determined by their channel conditions, the ergodic rate becomes an important metric for performance evaluation.

Hence, the performance of the proposed CNOMA scheme is characterized in terms of ergodic rates as shown below. First, we consider the ergodic rate of D_1 under H_1.

As above-stated, H_1 is divided into two situations E_1 and E_2. For the situation E_1, on the condition that the BS can decode x_2, the achievable rate of D_1 at the BS can be written as $R_{D_1}\big|\, H_1, P_d\left(|h_2|^2\right) = \frac{1}{2}\log\left(1+\gamma_{D_1\to BS}\right)$. Then the ergodic rate of D_1 under E_1 is calculated as

$$\begin{aligned} E\left[R_{D_1}\big|\, H_1, P_d\left(|h_2|^2\right)\right] &= \tfrac{1}{2}E\left[\log\left(1+\underbrace{\gamma_{D_1\to BS}}_{Y}\right)\right] \\ &= \tfrac{1}{2\ln 2}\int_0^\infty \tfrac{1}{1+y}\left(1-F_Y(y)\right)dy, \end{aligned} \tag{2.19}$$

where the CDF of Y, i.e., $F_Y(y)$, is calculated as follows.

$$F_Y(y) = \Pr\left(a_1|h_1|^2\rho < y\right) = 1 - e^{-\frac{1}{\Omega_1}\frac{y}{a_1\rho}}. \tag{2.20}$$

Substituting (2.20) into (2.19), we learn that the ergodic rate is written as

$$E\left[R_{D_1}\big|\, H_1, P_d\left(|h_2|^2\right)\right] = \frac{1}{2\ln 2}\int_0^\infty \frac{1}{1+y}e^{-\frac{1}{\Omega_1}\frac{y}{a_1\rho}}dy. \tag{2.21}$$

Based on the equation (3.352.4) in [88], we can obtain the ergodic rate of D_1 under E_1 as follows.

$$\begin{aligned} &E\left[R_{D_1}\big|\, H_1, P_d\left(|h_2|^2\right)\right] \\ &\quad = \tfrac{1}{2\ln 2}\left(-e^{\frac{1}{\Omega_1 a_1\rho}}\mathrm{Ei}\left(-\tfrac{1}{\Omega_1 a_1\rho}\right)\right). \end{aligned} \tag{2.22}$$

For situation E_2 where miss detection happens, D_1 only transmits its own message x_1. In this case, the received SNR at the BS to decode x_1, i.e., $\gamma'_{D_1\to BS}$, is calculated as (2.7). Thus the achievable rate of D_1 at the BS, on the condition that the BS can decode x_2, is written as $R_{D_1}\big|\, H_1, P_m\left(|h_2|^2\right) = \frac{1}{2}\log\left(1+\gamma'_{D_1\to BS}\right)$. Then similar to the

above derivation under E_1, the ergodic rate under E_2 is expressed as

$$E\left[R_{D_1}\middle|H_1, P_m\left(|h_2|^2\right)\right] = \frac{1}{2\ln 2}\left(-e^{\frac{1}{\Omega_1\rho}}\mathrm{Ei}\left(-\frac{1}{\Omega_1\rho}\right)\right). \tag{2.23}$$

Accordingly, the closed-form ergodic rate of D_1 under the hypothesis of H_1 is calculated as (2.24).

$$\begin{aligned}
&E\left[R_{D_1}|H_1\right] \\
&= \int_0^\infty \left(E\left[R_{D_1}\middle|H_1, P_d\left(|h_2|^2\right)\right] \times P_d\left(|h_2|^2\right) + E\left[R_{D_1}\middle|H_1, P_m\left(|h_2|^2\right)\right] \times P_m\left(|h_2|^2\right)\right) f_{|h_2|^2}\left(|h_2|^2\right) d|h_2|^2 \\
&= \frac{1}{2\ln 2}\left(-e^{\frac{1}{\Omega_1 a_1\rho}}\mathrm{Ei}\left(-\frac{1}{\Omega_1 a_1\rho}\right)\right)\int_0^\infty P_d(x) f_X(x) dx + \frac{1}{2\ln 2}\left(-e^{\frac{1}{\Omega_1\rho}}\mathrm{Ei}\left(-\frac{1}{\Omega_1\rho}\right)\right)\left(1 - \int_0^\infty P_d(x) f_X(x) dx\right)
\end{aligned} \tag{2.24}$$

Still, numerically, $\int_0^\infty P_d(x) f_X(x)\, dx$ can be worked out by substituting $\phi_2 = 0$ into (2.14).

Ergodic Rate of D_1 under H_0: Under situation E_3, D_1 mistakenly identifies the received noise signal, i.e., n_{D_1}, as D_2's message. Then similar with (2.22), on the condition that the BS can decode the "mistaken x_2", the ergodic rate of D_1 can be written as $\frac{1}{2\ln 2}\left(-e^{\frac{1}{\Omega_1 a_1\rho}}\mathrm{Ei}\left(-\frac{1}{\Omega_1 a_1\rho}\right)\right)$. Under E_4, D_1 only transmits its own signal x_1 and therefore similar to (2.23), its corresponding ergodic rate is $\frac{1}{2\ln 2}\left(-e^{\frac{1}{\Omega_1\rho}}\mathrm{Ei}\left(-\frac{1}{\Omega_1\rho}\right)\right)$. In summary, under H_0, the ergodic rate of D_1 under H_0 is given by

$$\begin{aligned}
E\left[R_{D_1}\middle|H_0\right] = &\frac{1}{2\ln 2}\left(-e^{\frac{1}{\Omega_1 a_1\rho}}\mathrm{Ei}\left(-\frac{1}{\Omega_1 a_1\rho}\right)\right)P_f^{pre} \\
&+ \frac{1}{2\ln 2}\left(-e^{\frac{1}{\Omega_1\rho}}\mathrm{Ei}\left(-\frac{1}{\Omega_1\rho}\right)\right)\left(1 - P_f^{pre}\right).
\end{aligned} \tag{2.25}$$

Ergodic Rate of D_2 under H_1: Under E_1, since x_2 should be decoded at D_1 as well as at the BS for SIC, the achievable rate of D_2 is written as $R_{D_2}\middle|H_1, P_d\left(|h_2|^2\right) = \frac{1}{2}\log\left(1 + \min\left(\gamma_{D_2\to D_1}, \gamma_{D_2\to BS,rel}\right)\right)$ and the ergodic rate is given by $E\left[R_{D_2}\middle|H_1, P_d\left(|h_2|^2\right)\right] = \frac{1}{2}E\left[\log\left(1 + \min\left(\gamma_{D_2\to D_1}, \gamma_{D_2\to BS,rel}\right)\right)\right]$. Obviously, it is difficult to obtain the CDF of $\min\left(\gamma_{D_2\to D_1}, \gamma_{D_2\to BS,rel}\right)$. Considering the subsequent even more complicated derivation

based on its CDF, we focus on the high SNR and present the high approximation of $E\left[R_{D_2}\middle| H_1, P_d\left(|h_2|^2\right)\right]$, just like [84], so that we may finally manage to derive a closed-form expression for this ergodic rate to make the performance evaluation possible. Considering $\lim\limits_{\rho\to\infty}\gamma_{D_2\to D_1} = |h_2|^2\rho$ and $\lim\limits_{\rho\to\infty}\gamma_{D_2\to BS,rel} = \frac{a_2}{a_1}$, we learn that the asymptotic expression for ergodic rate of D_2 under E_1 in the high SNR region is

$$\begin{aligned} &E\left[R_{D_2}^{\infty}\middle| H_1, P_d\left(|h_2|^2\right)\right] \\ &= \tfrac{1}{2}E\left[\log\left(1+\underbrace{\min\left(|h_2|^2\rho, \frac{a_2}{a_1}\right)}_{Y'}\right)\right] \\ &= \tfrac{1}{2\ln 2}\int_0^{\infty}\tfrac{1}{1+y'}\left(1-F_{Y'}\left(y'\right)\right)dy'. \end{aligned} \tag{2.26}$$

The CDF of Y' is expressed as

$$\begin{aligned} F_{Y'}\left(y'\right) &= 1-\Pr\left(|h_2|^2\rho > y', \tfrac{a_2}{a_1} > y'\right) \\ &= 1-U\left(\tfrac{a_2}{a_1}-y'\right)\Pr\left(|h_2|^2 > \tfrac{y'}{\rho}\right), \end{aligned} \tag{2.27}$$

where $U\left(y'\right)$ is unit step function as $U\left(y'\right) = \begin{cases} 1, & y' > 0 \\ 0, & y' < 0 \end{cases}$. Substitute (2.27) into (2.26) and we obtain the high SNR approximation of the ergodic rate for D_2 under E_1, as shown in (2.28).

$$\begin{aligned} &E\left[R_{D_2}^{\infty}\middle| H_1, P_d\left(|h_2|^2\right)\right] \\ &= \tfrac{1}{2\ln 2}\int_0^{\infty}\tfrac{1}{1+y'}\left(U\left(\tfrac{a_2}{a_1}-y'\right)\Pr\left(|h_2|^2 > \tfrac{y'}{\rho}\right)\right)dy'. \end{aligned} \tag{2.28}$$

As to E_2, the BS cannot decode x_2 since D_1 fails to detect and forward x_2. Thus, the ergodic rate expression of D_2 is $E\left[R_{D_2}^{\infty}\middle| H_1, P_m\left(|h_2|^2\right)\right] = 0$.

In summary, the high SNR approximation of the ergodic rate for D_2 under H_1 is

given by (2.29).

$$\begin{aligned} E\left[R_{D_2}^{\infty}|H_1\right] &\to \tfrac{1}{2\ln 2}\int_0^{\frac{a_2}{a_1}} \tfrac{1}{1+y'}\left(\int_{\frac{y'}{\rho}}^{\infty} P_d(x)\, f_X(x)\, dx\right) dy' \\ &\to \tfrac{1}{2\ln 2}\int_0^{\frac{a_2}{a_1}} \tfrac{1}{1+y'}\left(e^{-\frac{y'}{\Omega_2\rho}} Q\left(-\sqrt{\tfrac{K}{2}}\right)\right) dy' \\ &\to \tfrac{1}{2\ln 2} Q\left(-\sqrt{\tfrac{K}{2}}\right)\int_0^{\frac{a_2}{a_1}} \tfrac{1}{1+y'} e^{-\frac{y'}{\Omega_2\rho}} dy'. \end{aligned} \tag{2.29}$$

Based on (3.352.1) in [88], we further calculate the asymptotic expression for ergodic rate of D_2 under H_1 in the high SNR region as follows.

$$\begin{aligned} &E\left[R_{D_2}^{\infty}|H_1\right] \to \\ &\tfrac{1}{2\ln 2} Q\left(-\sqrt{\tfrac{K}{2}}\right) e^{\frac{1}{\Omega_2\rho}}\left(\mathrm{Ei}\left(-\tfrac{1}{\Omega_2\rho}\tfrac{a_2}{a_1} - \tfrac{1}{\Omega_2\rho}\right) - \mathrm{Ei}\left(-\tfrac{1}{\Omega_2\rho}\right)\right) \end{aligned} \tag{2.30}$$

Ergodic Rate of D_2 under H_0: This case needs not to be considered since D_2 does not exist under such hypothesis.

2.3.1.4 Throughput in Delay-Tolerant Transmission Mode

In this subsection, the closed-form expression of system throughput in delay-tolerant transmission mode under the hypothesis of $\mathcal{H}$ is presented. First, we consider the hypothesis of H_1. The throughput is determined by evaluating the ergodic rate. Using (2.24) and (2.30), the asymptotic expression of system throughput under H_1 is given by

$$R_t^{\infty}|H_1 = E\left[R_{D_1}|H_1\right] + E\left[R_{D_2}^{\infty}|H_1\right]. \tag{2.31}$$

As to the hypothesis H_0, by using (2.25), the system throughput under H_0 is given by

$$R_t|H_0 = E\left[R_{D_1}|H_0\right]. \tag{2.32}$$

Accordingly, the asymptotic expression of system throughput under $\mathcal{H}$ is expressed as

$$R_t^{\infty}|\mathcal{H} = \left(R_t^{\infty}|H_1\right) P(H_1) + \left(R_t|H_0\right) P(H_0), \tag{2.33}$$

where $R_t^{\infty}|H_1$ and $R_t|H_0$ are worked out based on (2.31) and (2.32).

2.3.2 Scenario with Direct Link

Direct link makes no difference under H_0. Therefore, here we only focus on hypothesis H_1 .

2.3.2.1 Outage Probability

Outage Probability of D_1 under H_1: Under E_1, the complementary events of communication outage at D_1 are explained as follows. If D_1 fails to decode x_2, the BS needs to decode that mistakenly decoded message by the SU, and to decode x_1, only via the relaying link. If D_1 successfully decodes x_2, the BS needs to decode x_2 after MRC, and to decode x_1 as well. Then the outage probability under E_1 is (2.34),

$$\begin{aligned} P_{D_1,dir}\Big| H_1, P_d\left(|h_2|^2\right) = 1 - \big(&\Pr\left(\gamma_{D_2\to D_1} < \phi_2, \gamma_{D_2\to BS,rel} > \phi_2, \gamma_{D_1\to BS} > \phi_1\right) \\ &+ \Pr\left(\gamma_{D_2\to D_1} > \phi_2, \gamma_{D_2}^{MRC} > \phi_2, \gamma_{D_1\to BS} > \phi_1\right)\big) = 1 - \Pr\left(|h_2|^2\rho < \phi_2\right) \\ \times \underbrace{\Pr\left(\frac{a_2|h_1|^2\rho}{a_1|h_1|^2\rho+1} > \phi_2, a_1|h_1|^2\rho > \phi_1\right)}_{J_1} &- \Pr\left(|h_2|^2\rho > \phi_2\right) \underbrace{\Pr\left(|h_0|^2\rho + \frac{a_2|h_1|^2\rho}{a_1|h_1|^2\rho+1} > \phi_2, a_1|h_1|^2\rho > \phi_1\right)}_{J_2} \end{aligned} \tag{2.34}$$

where after proper integral calculation, we learn that

$$J_1 = e^{-\frac{1}{\Omega_1}\theta_{D_1,dir}}, \tag{2.35}$$

where $\theta_{D_1,dir} = \max\left(\frac{\phi_1}{\rho a_1}, \frac{\phi_2}{\rho(a_2 - a_1\phi_2)}\right)$. With the help of Taylor expansion and the integral formula (3.351.4) in [88], we learn that J_2 is calculated as (2.36),

$$J_2 = \begin{cases} e^{-\frac{\tau_2}{\Omega_1}}, & \tau_2 \geq \tau_1 \\ \frac{1}{\Omega_1}\frac{1}{a_1\rho} e^{p' - \frac{1}{\Omega_0}\frac{\phi_2}{\rho} + \frac{1}{\Omega_1}\frac{1}{a_1\rho}} \sum\limits_{n=0}^{\infty} \frac{(-1)^n \left(\frac{1}{\Omega_1}\frac{1}{a_1\rho}\right)^n}{n!} & \\ \quad \times \left((-1)^{n+2} \frac{p'^{n+1}}{(n+1)!} \left(\mathrm{Ei}(\varphi_1) - \mathrm{Ei}(\varphi_2)\right) + \left(\sum\limits_{k=0}^{n} \frac{\frac{e^{\varphi_1}\varphi_1^k}{u_1^{n+1}} - \frac{e^{\varphi_2}\varphi_2^k}{u_2^{n+1}}}{(n+1)n(n-1)\cdots(n-k+1)} \right) \right) + e^{-\frac{\tau_1}{\Omega_1}}, & \tau_2 < \tau_1 \end{cases} \tag{2.36}$$

where $\tau_1 = \frac{\phi_2}{\rho(a_2 - a_1\phi_2)}$, $\tau_2 = \frac{\phi_1}{a_1\rho}$, $p' = \frac{1}{\Omega_0}\frac{a_2}{a_1\rho}$, $u_1 = \frac{1}{a_1\rho\tau_1 + 1}$, $u_2 = \frac{1}{a_1\rho\tau_2 + 1}$, $\varphi_1 = -p'u_1$ and $\varphi_2 = -p'u_2$.

For situation E_2, the outage probability is

$$\begin{aligned} &P_{D_1,dir}\left| H_1, P_m\left(|h_2|^2\right)\right. \\ &\quad = \Pr\left(\gamma'_{D_1 \to BS} < \phi_1\right) = 1 - e^{-\frac{1}{\Omega_1}\frac{\phi_1}{\rho}}. \end{aligned} \tag{2.37}$$

Based on (2.34) and (2.37), the outage probability of D_1 under H_1 is calculated as

$$\begin{aligned} P_{D_1,dir}\left| H_1 \right. &= 1 - e^{-\frac{1}{\Omega_1}\frac{\phi_1}{\rho}} \\ &+ \left(e^{-\frac{1}{\Omega_1}\frac{\phi_1}{\rho}} - J_1\right) \int_0^{\infty} P_d(x) f_X(x) dx \\ &+ (J_1 - J_2) \int_{\frac{\phi_2}{\rho}}^{\infty} P_d(x) f_X(x) dx. \end{aligned} \tag{2.38}$$

Again, $\int_{\frac{\phi_2}{\rho}}^{\infty} P_d(x) f_X(x) dx$ can be obtained from (2.14).

Outage Probability of D_2 under H_1: Under E_1, the complementary events of outage at D_2 are described as follows. D_1 successfully decodes x_2 and the BS also decodes x_2 after MRC, or D_1 fails to decode x_2 but the BS decodes x_2 merely via the direct link.

Therefore,

$$\begin{aligned} & P_{D_2,dir}\big| H_1, P_d\left(|h_2|^2\right) \\ &= 1-\Big(\Pr\left(\gamma_{D_2\to D_1}>\phi_2, \gamma_{D_2}^{MRC}>\phi_2\right) \\ &\qquad +\Pr\left(\gamma_{D_2\to D_1}<\phi_2, \gamma_{D_2\to BS,dir}>\phi_2\right)\Big) \\ &= 1-\Pr\left(|h_2|^2\rho>\phi_2\right)J'_1-\Pr\left(|h_2|^2\rho<\phi_2\right)e^{-\frac{1}{\Omega_0}\frac{\phi_2}{\rho}}. \end{aligned} \tag{2.39}$$

Through similar calculation with the situation of D_1 under H_1 in Section 2.3.2.1, we find that $J'_1 = \Pr\left(|h_0|^2\rho+\frac{a_2|h_1|^2\rho}{a_1|h_1|^2\rho+1}>\phi_2\right)$ is numerically equal to (2.36) after substituting $\tau_2 = \phi_1 = 0$ into (2.36). Under E_2, the outage probability is written as $P_{D_2,dir}\big| H_1, P_m\left(|h_2|^2\right) = \Pr\left(\gamma_{D_2\to BS,dir}<\phi_2\right) = 1-e^{-\frac{1}{\Omega_0}\frac{\phi_2}{\rho}}$.

Accordingly, the outage probability of D_2 under H_1 is

$$\begin{aligned} & P_{D_2,dir}\big| H_1 \\ &= 1-e^{-\frac{1}{\Omega_0}\frac{\phi_2}{\rho}}+\left(e^{-\frac{1}{\Omega_0}\frac{\phi_2}{\rho}}-J'_1\right)\int_{\frac{\phi_2}{\rho}}^{\infty}P_d(x)\,f_X(x)dx. \end{aligned} \tag{2.40}$$

$\int_{\frac{\phi_2}{\rho}}^{\infty}P_d(x)\,f_X(x)\,dx$ is obtained according to (2.14).

2.3.2.2 Throughput in Delay-Limited Transmission Mode

The system throughput is given by

$$\begin{aligned} & R_{l,dir}|\mathcal{H} = \left(1-P_{D_1}\big| H_0\right)R_1P(H_0)+ \\ & \left(\left(1-P_{D_1,dir}\big| H_1\right)R_1+\left(1-P_{D_2,dir}\big| H_1\right)R_2\right)P(H_1), \end{aligned} \tag{2.41}$$

where $P_{D_1}\big| H_0$, $P_{D_1,dir}\big| H_1$ and $P_{D_2,dir}\big| H_1$ are worked out based on (2.15), (2.38) and (2.40).

2.3.2.3 Ergodic Rate

Ergodic Rate of D_1 under H_1: First, for the situation E_1, the achievable rate of D_1 at the BS can be expressed as $R_{D_1,dir}\big| H_1, P_d\left(|h_2|^2\right) = \frac{1}{2}\log\left(1+\gamma_{D_1\to BS}\right)$. Then the

ergodic rate of D_1 under E_1 is

$$\begin{aligned} E\left[R_{D_1,dir}\middle| H_1, P_d\left(|h_2|^2\right)\right] &= \tfrac{1}{2}E\left[\log\left(1+\underbrace{\gamma_{D_1\to BS}}_{Y}\right)\right] \\ &= \tfrac{1}{2\ln 2}\int_0^\infty \tfrac{1}{1+y}\left(1-F_Y(y)\right)dy, \end{aligned} \tag{2.42}$$

where the CDF of Y, i.e., $F_Y(y)$, is calculated as follows.

$$F_Y(y) = \Pr\left(a_1|h_1|^2\rho < y\right) = 1 - e^{-\frac{1}{\Omega_1}\frac{y}{a_1\rho}}. \tag{2.43}$$

Substituting (2.43) into (2.42), we learn that the ergodic rate is written as

$$E\left[R_{D_1,dir}\middle| H_1, P_d\left(|h_2|^2\right)\right] = \frac{1}{2\ln 2}\int_0^\infty \frac{1}{1+y}e^{-\frac{1}{\Omega_1}\frac{y}{a_1\rho}}dy. \tag{2.44}$$

Based on (3.352.4) in [88], we can obtain the ergodic rate of D_1 under E_1 as follows.

$$\begin{aligned} &E\left[R_{D_1,dir}\middle| H_1, P_d\left(|h_2|^2\right)\right] \\ &\quad= \tfrac{1}{2\ln 2}\left(-e^{\frac{1}{\Omega_1 a_1\rho}}\mathrm{Ei}\left(-\tfrac{1}{\Omega_1 a_1\rho}\right)\right). \end{aligned} \tag{2.45}$$

For situation E_2, the achievable rate of D_1 at the BS, on the condition that the BS can decode x_2, is written as $R_{D_1,dir}\middle| H_1, P_m\left(|h_2|^2\right) = \frac{1}{2}\log\left(1+\gamma'_{D_1\to BS}\right)$. Then similar to the above derivation under E_1, the ergodic rate under E_2 is

$$E\left[R_{D_1,dir}\middle| H_1, P_m\left(|h_2|^2\right)\right] = \frac{1}{2\ln 2}\left(-e^{\frac{1}{\Omega_1\rho}}\mathrm{Ei}\left(-\frac{1}{\Omega_1\rho}\right)\right) \tag{2.46}$$

Accordingly, the closed-form ergodic rate of D_1 under the hypothesis of H_1 is cal-

culated as (2.47).

$$\begin{aligned}
&E\left[R_{D_1,dir}|H_1\right] \\
&= \int_0^\infty \left(E\left[R_{D_1,dir}\middle| H_1, P_d\left(|h_2|^2\right)\right] \times P_d(x) + E\left[R_{D_1,dir}\middle| H_1, P_m\left(|h_2|^2\right)\right] \times \left(1 - P_d(x)\right)\right) f_X(x)\, dx \\
&= \frac{1}{2\ln 2}\left(-e^{\frac{1}{\Omega_1 a_1 \rho}} \mathrm{Ei}\left(-\frac{1}{\Omega_1 a_1 \rho}\right)\right) \int_0^\infty P_d(x)\, f_X(x) dx + \frac{1}{2\ln 2}\left(-e^{\frac{1}{\Omega_1 \rho}} \mathrm{Ei}\left(-\frac{1}{\Omega_1 \rho}\right)\right)\left(1 - \int_0^\infty P_d(x)\, f_X(x) dx\right)
\end{aligned} \tag{2.47}$$

Still, numerically, $\int_0^\infty P_d(x)\, f_X(x)\, dx$ can be worked out by substituting $\phi_2 = 0$ into (2.14).

Ergodic Rate of D_2 under H_1: Under E_1, x_2 should be decoded at D_1 as well as at the BS for SIC. Then the achievable rate of D_2 is written as $R_{D_2,dir}\middle| H_1, P_d\left(|h_2|^2\right) = \frac{1}{2}\log\left(1 + \min\left(\gamma_{D_2\to D_1}, \gamma_{D_2}^{MRC}\right)\right)$ and the ergodic rate is given by $E\left[R_{D_2,dir}\middle| H_1, P_d\left(|h_2|^2\right)\right] = \frac{1}{2}E\left[\log\left(1 + \min\left(\gamma_{D_2\to D_1}, \gamma_{D_2}^{MRC}\right)\right)\right]$. Still, we focus on the high SNR and present the high approximation of $E\left[R_{D_2,dir}\middle| H_1, P_d\left(|h_2|^2\right)\right]$, just like [84]. Considering $\lim_{\rho\to\infty} \gamma_{D_2\to D_1} = |h_2|^2\rho$ and $\lim_{\rho\to\infty} \gamma_{D_2}^{MRC} = |h_0|^2\rho + \frac{a_2}{a_1}$, the asymptotic expression for ergodic rate of D_2 under E_1 in the high SNR region is

$$\begin{aligned}
&E\left[R_{D_2,dir}^{\infty}\middle| H_1, P_d\left(|h_2|^2\right)\right] \\
&= \frac{1}{2}E\left[\log\left(1 + \underbrace{\min\left(|h_2|^2\rho, |h_0|^2\rho + \frac{a_2}{a_1}\right)}_{Z'}\right)\right] \\
&= \frac{1}{2\ln 2}\int_0^\infty \frac{1}{1+z'}\left(1 - F_{Z'}(z')\right) dz'.
\end{aligned} \tag{2.48}$$

The CDF of Z' is expressed as

$$\begin{aligned}
F_{Z'}(z') &= 1 - \Pr\left(|h_2|^2\rho > z', |h_0|^2\rho + \frac{a_2}{a_1} > z'\right) \\
&= 1 - \Pr\left(|h_2|^2 > \frac{z'}{\rho}\right) \\
&\quad \times \left(U\left(z' - \frac{a_2}{a_1}\right) e^{-\frac{1}{\Omega_0}\left(\frac{z'}{\rho} - \frac{a_2}{a_1\rho}\right)} + U\left(\frac{a_2}{a_1} - z'\right)\right).
\end{aligned} \tag{2.49}$$

After substituting (2.49) into (2.48), we get the high SNR approximation of the ergodic rate for D_2 under E_1, as calculated in (2.50).

$$\begin{aligned} E\left[R_{D_2,dir}^{\infty}\middle| H_1, P_d\left(|h_2|^2\right)\right] &= \frac{1}{2\ln 2}\int_0^{\infty}\frac{1}{1+z'}\Pr\left(|h_2|^2 > \frac{z'}{\rho}\right)\left(U\left(z'-\frac{a_2}{a_1}\right)e^{-\frac{1}{\Omega_0}\left(\frac{z'}{\rho}-\frac{a_2}{a_1\rho}\right)} + U\left(\frac{a_2}{a_1}-z'\right)\right)dz' \\ &= \frac{1}{2\ln 2}\left(\int_{\frac{a_2}{a_1}}^{\infty}\frac{1}{1+z'}e^{-\frac{1}{\Omega_0}\left(\frac{z'}{\rho}-\frac{a_2}{a_1\rho}\right)}\Pr\left(|h_2|^2 > \frac{z'}{\rho}\right)dz' + \int_0^{\frac{a_2}{a_1}}\frac{1}{1+z'}\Pr\left(|h_2|^2 > \frac{z'}{\rho}\right)dz'\right) \end{aligned} \tag{2.50}$$

As to E_2, even though D_1 fails to detect x_2, the BS could be capable of decoding x_2 via the direct link. Thus, we obtain the ergodic rate expression of D_2 as follows.

$$E\left[R_{D_2,dir}\middle| H_1, P_m\left(|h_2|^2\right)\right] = \frac{1}{2\ln 2}\left(-e^{\frac{1}{\Omega_0\rho}}\mathrm{Ei}\left(-\frac{1}{\Omega_0\rho}\right)\right). \tag{2.51}$$

To summarise, the high SNR approximation of the ergodic rate for D_2 under H_1 with direct link is given by (2.52).

$$\begin{aligned} &E\left[R_{D_2,dir}^{\infty}|H_1\right] \\ &= \int_0^{\infty}\left(E\left[R_{D_2,dir}^{\infty}\middle| H_1, P_d\left(|h_2|^2\right)\right]\times P_d\left(|h_2|^2\right) + E\left[R_{D_2,dir}\middle| H_1, P_m\left(|h_2|^2\right)\right]\times P_m\left(|h_2|^2\right)\right)f_{|h_2|^2}\left(|h_2|^2\right)d|h_2|^2 \\ &= \frac{1}{2\ln 2}\int_{\frac{a_2}{a_1}}^{\infty}\frac{1}{1+z'}e^{-\frac{1}{\Omega_0}\left(\frac{z'}{\rho}-\frac{a_2}{a_1\rho}\right)}\left(\int_{\frac{z'}{\rho}}^{\infty}P_d(x)\,f_X(x)\,dx\right)dz' + \frac{1}{2\ln 2}\int_0^{\frac{a_2}{a_1}}\frac{1}{1+z'}\left(\int_{\frac{z'}{\rho}}^{\infty}P_d(x)\,f_X(x)\,dx\right)dz' \\ &+\frac{1}{2\ln 2}\left(-e^{\frac{1}{\Omega_0\rho}}\mathrm{Ei}\left(-\frac{1}{\Omega_0\rho}\right)\right)\left(\int_0^{\infty}(1-P_d(x))\,f_X(x)dx\right) \\ &= \frac{1}{2\ln 2}\left(\int_{\frac{a_2}{a_1}}^{\infty}\frac{1}{1+z'}e^{-\frac{1}{\Omega_0}\left(\frac{z'}{\rho}-\frac{a_2}{a_1\rho}\right)}e^{-\frac{z'}{\Omega_2\rho}}Q\left(-\sqrt{\frac{K}{2}}\right)dz' + \int_0^{\frac{a_2}{a_1}}\frac{1}{1+z'}e^{-\frac{z'}{\Omega_2\rho}}Q\left(-\sqrt{\frac{K}{2}}\right)dz'\right) \\ &+\frac{1}{2\ln 2}\left(-e^{\frac{1}{\Omega_0\rho}}\mathrm{Ei}\left(-\frac{1}{\Omega_0\rho}\right)\right)\left(\int_0^{\infty}(1-P_d(x))\,f_X(x)dx\right) \\ &= \underbrace{\frac{1}{2\ln 2}Q\left(-\sqrt{\frac{K}{2}}\right)e^{\frac{1}{\Omega_0}\left(\frac{a_2}{a_1\rho}\right)}\int_{\frac{a_2}{a_1}}^{\infty}\frac{1}{1+z'}e^{\left(-\frac{1}{\Omega_0\rho}-\frac{1}{\Omega_2\rho}\right)z'}dz'}_{\Theta_1} + \underbrace{\frac{1}{2\ln 2}Q\left(-\sqrt{\frac{K}{2}}\right)\int_0^{\frac{a_2}{a_1}}\frac{1}{1+z'}e^{\frac{z'}{\Omega_2\rho}}dz'}_{\Theta_2} \\ &+\frac{1}{2\ln 2}\left(-e^{\frac{1}{\Omega_0\rho}}\mathrm{Ei}\left(-\frac{1}{\Omega_0\rho}\right)\right)\left(\int_0^{\infty}(1-P_d(x))\,f_X(x)dx\right) \end{aligned} \tag{2.52}$$

Based on (3.352.2) in [88], we further work out Θ_1 and Θ_2 in (2.52), and then accordingly obtain the following asymptotic expression for ergodic rate of D_2 under H_1 in the

high SNR region.

$$\begin{aligned} & E\left[R_{D_2,dir}^{\infty}|H_1\right] \\ & = \frac{1}{2\ln 2}Q\left(-\sqrt{\frac{K}{2}}\right)\left(\ln\left(\left(\frac{a_2}{a_1}+1\right)\left(\frac{1}{\Omega_0\rho}+\frac{1}{\Omega_2\rho}\right)\right)+C_E\right) \\ & +\frac{1}{2\ln 2}Q\left(-\sqrt{\frac{K}{2}}\right)\ln\left(\frac{a_2}{a_1}+1\right)-\frac{1}{2\ln 2}\left(1+\frac{1}{\Omega_0\rho}\right) \\ & \times\left(\ln\frac{1}{\Omega_0\rho}+C_E\right)\left(\int_0^{\infty}\left(1-P_d\left(x\right)\right)f_X\left(x\right)dx\right). \end{aligned} \tag{2.53}$$

$\int_0^{\infty} P_d\left(x\right) f_X\left(x\right)dx$ is obtained from (2.14). C_E is the Euler constant.

2.3.2.4 Throughput in Delay-Tolerant Transmission Mode

First, we consider the hypothesis of H_1. The throughput is determined by evaluating the ergodic rate. Based on (2.47) and (2.53), the asymptotic expression of system throughput under H_1 is given by

$$R_{t,dir}^{\infty}|H_1 = E\left[R_{D_1,dir}|H_1\right] + E\left[R_{D_2,dir}^{\infty}|H_1\right]. \tag{2.54}$$

As to the hypothesis H_0, using (2.25), the system throughput under H_0 is given by

$$R_{t,dir}|H_0 = E\left[R_{D_1}|H_0\right]. \tag{2.55}$$

Accordingly, the asymptotic expression of system throughput under $\mathcal{H}$ is expressed as

$$R_{t,dir}^{\infty}|\mathcal{H} = \left(R_{t,dir}^{\infty}|H_1\right)P\left(H_1\right) + \left(R_{t,dir}|H_0\right)P\left(H_0\right), \tag{2.56}$$

where $R_{t,dir}^{\infty}|H_1$ and $R_{t,dir}|H_0$ are worked out based on (2.54) and (2.55).

2.4 Numerical Results

Numerical simulation results are presented to validate the derived closed-form expressions in Section 2.3, verify the effectiveness of adopting spectrum sensing technique,

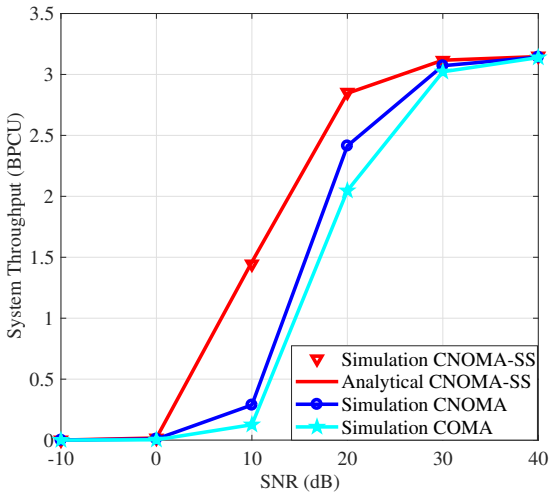

Figure 2.2: System throughput in delay-limited transmission mode versus SNR under $\mathcal{H}$ without direct link.

and further evaluate the achievable performance of the proposed CNOMA scheme.

Figure 2.2 plots the system throughput in delay-limited transmission mode for the proposed scheme based on spectrum sensing, which is referred to as CNOMA-SS ("SS" refers to spectrum sensing) in the simulation figures of this chapter, and two benchmarks, i.e., the CNOMA scheme proposed in [17] and the conventional COMA described in [84], versus SNR without direct link under $\mathcal{H}$. Both benchmarks are carried out in their uplink forms. To be specific, the communication process of COMA is finished in three slots. The far user sends its message x_2 in the first slot. The near user then decodes and forwards x_2 to the BS in the second slot. Finally, the near user sends its own message x_1 to the BS. As to CNOMA, two slots are needed. In the first slot, the far user sends x_2. The near user then decodes x_2 and transmits the superimposed NOMA signal consisting of x_2 and its own message x_1 to the BS in the second slot. In fact, CNOMA which fails to consider the existing spectrum holes is equivalent to CNOMA-SS when the false alarm probability is set to be 1. Without loss of generality, we assume that the distance between the BS and D_2 is normalized to unity. $\Omega_0 = 1$, $\Omega_1 = d^{-\alpha}$ and $\Omega_2 = (1-d)^{-\alpha}$, where d denotes the normalised distance between the BS and D_1, and α is the pathloss exponent. $d = 0.3$. $\alpha = 2$. As to other param-

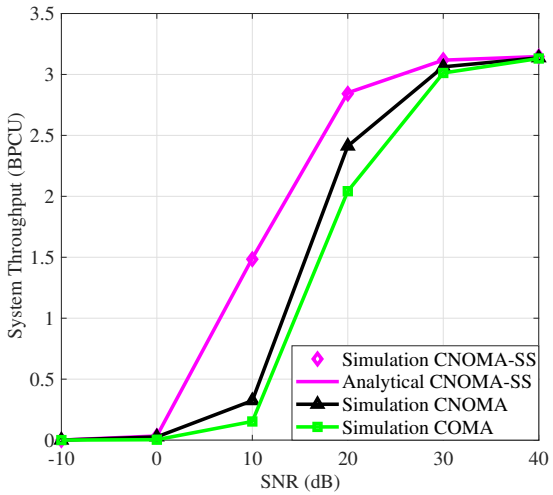

Figure 2.3: System throughput in delay-limited transmission mode versus SNR under $\mathcal{H}$ with direct link.

eters, $a_1 = 0.2$, $a_2 = 0.8$, $R_1 = 3$ bit per channel use (BPCU) and $R_2 = 1$ BPCU. $P_f^{pre} = 0.1$. $K = 30$. $P(H_1) = 0.15$ and $P(H_0) = 0.85$ [90]. The throughput analytical results for CNOMA-SS are worked out according to (2.12), (2.15), (2.17) and (2.18). Obviously, the analytical curve matches well with Monte Carlo simulation results, validating the involved derivation results. Also, it is observed that CNOMA-SS achieves higher throughput than CNOMA and COMA. To be specific, the system throughput of the proposed CNOMA-SS scheme respectively exceeds the two benchmarks CNOMA and COMA by 18.19% and 39.42% when SNR is 20 dB. This is because by spectrum sensing, the user-relay D_1 is capable of identifying the spectrum holes. It does not need to forward the received signals if D_2 is claimed to be absent. So useless transmission is avoided. Overall, the system resources are utilized more efficiently and thus the system throughput is improved compared with CNOMA and COMA. Then in fact, such phenomenon verifies that by adopting spectrum sensing technique, the proposed CNOMA-SS scheme is indeed able to make the system improve its capacity.

Figure 2.3 presents the system throughput in delay-limited transmission mode for CNOMA-SS, CNOMA and COMA with direct link under $\mathcal{H}$. The analytical curve for CNOMA-SS is plotted based on (2.15), (2.38), (2.40) and (2.41). Well-matched

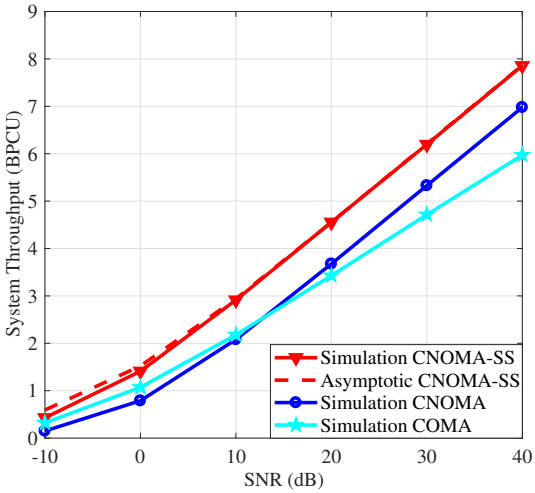

Figure 2.4: System throughput in delay-tolerant transmission mode versus SNR under $\mathcal{H}$ without direct link.

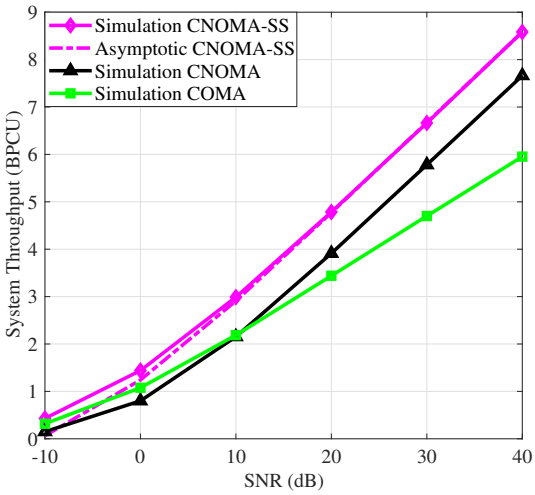

Figure 2.5: System throughput in delay-tolerant transmission mode versus SNR under $\mathcal{H}$ with direct link.

analytical results and simulation results validate our derived closed-form expressions. Similarly, the achieved system throughput by CNOMA-SS is higher than two benchmarks in the scenario with direct link. Compare Fig. 2.2 and Fig. 2.3, and we find that each scheme obtains slightly larger throughput with direct link than without direct link. This is because the direct link is able to provide spatial diversity by offering another chance for signal transmission.

Figure 2.4 and Fig. 2.5 plot the simulated and asymptotic results of the system

throughput in delay-tolerant transmission mode versus SNR under $\mathcal{H}$, respectively without or with the direct link. The asymptotic results of system throughput for the proposed CNOMA-SS are respectively worked out based on (2.33) and (2.56). It is observed from Fig. 2.4 and Fig. 2.5 that simulation curves approximate their corresponding asymptotic curves very well. Therefore, the relevant throughput derivation results are validated. In fact, according to (2.33) and (2.56), the system throughput should be obtained on the basis of the calculation of corresponding ergodic rates. Thus the correctness of the closed-form expressions of ergodic rates is also verified by Fig. 2.4 and Fig. 2.5. Moreover, it is shown that the CNOMA-SS scheme achieves larger system throughput in delay-tolerant transmission mode than CNOMA and COMA, in both of the scenarios with or without the direct link, verifying the effectiveness of adopting spectrum sensing in our proposed scheme. When SNR is 20 dB, the proposed CNOMA-SS scheme respectively outperforms CNOMA and COMA in the scenario without direct link in terms of system throughput by 23.9% and 32.84%. When the direct link exists, CNOMA-SS respectively outperforms the two benchmarks by 22.31% and 39.12%. After comparing Fig. 2.4 and Fig. 2.5, it is observed that each scheme obtains larger throughput with direct link than without direct link, because of the additional spatial diversity brought by the direct link when offering another chance for signal transmission.

By comparing Figs. 2.2, 2.3 and Figs. 2.4, 2.5, we find out that the system throughput under delay-limited transmission mode has an upper limit while the throughput under delay-tolerant mode does not. The reason is presented as follows. In the delay-limited mode, each user has a target data rate. The message of each user is sent at a fixed rate. Therefore, the best situation with the largest system throughput is that outage probabilities of both users are approximately equal to 0. In such case, the system throughput achieves its upper limit and it is equal to the sum of target rates of the two users. As to the delay-tolerant mode, users' target rates are allocated opportunistically and the transmitted data rates are adaptively determined according to these users' chan-

nel conditions. As the SNR ρ becomes larger and larger, the received SNR and SINR values at D_1 and the BS increase as well based on (2.2), (2.5)-(2.9). Accordingly, the values of corresponding ergodic rates get larger without any upper limit as ρ increases.

2.5 Summary

This chapter has proposed a HD CNOMA scheme based on spectrum sensing with the ability of identifying the spectrum holes of a CNOMA system, to avoid useless transmission, to adequately utilize the system resources and to eventually increase the system throughput in both delay-limited and delay-tolerant transmission modes under the scenarios with and without the direct link. To characterize the performance of the proposed scheme, we derived the closed-form expressions of outage probabilities and ergodic rates for two NOMA users with the practical assumption of imperfect spectrum sensing. Accordingly, the system throughput in the delay-limited and delay-tolerant transmission modes was worked out. Based on the simulation results, we validated these closed-form expressions, verified the effectiveness of employing spectrum sensing for better system performance, and demonstrated that the proposed scheme achieved larger throughput than two cooperative benchmarks, in both transmission modes with and without the direct link. Furthermore, based on the simulation results, we learned that all of the involved cooperative schemes obtained larger system throughput with direct link than without it, since the direct link was able to provide spatial diversity by offering additional opportunity for signal transmission.

In the next chapter, we look into a FD relaying CNOMA scheme which has the potential to further increase the spectrum efficiency compared with HD mode, due to the feature of simultaneously receiving and transmitting signals.

Chapter 3

Full-Duplex Cooperative NOMA Based on Spectrum Sensing

3.1 Introduction

In this chapter, we propose a FD CNOMA scheme based on spectrum sensing and then further characterize its performance. To be specific, we first introduce the system model of the considered FD relaying CNOMA scheme and then explain the signal sensing and transmission process of our proposed FD CNOMA scheme. Afterwards, expressions of ergodic rates are derived under practical assumptions of imperfect spectrum sensing and imperfect SI cancellation. For more insights, we work out their corresponding high-SNR slopes. Moreover, we obtain the system throughput according to the derived ergodic rates. Finally, numerical simulations are performed to verify the correctness of these derived expressions and to illustrate that the proposed FD CNOMA scheme outperforms other benchmarks in terms of ergodic rate and system throughput.

3.2 System Model

We consider the FD relaying CNOMA scheme consisting of one BS and two users, i.e., the SU D_1 and the PU D_2. Figure 3.1 takes uplink as an example and presents the studied system model. The far user D_2 from the BS intends to communicate with the BS under the assistance of the near user-relay D_1. D_1 is equipped with one transmit antenna and one receive antenna, while BS and D_2 are respectively equipped with one receive antenna and one transmit antenna. All wireless links among the BS, D_1 and D_2 are assumed to be independent non-selective block Rayleigh fading channels and they are disturbed by additive white Gaussian noise with the power of N_0. h_1, h_2 and h_0 denote the channel coefficients of $D_1 \rightarrow BS$, $D_2 \rightarrow D_1$ and $D_2 \rightarrow BS$ links, respectively. The channel power gains $|h_1|^2$, $|h_2|^2$ and $|h_0|^2$ are exponentially distributed random variables with Ω_i, $i \in \{0, 1, 2\}$, referring to their mean values [45]. We assume that an imperfect self-interference cancellation scheme is executed by D_1. The residual loop self-interference (LI) refers to the signals that are transmitted by a FD user-relay and looped back to the receiver simultaneously. By self-interference suppression techniques [52], [91] and [92], those LI signals can be suppressed to the same level with noise floor [92, 93]. Similar to previous works [44, 94, 95], we assume that the LI signal x_{LI} is zero-mean, additive and Gaussian. The assumption of a Gaussian distribution might hold in reality because of the various sources of imperfections in the cancellation process (based on the central limit theorem (CLT)). Meanwhile, similar to [53, 92, 96], the variance of the Gaussian LI signal is $\Omega_{LI} P_r$, where P_r represents the normalized transmit power of the user-relay D_1 and Ω_{LI} is the LI cancellation coefficient. x_1 and x_2 denote the messages of D_1 and D_2. It is noted that x_1 and x_2 are assumed to be normalized unity power signals, i.e., $E\left[x_1^2\right] = E\left[x_2^2\right] = 1$.

FD mode is adopted by the SU D_1 in our proposed FD CNOMA scheme. D_1 receives and detects x_2 while simultaneously transmitting x_1 and x_2 (or only transmitting x_1). So on average, the entire communication process of FD CNOMA is finished in just

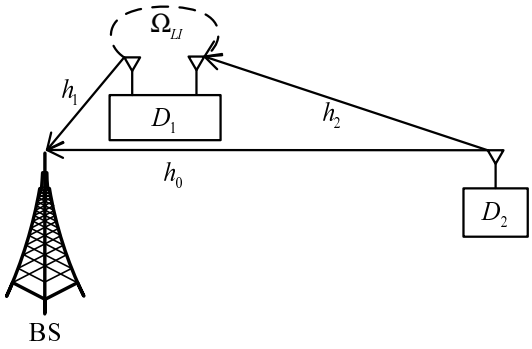

Figure 3.1: System model.

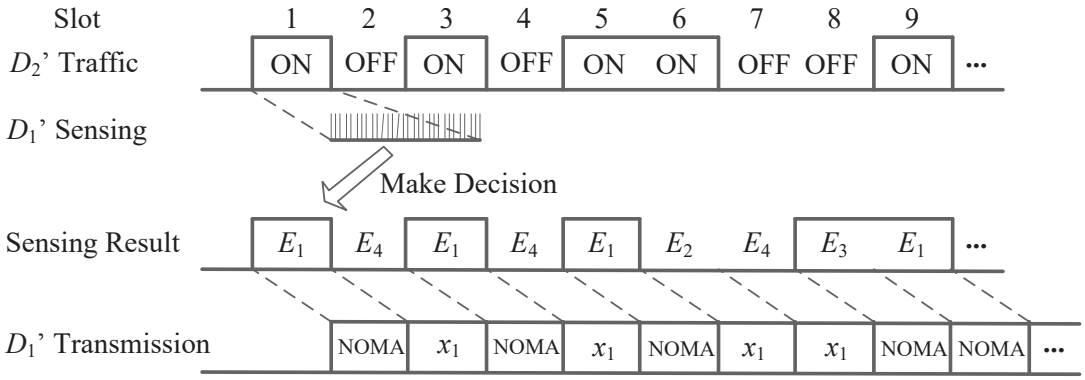

Figure 3.2: Sensing and transmission process of FD CNOMA.

one slot. By referring to the FD-CR scheme of D_1 in [97], we employ the sensing and transmission process presented in Fig. 3.2. D_1 keeps sensing D_2's message all the time in the entire time slots without dedicated sensing or transmission slots, and determines whether the PU D_2 exists or not. Since FD mode is adopted, D_1 also keeps transmitting all the time. If the spectrum sensing result claims the existence of D_2, then D_1 will decode D_2's message, and transmit x_1 and x_2 together as a superimposed NOMA signal to the BS, as shown in the first slot of Fig. 3.2. Otherwise, if the sensing result claims the non-existence of D_2, D_1 will transmit its own message x_1 using full power, as shown in the second slot. In this way, spectrum holes are identified and utilized timely. When D_2 exists, the licensed spectrum band is shared by D_1 and D_2, leading to larger spectrum efficiency than merely D_2 occupying it. The feature of sensing and transmitting signals simultaneously overcomes the inherent issues of conventional CRNs which are pointed out in Chapter 1. In this chapter, all derivations are discussed

under two hypotheses: H_1 and H_0, i.e., with or without the existence of D_2. H_1 and H_0 can be divided into the following four situations. Under E_1, D_2 does exist and is sensed by D_1, such as the first slot in Fig. 3.2. Under miss detection situation E_2, D_2 does exist but D_1 fails to sense it because of the possibly incorrect sensing results, such as the sixth slot. Under false alarm situation E_3, D_2 does not exist but D_1 mistakenly believes it exists, such as the eighth slot. Under E_4, D_2 does not exist and is not sensed by D_1, such as the second slot.

Next we will present all involved SNR and signal to interference and noise ratio (SINR) values for performance parameter derivation in Section 3.3. During the k-th time slot, the observation at D_1 can be expressed as

$$y_{D_1}^r[k] = \begin{cases} \sqrt{P_s} h_2 x_2[k] + x_{LI}[k] + n_{D_1}[k], & H_1 \\ x_{LI}[k] + n_{D_1}[k], & H_0 \end{cases} \tag{3.1}$$

where x_{LI} is the loop interference signal and n_{D_1} is the noise signal. P_s represents the normalized transmit power of D_2. In the following analysis, we assume that $P_r = P_s$ to simplify the derivation process[1]. First, we consider the situation E_1. The received SINR at D_1 to decode x_2 is calculated as

$$\gamma_{D_2 \to D_1}^{FD} = \frac{|h_2|^2 \rho}{\Omega_{LI} \rho + 1}, \tag{3.2}$$

where $\rho = \frac{P_r}{N_0} = \frac{P_s}{N_0}$ is the transmit SNR. The superimposed NOMA signal transmitted by D_1 is written as

$$y_{D_1}^t[k] = \sqrt{P_r a_1} x_1[k] + \sqrt{P_r a_2} x_2[k - \tau], \tag{3.3}$$

where τ denotes the processing delay at D_1 with an integer $\tau \geq 1$. Actually we take $\tau = 1$ as an example in Fig. 3.2. a_1 and a_2 denote the power allocation coefficients of

[1] A similar technique can be applied when $P_r \neq P_s$.

x_1 and x_2. To stipulate better fairness between the two users, we assume that $a_2 > a_1$ [45, 46] on the premise of $a_1 + a_2 = 1$ based on the NOMA principle [2]. Therefore, the received signals at the BS for the relaying link equals

$$y_{BS}[k] = h_1 y^t_{D_1}[k] + n_{BS}[k], \tag{3.4}$$

where n_{BS} is the noise signal at the BS. In the considered system shown in Fig. 3.1, the relaying link arrives at the BS with a small processing time delay compared with the direct link. In other words, there is some temporal separation between the signals from D_2 to BS via the relaying link and the direct link. Therefore, these signals can be appropriately co-phased and merged by using maximal ratio combining (MRC) [42]. To derive the theoretical results for FD relaying CNOMA system, we assume that signals from D_2 to BS via the two paths are fully resolvable by the BS, as also assumed in [42, 45, 46]. According to the NOMA principle, successive interference cancellation (SIC) is adopted at the BS. The received SINR at the BS to decode x_2 only using the relaying link is

$$\gamma^{FD}_{D_2 \to D_1 \to BS} = \frac{a_2 |h_1|^2 \rho}{a_1 |h_1|^2 \rho + 1}. \tag{3.5}$$

The received SNR at the BS to decode for the direct link is

$$\gamma^{FD}_{D_2 \to BS} = |h_0|^2 \rho. \tag{3.6}$$

After MRC, the received SINR at the BS for decoding x_2 can be expressed as [17, 46]

$$\gamma^{FD,MRC}_{D_2} = \gamma^{FD}_{D_2 \to BS} + \gamma^{FD}_{D_2 \to D_1 \to BS}. \tag{3.7}$$

According to SIC, after detecting and then subtracting x_2 from the received signals, the

[2] See detailed power allocation coefficient calculation method in our published paper [98].

BS needs to decode x_1 with the received SNR written as

$$\gamma_{D_1 \to BS}^{FD} = a_1 |h_1|^2 \rho. \tag{3.8}$$

The SNR and SINR values under E_2, E_3 and E_4 can be worked out in a similar way with situation E_1.

3.3 Performance Analysis

3.3.1 Ergodic Rate

3.3.1.1 Ergodic rate of D_1 under H_1

Ergodic rate is defined under a delay-tolerant transmission mode where target data transmission rates for users are set opportunistically. The codeword can span over all the fading states if necessary by being designed arbitrarily long. Therefore, the premise of ergodic rate calculation is that signals are successfully decoded [45, 99]. Note that each entire communication process of FD CNOMA is completed in one time slot but HD CNOMA takes two. Referring to the ergodic rate expression of D_1 under situation E_1 for the proposed HD CNOMA scheme by Chapter 2, as presented by (2.22), the corresponding ergodic rate for our proposed FD CNOMA scheme in this chapter can be derived in a similar way as

$$E\left[R_{D_1}^{FD} \middle| H_1, P_d^{FD}\left(|h_2|^2\right)\right] = \frac{1}{\ln 2}\left(-e^{\frac{1}{\Omega_1 a_1 \rho}} \mathrm{Ei}\left(-\frac{1}{\Omega_1 a_1 \rho}\right)\right) \tag{3.9}$$

where $P_d^{FD}\left(|h_2|^2\right)$ refers to the detection probability at D_1 to detect x_2 and it is a function of $|h_2|^2$. $\mathrm{Ei}(\cdot)$ denotes Exponential integral function.

For situation E_2, D_1 only transmits x_1. In a similar way with (2.23) in Chapter 2,

the ergodic rate under E_2 is expressed as

$$E\left[R_{D_1}^{FD}\middle| H_1, P_m^{FD}\left(|h_2|^2\right)\right] = \frac{1}{\ln 2}\left(-e^{\frac{1}{\Omega_1\rho}}\mathrm{Ei}\left(-\frac{1}{\Omega_1\rho}\right)\right) \tag{3.10}$$

where $P_m^{FD}\left(|h_2|^2\right)$ is the miss detection probability at D_1. The notation $R_{D_1}^{FD}\middle| H_1, P_m^{FD}\left(|h_2|^2\right)$ denotes the achievable rate under H_1 when x_2 fails to be detected by D_1, and thus it is corresponding to the situation E_2.

By combining (3.9) and (3.10), we obtain the ergodic rate of D_1 under H_1 as shown in (3.11),

$$\begin{aligned}
&E\left[R_{D_1}^{FD}|H_1\right] \\
&= \int_0^\infty \left(E\left[R_{D_1}^{FD}\middle| H_1, P_d^{FD}\left(|h_2|^2\right)\right] \times P_d^{FD}\left(|h_2|^2\right) + E\left[R_{D_1}^{FD}\middle| H_1, P_m^{FD}\left(|h_2|^2\right)\right] \times P_m^{FD}\left(|h_2|^2\right)\right) f_{|h_2|^2}\left(|h_2|^2\right) d|h_2| \\
&= \int_0^\infty \left(E\left[R_{D_1}^{FD}\middle| H_1, P_d^{FD}\left(|h_2|^2\right)\right] \times P_d^{FD}(x) + E\left[R_{D_1}^{FD}\middle| H_1, P_m^{FD}\left(|h_2|^2\right)\right] \times \left(1 - P_d^{FD}(x)\right)\right) f_X(x)\, dx \\
&= \frac{1}{\ln 2}\left(-e^{\frac{1}{\Omega_1 a_1\rho}}\mathrm{Ei}\left(-\frac{1}{\Omega_1 a_1\rho}\right)\right)\int_0^\infty P_d^{FD}(x)\, f_X(x)dx + \frac{1}{\ln 2}\left(-e^{\frac{1}{\Omega_1\rho}}\mathrm{Ei}\left(-\frac{1}{\Omega_1\rho}\right)\right)\left(1 - \int_0^\infty P_d^{FD}(x)\, f_X(x)dx\right)
\end{aligned} \tag{3.11}$$

where $f_{|h_2|^2}\left(|h_2|^2\right)$ denotes the PDF of $|h_2|^2$ and x represents $|h_2|^2$ to simplify the following derivation. Next we focus on the key of (3.11), i.e., $\int_0^\infty P_d^{FD}(x)\, f_X(x)dx$.

Theorem 1. *$\int_0^\infty P_d^{FD}(x)\, f_X(x)dx$ can be worked out as*

$$\begin{aligned}
\int_0^\infty P_d^{FD}(x)\, f_X(x)dx = \frac{1}{2} - \frac{A}{\sqrt{\pi}}\sum_{m=0}^{\infty}\frac{(-1)^m\left(\frac{1}{\sqrt{2}}\right)^{2m+1}}{(m!)(2m+1)} \\
\times\left(\left(-\sqrt{\frac{K}{2}}\right)^{2m+1}\frac{1}{p}e^{-p} + \sum_{i=1}^{2m+1}C_{2m+1}^{i}\left(-\sqrt{\frac{K}{2}}\right)^{2m+1-i}B^i\left((-1)^i\frac{p^{i-1}\mathrm{Ei}(-p)}{(i-1)!} + e^{-p}\sum_{j=0}^{i-2}\frac{(-p)^j}{(i-1)(i-2)\cdots(i-j-1)}\right)\right)
\end{aligned} \tag{3.12}$$

where $A = pe^p$, $B = \frac{Q^{-1}\left(P_f^{FD,pre}\right)\sqrt{2/K}+1}{\sqrt{2/K}}$ and $p = \frac{1}{\Omega_2}\frac{\Omega_{LI}\rho+1}{\rho}$.

Proof. See Appendix 3. □

Finally, substitute (3.12) into (3.11) and we obtain the ergodic rate of D_1 under H_1, i.e., $E\left[R_{D_1}^{FD}|H_1\right]$.

It is noted that expressions in this chapter are derived under the assumption of imperfect spectrum sensing. This practical assumption is consistent with real-world

systems. However, it makes the analysis very complicated. Therefore, we also present derivation results under the assumption of perfect spectrum sensing (pSS) as corollaries to simplify the expressions and to make it easier to understand our derivation process.

Corollary 1. *Under pSS assumption, the detection probability is equal to one, and thus H_1 is equivalent with E_1. The ergodic rate* (3.11) *of D_1 is simplified into the ergodic rate* (3.9)*. So*

$$E\left[R_{D_1,pSS}^{FD}\middle|H_1\right] = \frac{1}{\ln 2}\left(-e^{\frac{1}{\Omega_1 a_1 \rho}}\mathrm{Ei}\left(-\frac{1}{\Omega_1 a_1 \rho}\right)\right). \tag{3.13}$$

3.3.1.2 Ergodic rate of D_1 under H_0

In a similar way with (2.25) of Chapter 2, we get the following ergodic rate under H_0.

$$\begin{aligned} E\left[R_{D_1}^{FD}\middle|H_0\right] = {} & \frac{1}{\ln 2}\left(-e^{\frac{1}{\Omega_1 a_1 \rho}}\mathrm{Ei}\left(-\frac{1}{\Omega_1 a_1 \rho}\right)\right)P_f^{FD,pre} \\ & + \frac{1}{\ln 2}\left(-e^{\frac{1}{\Omega_1 \rho}}\mathrm{Ei}\left(-\frac{1}{\Omega_1 \rho}\right)\right)\left(1 - P_f^{FD,pre}\right). \end{aligned} \tag{3.14}$$

Corollary 2. *Under pSS assumption, the false alarm probability is equal to zero, and thus H_0 is equivalent with E_4. Then the ergodic rate* (3.14) *of D_1 under H_0 is simplified into*

$$E\left[R_{D_1,pSS}^{FD}\middle|H_0\right] = \frac{1}{\ln 2}\left(-e^{\frac{1}{\Omega_1 \rho}}\mathrm{Ei}\left(-\frac{1}{\Omega_1 \rho}\right)\right). \tag{3.15}$$

3.3.1.3 Ergodic Rate of D_2 under H_1

Under E_1, the message x_2 is decoded at both D_1 and the BS. So the achievable rate of D_2 is written as

$$\begin{aligned} & R_{D_2}^{FD}\middle|H_1, P_d^{FD}\left(|h_2|^2\right) \\ & \quad = \log\left(1 + \min\left(\gamma_{D_2\to D_1}^{FD}, \gamma_{D_2}^{FD,MRC}\right)\right). \end{aligned} \tag{3.16}$$

The ergodic rate is $E\left[R_{D_2}^{FD}\middle|H_1, P_d^{FD}\left(|h_2|^2\right)\right] = E\left[\log\left(1 + \min\left(\gamma_{D_2\to D_1}^{FD}, \gamma_{D_2}^{FD,MRC}\right)\right)\right]$. Obviously, it is extremely difficult to work out the CDF of $\min\left(\gamma_{D_2\to D_1}^{FD}, \gamma_{D_2}^{FD,MRC}\right)$. We focus on the high SNR region and present the high approximation of ergodic rate, just like [45]. In fact according to [100], ergodic rate performance in high SNR

regime is particularly important since the system is degree-of-freedom limited instead of power limited. Based on (3.2) and (3.7), we have $\lim_{\rho\to\infty} \gamma_{D_2\to D_1}^{FD} = \frac{1}{\Omega_{LI}}|h_2|^2$ and $\lim_{\rho\to\infty} \gamma_{D_2}^{FD,MRC} = |h_0|^2\rho + \frac{a_2}{a_1}$. Accordingly, the asymptotic ergodic rate of D_2 under E_1 in the high SNR region is

$$\begin{aligned} & E\left[R_{D_2}^{FD,\infty}\middle| H_1, P_d^{FD}\left(|h_2|^2\right)\right] \\ &= E\left[\log\left(1+\underbrace{\min\left(\frac{|h_2|^2}{\Omega_{LI}}, |h_0|^2\rho+\frac{a_2}{a_1}\right)}_{Y'}\right)\right] \\ &= \tfrac{1}{\ln 2}\int_0^\infty \tfrac{1}{1+y'}\left(1-F_{Y'}\left(y'\right)\right)dy', \end{aligned} \tag{3.17}$$

where the CDF of Y' is expressed as

$$\begin{aligned} & F_{Y'}\left(y'\right) = 1-\Pr\left(\tfrac{|h_2|^2}{\Omega_{LI}} > y', |h_0|^2\rho+\tfrac{a_2}{a_1} > y'\right) \\ &= 1-\Pr\left(|h_2|^2 > \Omega_{LI}y'\right) \\ &\quad \times\left(U\left(y'-\tfrac{a_2}{a_1}\right)e^{-\frac{1}{\Omega_0}\left(\frac{y'}{\rho}-\frac{a_2}{a_1\rho}\right)} + U\left(\tfrac{a_2}{a_1}-y'\right)\right), \end{aligned} \tag{3.18}$$

where $U\left(y'\right)$ is unit step function as $U\left(y'\right) = \begin{cases} 1, & y' > 0 \\ 0, & y' < 0 \end{cases}$. Substitute (3.18) into (3.17) and we obtain the following high SNR approximation of the ergodic rate for D_2 under E_1.

$$\begin{aligned} & E\left[R_{D_2}^{FD,\infty}\middle| H_1, P_d^{FD}\left(|h_2|^2\right)\right] \\ &= \tfrac{1}{\ln 2}\int_0^\infty \tfrac{1}{1+y'}\Pr\left(|h_2|^2 > \Omega_{LI}y'\right) \\ &\times\left(U\left(y'-\tfrac{a_2}{a_1}\right)e^{-\frac{1}{\Omega_0}\left(\frac{y'}{\rho}-\frac{a_2}{a_1\rho}\right)} + U\left(\tfrac{a_2}{a_1}-y'\right)\right)dy' \\ &= \tfrac{1}{\ln 2}\left(\int_{\frac{a_2}{a_1}}^\infty \tfrac{1}{1+y'}e^{-\frac{1}{\Omega_0}\left(\frac{y'}{\rho}-\frac{a_2}{a_1\rho}\right)}\Pr\left(|h_2|^2 > \Omega_{LI}y'\right)dy'\right. \\ &\left.+\int_0^{\frac{a_2}{a_1}} \tfrac{1}{1+y'}\Pr\left(|h_2|^2 > \Omega_{LI}y'\right)dy'\right). \end{aligned} \tag{3.19}$$

As to E_2, the BS should be capable of decoding x_2 via the direct link even though

D_1 fails to detect x_2. The corresponding ergodic rate expression of D_2 is

$$E\left[R_{D_2}^{FD}\middle| H_1, P_m^{FD}\left(|h_2|^2\right)\right] = \frac{1}{\ln 2}\left(-e^{\frac{1}{\Omega_0\rho}}\mathrm{Ei}\left(-\frac{1}{\Omega_0\rho}\right)\right). \tag{3.20}$$

After combining (3.19) and (3.20), the high SNR approximation of the ergodic rate for D_2 under H_1 is obtained as shown in (3.21),

$$\begin{aligned}
&E\left[R_{D_2}^{FD,\infty}|H_1\right] \\
&= \int_0^{\infty}\left(E\left[R_{D_2}^{FD,\infty}\middle| H_1, P_d^{FD}\left(|h_2|^2\right)\right]\times P_d^{FD}\left(|h_2|^2\right) + E\left[R_{D_2}^{FD}\middle| H_1, P_m^{FD}\left(|h_2|^2\right)\right]\times P_m^{FD}\left(|h_2|^2\right)\right) f_{|h_2|^2}\left(|h_2|^2\right) d|h_2|^2 \\
&= \underbrace{\frac{1}{\ln 2}\left(\int_{\frac{a_2}{a_1}}^{\infty}\frac{1}{1+y'}e^{-\frac{1}{\Omega_0}\left(\frac{y'}{\rho}-\frac{a_2}{a_1\rho}\right)}\left(\int_{\Omega_{LI}y'}^{\infty}P_d^{FD}(x)\,f_X(x)\,dx\right)dy' + \int_0^{\frac{a_2}{a_1}}\frac{1}{1+y'}\left(\int_{\Omega_{LI}y'}^{\infty}P_d^{FD}(x)\,f_X(x)\,dx\right)dy'\right)}_{\Theta} \\
&+\frac{1}{\ln 2}\left(-e^{\frac{1}{\Omega_0\rho}}\mathrm{Ei}\left(-\frac{1}{\Omega_0\rho}\right)\right)\left(1-\int_0^{\infty}P_d^{FD}(x)\,f_X(x)dx\right)
\end{aligned} \tag{3.21}$$

where $\int_0^{\infty}P_d^{FD}(x)\,f_X(x)dx$ is worked out by (3.12).

So the main focus now is to calculate Θ in (3.21). Let $f_{E_y}(y') = \int_{\Omega_{LI}y'}^{\infty}P_d^{FD}(x)\,f_X(x)\,dx$ and we have

$$\begin{aligned}
\Theta = &\underbrace{\frac{1}{\ln 2}\int_{\frac{a_2}{a_1}}^{\infty}\frac{1}{1+y'}e^{-\frac{1}{\Omega_0}\left(\frac{y'}{\rho}-\frac{a_2}{a_1\rho}\right)}f_{E_y}(y')\,dy'}_{\Theta_1} \\
&+\underbrace{\frac{1}{\ln 2}\int_0^{\frac{a_2}{a_1}}\frac{1}{1+y'}f_{E_y}(y')\,dy'}_{\Theta_2}.
\end{aligned} \tag{3.22}$$

Afterwards, we work out the expression of $f_{E_y}(y')$ as presented in (3.23) where $u = y'+1$, $p' = \frac{\Omega_{LI}}{\Omega_2}$ and $A' = \frac{\Omega_{LI}}{\Omega_2}e^{\frac{\Omega_{LI}}{\Omega_2}}$, according to a similar method with (3.12).

$$\begin{aligned}
&f_{E_y}(y') = \int_{\Omega_{LI}y'}^{\infty}P_d^{FD}(x)\,f_X(x)\,dx = \frac{1}{2}e^{-\frac{\Omega_{LI}}{\Omega_2}y'} - \frac{A'}{\sqrt{\pi}}\sum_{m=0}^{\infty}\frac{(-1)^m\left(\frac{1}{\sqrt{2}}\right)^{2m+1}}{(m!)(2m+1)}\times \\
&\left(\left(-\sqrt{\frac{K}{2}}\right)^{2m+1}\frac{\Omega_2}{\Omega_{LI}}e^{-\frac{\Omega_{LI}}{\Omega_2}(y'+1)} + \sum_{i=1}^{2m+1}C_{2m+1}^{i}\left(-\sqrt{\frac{K}{2}}\right)^{2m+1-i}B^i\left((-1)^i\frac{p'^{i-1}\mathrm{Ei}(-p'u)}{(i-1)!} + \frac{e^{-p'u}}{u^{i-1}}\sum_{j=0}^{i-2}\frac{(-1)^j p'^j u^j}{(i-1)(i-2)\cdots(i-j-1)}\right)\right)
\end{aligned} \tag{3.23}$$

Then according to Gaussian-Chebyshev quadrature formula in [101], we have

$$\Theta_2 = \sum_{i=1}^{N} \frac{\pi}{N} \frac{1}{\ln 2} \frac{a_2}{2a_1} \frac{1}{1+\frac{a_2}{a_1}\frac{z_i+1}{2}} f_{E_y}\left(\frac{a_2}{a_1}\frac{z_i+1}{2}\right) \sqrt{1-z_i^2}, \tag{3.24}$$

where N is a parameter to ensure a complexity-accuracy trade-off and $z_i = \cos\frac{(2i-1)\pi}{2N}$. $f_{E_y}\left(\frac{a_2}{a_1}\frac{z_i+1}{2}\right)$ is obtained by substituting $y' = \frac{a_2}{a_1}\frac{z_i+1}{2}$ into (3.23). Similarly, we then get

$$\begin{aligned}\Theta_1 = \sum_{i=1}^{N} \frac{\pi}{N} \frac{1}{\ln 2} \frac{1}{1+\frac{2a_2}{a_1(z_i+1)}} e^{-\frac{1}{\Omega_0}\left(\frac{2a_2}{a_1\rho(z_i+1)}-\frac{a_2}{a_1\rho}\right)} \\ \times f_{E_y}\left(\frac{2a_2}{a_1(z_i+1)}\right) \frac{2a_2}{a_1} \frac{1}{(z_i+1)^2} \sqrt{1-z_i^2},\end{aligned} \tag{3.25}$$

where $f_{E_y}\left(\frac{2a_2}{a_1(z_i+1)}\right)$ is worked out by substituting $y' = \frac{2a_2}{a_1(z_i+1)}$ into (3.23). Combining (3.21), (3.22), (3.24) and (3.25) together, we eventually obtain the high SNR approximation of the ergodic rate of D_2 under H_1.

Corollary 3. *Under pSS assumption, H_1 is equivalent with E_1. Then the ergodic rate* (3.21) *of D_2 under H_1 is simplified into the ergodic rate* (3.17) *under E_1. So we have*

$$\begin{aligned}E\left[R_{D_2,pSS}^{FD,\infty}\middle| H_1\right] &= E\left[R_{D_2,pSS}^{FD,\infty}\middle| H_1, P_d^{FD}\right] \\ &= \frac{1}{\ln 2}\int_0^{\infty} \frac{1}{1+y'}\left(1-F_{Y'}\left(y'\right)\right) dy',\end{aligned} \tag{3.26}$$

where CDF of Y' is

$$\begin{aligned}F_{Y'}\left(y'\right) = 1 - \Pr\left(\frac{|h_2|^2}{\Omega_{LI}} > y', |h_0|^2\rho + \frac{a_2}{a_1} > y'\right) = 1- \\ e^{-\frac{1}{\Omega_2}\Omega_{LI}y'}\left(U\left(y'-\frac{a_2}{a_1}\right)e^{-\frac{1}{\Omega_0}\left(\frac{y'}{\rho}-\frac{a_2}{a_1\rho}\right)} + U\left(\frac{a_2}{a_1}-y'\right)\right).\end{aligned} \tag{3.27}$$

Substituting (3.27) *into* (3.26)*, we have*

$$\begin{aligned} & E\left[R_{D_2,pSS}^{FD,\infty}\middle| H_1\right] \\ &= \underbrace{\frac{1}{\ln 2} e^{\frac{1}{\Omega_0}\frac{a_2}{a_1\rho}} \int_{\frac{a_2}{a_1}}^{\infty} \frac{1}{1+y'} e^{-\left(\frac{1}{\Omega_2}\Omega_{LI}+\frac{1}{\Omega_0}\frac{1}{\rho}\right)y'} dy'}_{Y_1} \\ &+ \underbrace{\frac{1}{\ln 2} \int_0^{\frac{a_2}{a_1}} \frac{1}{1+y'} e^{-\frac{1}{\Omega_2}\Omega_{LI}y'} dy'}_{Y_2}. \end{aligned} \tag{3.28}$$

According to (3.352.1) and (3.352.2) in [76], we obtain

$$Y_1 = \frac{1}{\ln 2} e^{\frac{1}{\Omega_0}\frac{a_2}{a_1\rho}} \left(-e^{\mu_1}\mathrm{Ei}\left(-\mu_1 u_1 - \mu_1\right)\right), \tag{3.29}$$

$$Y_2 = \frac{1}{\ln 2} e^{\mu_2} \left(\mathrm{Ei}\left(-\mu_2 u_2 - \mu_2\right) - \mathrm{Ei}\left(-\mu_2\right)\right), \tag{3.30}$$

where $u_1 = u_2 = \frac{a_2}{a_1}$, $\mu_1 = \frac{1}{\Omega_2}\Omega_{LI} + \frac{1}{\Omega_0}\frac{1}{\rho}$ *and* $\mu_2 = \frac{1}{\Omega_2}\Omega_{LI}$. *Now we can work out the ergodic rate* $E\left[R_{D_2,pSS}^{FD,\infty}\middle| H_1\right]$ *of* D_2 *under* H_1 *by substituting* (3.29) *and* (3.30) *into* (3.28).

3.3.1.4 Ergodic Rate of D_2 under H_0

This case needs not to be considered since D_2 does not exist under such hypothesis.

3.3.2 Spatial Multiplexing Gain

According to [102] and [103], the physical meaning of high SNR slope for ergodic rate is spatial multiplexing gain. High SNR slope is defined as

$$S_D = \lim_{\rho\to\infty} \frac{E\left[R_D^{\infty}\right]}{\log\rho}, \tag{3.31}$$

where $E\left[R_D^{\infty}\right]$ is the high SNR approximation of the corresponding ergodic rate.

3.3.2.1 Spatial Multiplexing Gain of D_1 under H_1

Based on (3.11), when $\rho \to \infty$, by using $\mathrm{Ei}(-x) \approx \ln(x) + C_E$ where C_E is the Euler constant and $e^{-x} \approx 1 - x$, the asymptotic ergodic rate of D_1 under H_1 is

$$\begin{aligned} E\left[R_{D_1}^{FD,\infty}\middle|H_1\right] &= \lim_{\rho\to\infty} E\left[R_{D_1}^{FD}\middle|H_1\right] \\ &= \tfrac{1}{\ln 2}\left(-\left(1+\tfrac{1}{\Omega_1 a_1 \rho}\right)\left(\ln\tfrac{1}{\Omega_1 a_1 \rho} + C_E\right)\right) \\ &\qquad \times \int_0^\infty P_d^{FD}(x)\, f_X(x) dx \\ &+ \tfrac{1}{\ln 2}\left(-\left(1+\tfrac{1}{\Omega_1 \rho}\right)\left(\ln\tfrac{1}{\Omega_1 \rho} + C_E\right)\right) \\ &\qquad \times \left(1 - \int_0^\infty P_d^{FD}(x)\, f_X(x) dx\right). \end{aligned} \tag{3.32}$$

Moreover, substituting $\lim_{\rho\to\infty} p = \frac{\Omega_{LI}}{\Omega_2}$ into (3.12), we get

$$\lim_{\rho\to\infty} \int_0^\infty P_d^{FD}(x)\, f_X(x) dx \triangleq Q_1, \tag{3.33}$$

where Q_1 is a function independent of ρ. Therefore, the asymptotic ergodic rate of D_1 under H_1 is

$$\begin{aligned} &E\left[R_{D_1}^{FD,\infty}\middle|H_1\right] \\ &= \tfrac{1}{\ln 2}\left(-\left(1+\tfrac{1}{\Omega_1 a_1 \rho}\right)\left(\ln\tfrac{1}{\Omega_1 a_1 \rho} + C_E\right)\right) Q_1 \\ &+ \tfrac{1}{\ln 2}\left(-\left(1+\tfrac{1}{\Omega_1 \rho}\right)\left(\ln\tfrac{1}{\Omega_1 \rho} + C_E\right)\right)(1 - Q_1). \end{aligned} \tag{3.34}$$

Substituting (3.34) into (3.31), we have

$$S_{D_1}^{FD}|H_1 = \lim_{\rho\to\infty} \frac{E\left[R_{D_1}^{FD,\infty}\middle|H_1\right]}{\log\rho} = 1. \tag{3.35}$$

According to [100] and [104], the maximum high SNR slope in a system with m transmit antennas and n receive antennas is $\min(m, n)$. Therefore, regarding the considered system of Section 3.2, the maximum high SNR slope of D_1 is 1.

Remark 1. *The high SNR slope of the ergodic rate for D_1 under H_1 in the proposed FD CNOMA scheme is* 1*, which is the achievable maximum value in the considered*

system.

Corollary 4. *According to* (3.13)*, when* $\rho \to \infty$*, the asymptotic ergodic rate of* D_1 *under* H_1 *in pSS case becomes*

$$E\left[R_{D_1,pSS}^{FD,\infty}|H_1\right] = \frac{1}{\ln 2}\left(-\left(1+\frac{1}{\Omega_1 a_1 \rho}\right)\left(\ln\frac{1}{\Omega_1 a_1 \rho} + C_E\right)\right). \tag{3.36}$$

Substituting (3.36) *into* (3.31)*, we have* $S_{D_1,pSS}^{FD}|H_1 = \lim\limits_{\rho\to\infty} \frac{E\left[R_{D_1,pSS}^{FD,\infty}|H_1\right]}{\log\rho} = 1.$

3.3.2.2 Spatial Multiplexing Gain of D_1 under H_0

Based on (3.14), when $\rho \to \infty$, the asymptotic ergodic rate of D_1 under H_0 is

$$\begin{aligned} &E\left[R_{D_1}^{FD,\infty}\middle|H_0\right] = \lim_{\rho\to\infty} E\left[R_{D_1}^{FD}\middle|H_0\right] \\ &= \frac{P_f^{FD,pre}}{\ln 2}\left(-\left(1+\frac{1}{\Omega_1 a_1 \rho}\right)\left(\ln\left(\frac{1}{\Omega_1 a_1 \rho}\right) + C_E\right)\right) \\ &+\frac{\left(1-P_f^{FD,pre}\right)}{\ln 2}\left(-\left(1+\frac{1}{\Omega_1 \rho}\right)\left(\ln\left(\frac{1}{\Omega_1 \rho}\right) + C_E\right)\right). \end{aligned} \tag{3.37}$$

Substituting (3.37) into (3.31), we have

$$S_{D_1}^{FD}|H_0 = \lim_{\rho\to\infty} \frac{E\left[R_{D_1}^{FD,\infty}\middle|H_0\right]}{\log\rho} = 1. \tag{3.38}$$

Remark 2. *The high SNR slope of the ergodic rate for* D_1 *under* H_0 *is also equal to* 1*, which is the achievable maximum value in the considered system.*

Corollary 5. *According to* (3.15)*, when* $\rho \to \infty$*, the asymptotic ergodic rate of* D_1 *under* H_0 *with pSS is written as*

$$E\left[R_{D_1,pSS}^{FD,\infty}|H_0\right] = \frac{1}{\ln 2}\left(-\left(1+\frac{1}{\Omega_1\rho}\right)\left(\ln\frac{1}{\Omega_1\rho} + C_E\right)\right). \tag{3.39}$$

Substituting (3.39) *into* (3.31)*, we have* $S_{D_1,pSS}^{FD}|H_0 = \lim\limits_{\rho\to\infty} \frac{E\left[R_{D_1,pSS}^{FD,\infty}|H_0\right]}{\log\rho} = 1.$

3.3.2.3 Spatial Multiplexing Gain of D_2 under H_1

Based on (3.21) and (3.33), we learn that the asymptotic ergodic rate of D_2 under H_1 can be further simplified as

$$\begin{aligned} &E\left[R_{D_2}^{FD,\infty}|H_1\right] \\ &= \Theta + \tfrac{1}{\ln 2}\left(-\left(1+\tfrac{1}{\Omega_0\rho}\right)\left(\ln\tfrac{1}{\Omega_0\rho}+C_E\right)\right)(1-Q_1)\,. \end{aligned} \tag{3.40}$$

By observing (3.22), (3.24) and (3.25), we find out that when $\rho \to \infty$, Θ is independent of ρ. After substituting (3.40) into (3.31), we learn that

$$S_{D_2}^{FD}|H_1 = \lim_{\rho\to\infty} \frac{E\left[R_{D_2}^{FD,\infty}\middle|H_1\right]}{\log\rho} = 1 - Q_1. \tag{3.41}$$

When $\rho \to \infty$, the detection performance of ED gets improved and the detection probability $P_d^{FD}\left(|h_2|^2\right)$ is usually quite large. Thus, when $\rho \to \infty$, the asymptotic detection probability ${Q_1}^3$ is close to 1. So we have the following remark.

Remark 3. *The high SNR slope of the ergodic rate for D_2 is equal to the miss detection probability which is much smaller than slopes of D_1 due to the effects of residual LI caused by imperfect interference cancellation.*

Corollary 6. *According to* (3.28)*, when $\rho \to \infty$, the high SNR slope of the asymptotic ergodic rate $E\left[R_{D_2,pSS}^{FD,\infty}\middle|H_1\right]$ of D_2 under H_1 under pSS assumption is*

$$S_{D_2,pSS}^{FD}|H_1 = \lim_{\rho\to\infty} \frac{E\left[R_{D_2,pSS}^{FD,\infty}|H_1\right]}{\log\rho} = \lim_{\rho\to\infty} \frac{Y_1}{\log\rho} = 0. \tag{3.42}$$

3.3.2.4 Spatial Multiplexing Gain of D_2 under H_0

This case needs not to be considered since D_2 does not exist under such hypothesis.

[3] In fact, $\int_0^\infty P_d^{FD}(x)\, f_X(x)dx = E\left[P_d^{FD}\left(|h_2|^2\right)\right]$.

3.3.3 Throughput

3.3.3.1 Hypothesis H_1

Using (3.11) and (3.21), the asymptotic expression of system throughput for FD CNOMA under H_1 is

$$R_t^{FD,\infty}|H_1 = E\left[R_{D_1}^{FD}|H_1\right] + E\left[R_{D_2}^{FD,\infty}|H_1\right]. \tag{3.43}$$

3.3.3.2 Hypothesis H_0

Using (3.14), the system throughput under H_0 is

$$R_t^{FD}|H_0 = E\left[R_{D_1}^{FD}|H_0\right]. \tag{3.44}$$

3.3.3.3 Hypothesis $\mathcal{H}$

The hypothesis $\mathcal{H}$ is the combination of H_1 and H_0. Under $\mathcal{H}$, we do not know whether D_2 exists or not. D_2 randomly chooses to use its spectrum band for a particular time slot with a constant probability [105]. Such a combined hypothesis is in fact more practical in real-world networks. The asymptotic expression of system throughput under $\mathcal{H}$ is expressed as

$$R_t^{FD,\infty}|\mathcal{H} = \left(R_t^{FD,\infty}|H_1\right)P(H_1) + \left(R_t^{FD}|H_0\right)P(H_0), \tag{3.45}$$

where $R_t^{FD,\infty}|H_1$ and $R_t^{FD}|H_0$ are worked out based on (3.43) and (3.44). $P(H_1)$ and $P(H_0)$ are a priori probabilities that D_2 uses and does not use its spectrum band [105].

3.4 Numerical Results

Numerical simulation results are presented in this section to verify the correctness of derived exact and asymptotic expressions in Section 3.3, illustrate the effectiveness of

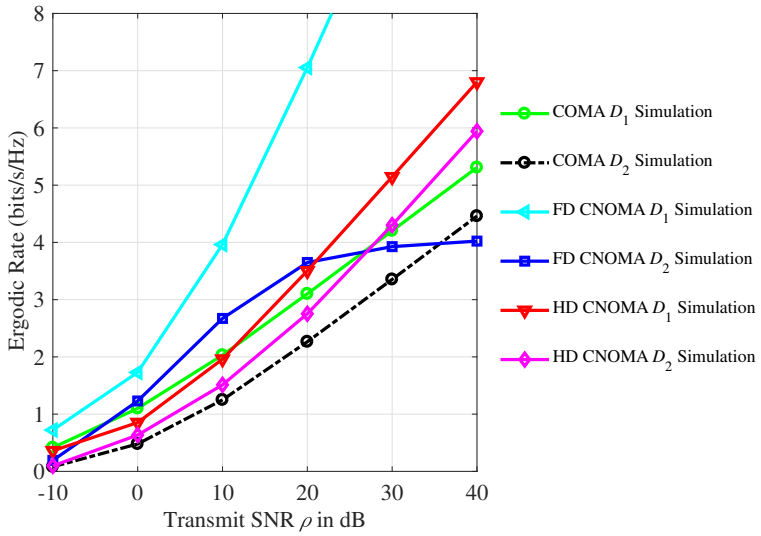

Figure 3.3: Simulated ergodic rates versus transmit SNR under the hypothesis of H_1.

adopting spectrum sensing, and compare the achieved performance of our proposed FD CNOMA scheme based on spectrum sensing with two cooperative benchmarks, i.e., HD CNOMA presented in [17] and COMA described in [45]. Both of them work in their uplink forms since we consider an uplink system as shown in Fig. 3.1 of this chapter. In order to guarantee the comparison fairness and thus to make the comparison convincing, we assume that user-relays of these benchmarks also have the capability of spectrum sensing. Access procedures of these two benchmarks are basically the same with our proposed FD CNOMA scheme, except that their user-relays work in HD mode or OMA mode, respectively, during receiving, detecting, decoding and transmitting signals. Without loss of generality, we assume that the distance between the BS and D_2 is normalized to unity, i.e., $\Omega_0 = 1$. $\Omega_1 = d^{-\alpha}$ and $\Omega_2 = (1-d)^{-\alpha}$ with d denoting the normalized distance between the BS and the SU D_1. α is the path-loss exponent. $P_f^{HD,pre}$ and $P_f^{OMA,pre}$ are used to denote the preset false alarm probabilities for HD CNOMA and COMA during ED. Unless otherwise stated, the following values are used in our simulations and analyses. $d = 0.3$, $\alpha = 2$, $a_1 = 0.2$, $a_2 = 0.8$, $K = 30$, $N = 20$, $\Omega_{LI} = -10$ dB, and $P_f^{FD,pre} = P_f^{HD,pre} = P_f^{OMA,pre} = 0.1$.

In Fig. 3.3, we compare the simulated ergodic rates of D_1 and D_2 in bits/s/Hz

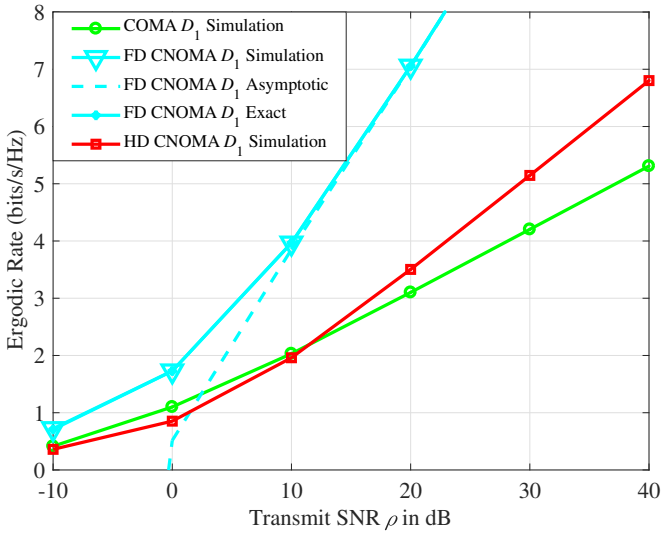

Figure 3.4: Simulated, asymptotic and exact ergodic rates versus transmit SNR of the strong user D_1 under the hypothesis of H_1.

versus SNR of our proposed FD CNOMA scheme with benchmarks HD CNOMA and COMA under H_1. First of all, it is observed that the ergodic rate of D_1 for FD CNOMA is always larger than benchmarks, since its entire communication process is completed in just one time slot, shorter than HD CNOMA and COMA. In this way, FD CNOMA utilizes resources more efficiently and has the potential to provide a higher transmission rate. As to D_2, FD CNOMA also outperforms HD CNOMA and COMA in the relatively low SNR region due to its short communication process duration. However, when the SNR is very large, beyond 27 dB in this case, LI becomes the dominating factor and limits FD CNOMA's ergodic rate until it is exceeded by HD CNOMA and even COMA. Similar simulation results about such effects of LI on the FD communication mode are also concluded in [45, 46, 99].

Figure 3.4 shows the simulated, asymptotic and exact ergodic rates of D_1 in a FD CNOMA system versus SNR under H_1. Exact results are worked out according to (3.11), while asymptotic results are calculated by (3.34). It is observed that the exact results match well with the Monte Carlo simulation results and the asymptotic curve approximates with its corresponding exact curve closely at the high SNR region. So

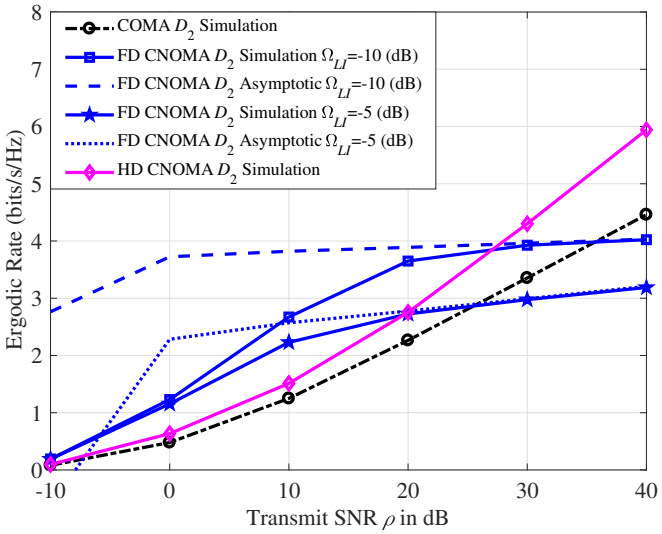

Figure 3.5: Simulated and asymptotic ergodic rates versus transmit SNR of the weak user D_2 under the hypothesis of H_1.

the above derivation results are validated. Moreover, considering the following two points $(10\text{ dB}, 3.8\text{ bits/s/Hz})$ and $(20\text{ dB}, 7.1\text{ bits/s/Hz})$ of the asymptotic curve of FD CNOMA in Fig. 3.4, we learn that the slope equals $3.3/10 = 0.33$, which matches Remark 1, i.e., $0.33 \cdot 10\lg 2 = 1$. The factor $10\lg 2$ appears between the actual slope "0.33" in Fig. 3.4 and the derived high SNR slope "1" in (3.35), since the x-axis in Fig. 3.4 is in dB while the denominator in (3.31) is in $\log(\cdot)$.

In Fig. 3.5, we present the simulated and asymptotic ergodic rates of D_2 under H_1 versus SNR with different self-interference cancellation coefficients. The asymptotic result of FD CNOMA is worked out based on (3.40). The simulation curve and the corresponding asymptotic curve match each other very well, which validates (3.40). In a similar way with Fig. 3.4, we learn that the high SNR slope of FD CNOMA with $\Omega_{LI} = -5$ dB in Fig. 3.5 is 0.022. Considering the parameter settings at the beginning of this section, we have $Q_1 = 0.9345$ based on (3.12) and (3.33). Since $0.022 \cdot 10\lg 2 \approx 1 - 0.9345$, the derivation result in (3.41) and Remark 3 are both verified. It is also observed that as to a fixed transmit SNR ρ, a smaller self-interference cancellation coefficient Ω_{LI} leads to a larger achieved ergodic rate for D_2 because the

intensity of residual LI in a FD CNOMA scheme is lower. On the other hand, as to a fixed Ω_{LI}, as ρ increases, the power of LI gets larger as well. It gradually affects FD CNOMA in a more obvious way. Eventually, the performance of FD CNOMA is exceeded by HD CNOMA and COMA in high SNR region. This result is consistent with Fig. 3.3. Therefore, the relationship between Ω_{LI} and ρ determines whether FD CNOMA is the best or not. The truth is that LI signal can be suppressed to the same level with the noise floor according to [92, 93] and [96]. Current self-interference suppression techniques are capable of reducing the LI's power $\Omega_{LI}P_r$ to N_0, which means $\Omega_{LI} = \frac{1}{\rho}$. In Fig. 3.5, (10 dB, 2.7 bits/s/Hz) and (5 dB, 1.7 bits/s/Hz) meet the above-mentioned relationship between Ω_{LI} and ρ in real-world scenarios and they belong to FD CNOMA curves respectively corresponding to $\Omega_{LI} = -10$ dB and $\Omega_{LI} = -5$ dB. FD CNOMA performs the best and has the largest ergodic rate at these two points. Therefore, FD CNOMA is already superior to HD CNOMA and COMA schemes with existing self-interference suppression techniques. Given the rapid development of suppression techniques, the superiority of FD CNOMA will be even more and more obvious. The fact that real-world scenarios with available self-interference suppression capability enable our FD CNOMA scheme to achieve the best performance greatly increases its significance in practical applications. Considering the rapidly-developing suppression techniques, our research on FD mode is necessary and meaningful.

Figure 3.6 shows the simulated, asymptotic and exact ergodic rates versus SNR under H_0. The PU D_2 does not exist under H_0 and therefore all curves are about D_1. Exact and asymptotic results of FD CNOMA are calculated according to (3.14) and (3.37). The well-matched exact and simulation curves and the well-approximated exact and asymptotic curves in the high SNR region validate these expressions. The performance of FD CNOMA always exceeds both benchmarks because of its shorter communication process duration. High SNR slope of FD CNOMA can be worked out according to Fig. 3.6, with the value of 0.33, verifying the calculation result in (3.38) and Remark 2. Finally, comparing ergodic rate curves in Fig. 3.6 with their

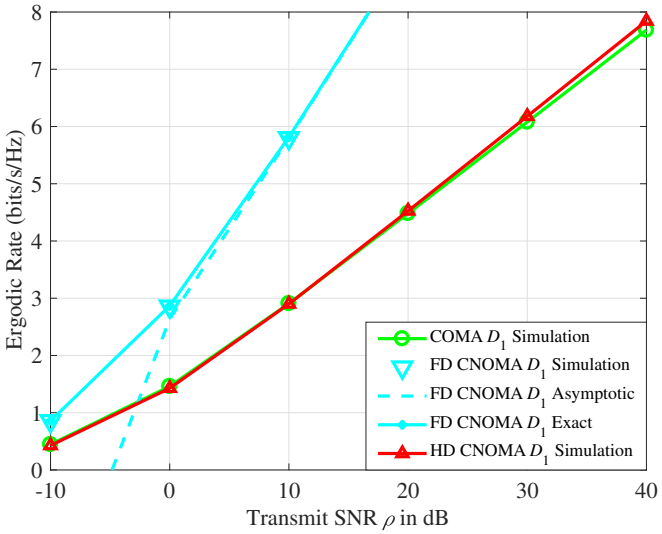

Figure 3.6: Simulated, asymptotic and exact ergodic rates versus transmit SNR of the strong user D_1 under the hypothesis of H_0.

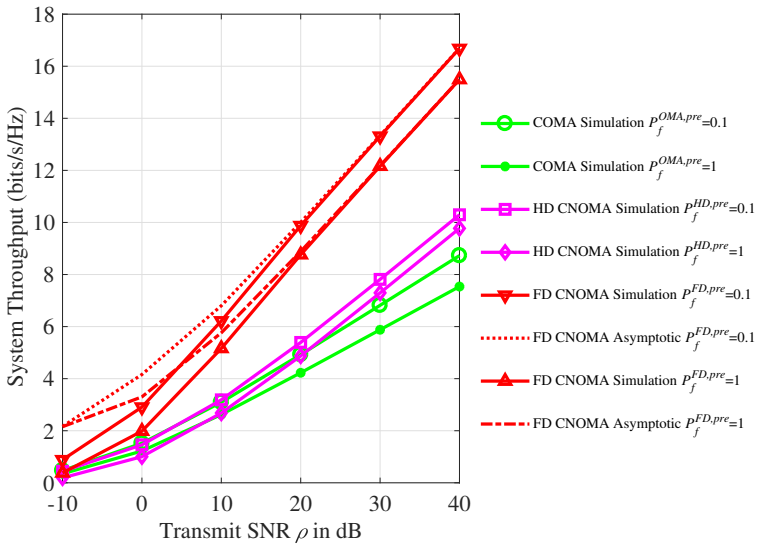

Figure 3.7: Simulated and asymptotic system throughput versus transmit SNR under the hypothesis of $\mathcal{H}$.

corresponding curves under H_1 in Fig. 3.4, we find out that D_1 achieves a larger ergodic rate under H_0 than H_1. It is because under the hypothesis of non-existence of D_2, D_1 tends to utilize its full transmit power to send its own message instead of assigning a large part of its power to send D_2's message.

Figure 3.7 plots the simulated and asymptotic results of the system throughput versus SNR under $\mathcal{H}$. We assume that $P(H_1) = P(H_0) = 0.5$. The asymptotic result of

system throughput for the proposed FD CNOMA scheme based on spectrum sensing is worked out based on (3.45). Still, simulation curves approximate their corresponding asymptotic curves very well. It is shown that FD CNOMA scheme achieves larger throughput than HD CNOMA and COMA. Afterwards, we compare the achieved system throughput with different preset false alarm probabilities and find out that for each scheme, the achieved throughput when false alarm probability is 0.1 is larger than when it is 1. If the false alarm probability is 1, spectrum sensing results will always claim the existence of the PU D_2, no matter whether D_2 actually exists or not. Therefore, the user-relay D_1 will always allocate a portion of its transmit power to forward its received signals even when D_2 does not exist and the received signals are nothing but interference and noise signals, leading to the wastes of power and spectrum hole resources. This is the reason why the achieved system throughput is smaller when the false alarm probability is 1. In fact, spectrum sensing becomes invalid if the false alarm probability is set to be 1. The comparison results of FD CNOMA curves with different false alarm probabilities in Fig. 3.7 actually verify the effectiveness of spectrum sensing in our proposed scheme for precisely identifying and sufficiently utilizing spectrum holes to increase the spectrum efficiency.

3.5 Summary

This chapter has proposed a FD CNOMA scheme based on spectrum sensing to sufficiently utilize both idle and underutilized spectrum resources, where a PU uploads messages to the BS with the assistance of a SU. By adopting the win-win collaboration scheme, the spectrum sensing technology, the NOMA strategy, and the FD communication mode, this FD CNOMA scheme achieves superior system performance in terms of ergodic rates and system throughput. In the meanwhile, it overcomes the inherent issues of conventional CRNs. The performance of FD CNOMA is investigated comprehensively. Exact and asymptotic expressions of ergodic rates have been de-

rived under the practical assumptions of imperfect spectrum sensing and imperfect SI cancellation. Corresponding high-SNR slopes of these ergodic rates are then worked out. In short, the high-SNR slope of SU is one, but the high-SNR slope of PU is equal to the miss detection probability which is much smaller than SU due to the effects of the imperfectly canceled SI. Afterward, we obtain the system throughput based on the worked out ergodic rates. According to the simulation results, these derivation expressions have been validated and the effectiveness of spectrum sensing for better system performance has been verified. Simulation results also demonstrate that the proposed FD CNOMA scheme always outperforms HD CNOMA and COMA in terms of ergodic rates and system throughput in the real-world scenario where the residual SI has the same level with the noise floor.

In the next chapter, we focus on the relay selection problem for the above-proposed FD CNOMA scheme.

Appendix 3: Proof of Theorem 1

We assume that SU adopts the widely-used energy detection spectrum sensing algorithm, since it is efficient and simple to be implemented in hardware. Its test statistic is

$$T_{ED} = \frac{1}{K}\sum_{k=1}^{K}\left(y_{D_1}^{r}[k]\right)^2, \tag{3.46}$$

where K is the the sampling number. The binary hypothesis test model of $y_{D_1}^{r}[k]$ is given in (3.1). Neyman-Pearson hypothesis testing is adopted since a priori probabilities are unknown in real-world scenarios. Therefore, detection threshold λ^{FD} of ED is determined by the preset false alarm probability $P_f^{FD,pre}$. According to the system model introduced in Section 3.2, we learn that $\frac{x_{LI}[k]+n_{D_1}[k]}{\sqrt{N_0+\Omega_{LI}N_0\rho}} \sim \mathcal{N}(0,1)$. So $\left(\frac{x_{LI}[k]+n_{D_1}[k]}{\sqrt{N_0+\Omega_{LI}N_0\rho}}\right)^2$ is subject to a chi-square distribution with 1-degree of freedom. According to CLT, the sum of statistically independent and identically distributed random

variables $\sum_{k=1}^{K}\left(\frac{x_{LI}[k]+n_{D_1}[k]}{\sqrt{N_0+\Omega_{LI}N_0\rho}}\right)^2$ is approximately subject to a Gaussian distribution when K is large enough. Therefore, we obtain the following distribution of the test statistic under H_0.

$$T_{ED}|H_0 \sim \mathcal{N}\left(N_0+\Omega_{LI}N_0\rho, \frac{2(N_0+\Omega_{LI}N_0\rho)^2}{K}\right). \tag{3.47}$$

Based on (3.47), the false alarm probability is

$$P_f^{FD} = Q\left(\frac{\lambda^{FD}/N_0-(1+\Omega_{LI}\rho)}{\sqrt{2/K}(1+\Omega_{LI}\rho)}\right). \tag{3.48}$$

As above-illustrated, the detection threshold λ^{FD} is determined by $P_f^{FD,pre}$. According to (3.48), we have

$$\lambda^{FD} = \left(Q^{-1}\left(P_f^{FD,pre}\right)\sqrt{\frac{2}{K}}+1\right)(1+\Omega_{LI}\rho)\,N_0, \tag{3.49}$$

where $Q(\cdot)$ denotes the Marcum Q-function and $Q^{-1}(\cdot)$ refers to its inverse function.

Similarly, we obtain the following distribution of the test statistic under H_1.

$$T_{ED}|H_1 \sim \mathcal{N}\left(N_0+\Omega_{LI}N_0\rho+\rho N_0|h_2|^2, \frac{2\left(N_0+\Omega_{LI}N_0\rho+\rho N_0|h_2|^2\right)^2}{K}\right). \tag{3.50}$$

The detection probability is calculated as

$$P_d^{FD}\left(|h_2|^2\right) = Q\left(\frac{\lambda^{FD}/N_0-\left(1+\Omega_{LI}\rho+|h_2|^2\rho\right)}{\sqrt{2/K}\left(1+\Omega_{LI}\rho+|h_2|^2\rho\right)}\right). \tag{3.51}$$

After substituting (3.49) into (3.51), we obtain

$$P_d^{FD}\left(|h_2|^2\right) = Q\left(\frac{Q^{-1}\left(P_f^{FD,pre}\right)\sqrt{\frac{2}{K}}(1+\Omega_{LI}\rho)-|h_2|^2\rho}{\sqrt{2/K}\left(1+\Omega_{LI}\rho+|h_2|^2\rho\right)}\right). \tag{3.52}$$

Substituting (3.52) into $\int_0^\infty P_d^{FD}(x) f_X(x)dx$, we have

$$\begin{aligned}&\int_0^\infty P_d^{FD}(x) f_X(x)dx\\ &\quad= \int_0^\infty Q\left(\frac{Q^{-1}\left(P_f^{FD,pre}\right)\sqrt{\frac{2}{K}}(1+\Omega_{LI}\rho)-\rho x}{\sqrt{2/K}(1+\Omega_{LI}\rho+\rho x)}\right)\frac{e^{-\frac{1}{\Omega_2}x}}{\Omega_2}dx.\end{aligned} \tag{3.53}$$

Let $z = \frac{\rho x}{\Omega_{LI}\rho+1} + 1$ and then (3.53) is written as

$$\begin{aligned}&\int_0^\infty P_d^{FD}(x) f_X(x)\,dx\\ &\quad= A\int_1^\infty Q\left(-\sqrt{\frac{K}{2}}+\frac{B}{z}\right)e^{-\frac{1}{\Omega_2}\frac{\Omega_{LI}\rho+1}{\rho}z}dz,\end{aligned} \tag{3.54}$$

where $A = pe^p$, $B = \frac{Q^{-1}\left(P_f^{FD,pre}\right)\sqrt{2/K}+1}{\sqrt{2/K}}$ and $p = \frac{1}{\Omega_2}\frac{\Omega_{LI}\rho+1}{\rho}$ for simplicity. Based on the expansion formula (3.321.1) in [76], the Marcum Q-function is expanded as

$$Q\left(-\sqrt{\frac{K}{2}}+\frac{B}{z}\right) = \frac{1}{2} - \frac{1}{\sqrt{\pi}}\sum_{m=0}^{\infty}\frac{(-1)^m\left(\frac{1}{\sqrt{2}}\left(-\sqrt{\frac{K}{2}}+\frac{B}{z}\right)\right)^{2m+1}}{(m!)(2m+1)}. \tag{3.55}$$

Substituting (3.55) into (3.54), we obtain (3.58). After binomial expansion, $\Theta_{1,m}$ in (3.56) is calculated as (3.57), where $C_m^i = \frac{m!}{i!(m-i)!}$. According to the integral formula (3.351.4) in [76], $\Theta_{2,i(i>0)}$ is written as (3.58).

$$\int_0^\infty P_d^{FD}(x) f_X(x)\,dx = \frac{A}{2}\frac{\Omega_2\rho}{\Omega_{LI}\rho+1}e^{-\frac{1}{\Omega_2}\frac{\Omega_{LI}\rho+1}{\rho}} - \frac{A}{\sqrt{\pi}}\sum_{m=0}^{\infty}\frac{(-1)^m\left(\frac{1}{\sqrt{2}}\right)^{2m+1}}{(m!)(2m+1)}\underbrace{\int_1^\infty\left(-\sqrt{\frac{K}{2}}+\frac{B}{z}\right)^{2m+1}e^{-\frac{1}{\Omega_2}\frac{\Omega_{LI}\rho+1}{\rho}z}dz}_{\Theta_{1,m}} \tag{3.56}$$

$$\begin{aligned}\Theta_{1,m} &= \int_1^\infty\sum_{i=0}^{2m+1}C_{2m+1}^i\left(-\sqrt{\frac{K}{2}}\right)^{2m+1-i}\left(\frac{B}{z}\right)^i e^{-\frac{1}{\Omega_2}\frac{\Omega_{LI}\rho+1}{\rho}z}dz\\ &= \left(-\sqrt{\frac{K}{2}}\right)^{2m+1}\frac{1}{p}e^{-p} + \sum_{i=1}^{2m+1}C_{2m+1}^i\left(-\sqrt{\frac{K}{2}}\right)^{2m+1-i}B^i\underbrace{\int_1^\infty\frac{1}{z^i}e^{-\frac{1}{\Omega_2}\frac{\Omega_{LI}\rho+1}{\rho}z}dz}_{\Theta_{2,i(i>0)}}\end{aligned} \tag{3.57}$$

$$\Theta_{2,i(i>0)} = (-1)^i\frac{p^{i-1}\mathrm{Ei}(-p)}{(i-1)!} + e^{-p}\sum_{j=0}^{i-2}\frac{(-p)^j}{(i-1)(i-2)\cdots(i-j-1)}. \tag{3.58}$$

Substituting (3.58) successively into (3.57) and (3.56), we eventually work out $\int_0^\infty P_d^{FD}(x) f_X(x)dx$ as shown in (3.12). The proof is completed.

Chapter 4

Three-Stage Relay Selection Strategy With Dynamic Power Allocation

4.1 Introduction

In this chapter, we propose a three-stage relay selection strategy with dynamic power allocation, i.e., TRSPA, which is applied to the FD CNOMA scheme proposed by Chapter 3. During the first stage, each relay, i.e., SU, senses the spectrum band to determine whether PU exists or not and then relays with positive sensing results further decode PU's signal. The second stage aims to further ensure the PU's successful transmissions from remaining relay candidates to the BS. In the third stage, the best relay is selected from remaining candidates and meanwhile, power allocation coefficients are dynamically determined according to instantaneous channel state information to realize the following optimization purpose of TRSPA. That is to find out the best relay to maximize the ergodic rate of that selected relay on the condition of guaranteeing successful transmissions of the PU's signal. It is noted that relevant proofs are presented to illustrate these power allocation coefficients are indeed the optimal results. Moreover, to evaluate the performance of TRSPA, we present the performance evaluation results of this proposed strategy in terms of outage probability and ergodic rate. Accordingly,

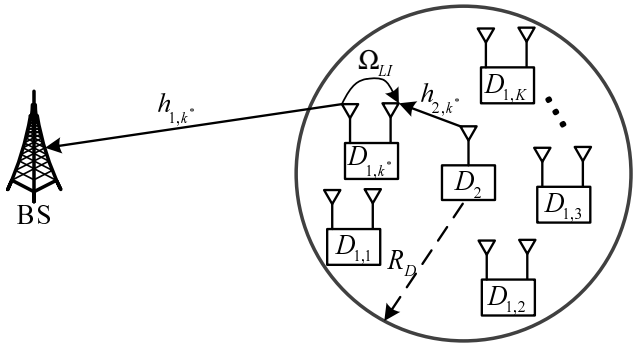

Figure 4.1: System model.

diversity orders and spatial multiplexing gains are derived. We further exploit the impact of SI on TRSPA for FD CNOMA and then compare its performance with TRSPA applied in other relaying modes, namely HD and OMA. Finally, numerical simulation results are provided to validate theoretical derivation results and to illustrate the superior performance of the proposed relay selection strategy compared to other relay selection strategies and other relaying modes.

4.2 Network Model

4.2.1 Network Description

We consider a FD relaying CNOMA scenario consisting of one BS, K FD user relays ($D_{1,k}$ with $1 \leq k \leq K$) and one user (D_2), in the uplink communication system as shown in Fig. 4.1. $\mathcal{S}$ denotes the set of relays in the network. The relays are equipped with two antennas, one for reception and one for transmission, while all other nodes are equipped with a single antenna. Like [80] and [106], this chapter assumes there does not exist any direct link between the BS and the weak user D_2 because of D_2's limited transmission capability [82] and the severe shadowing effects caused by physical obstacles. In such case, D_2 cannot upload signals to the BS all by itself, which is the main reason why it requires the assistance of a selected relay D_{1,k^*} ($D_{1,k^*} \in \mathcal{S}$) by our proposed relay selection strategy TRSPA in Section 4.2.3.1.

User relays that are not selected will send their respective messages to the BS using resource blocks other than the one occupied by D_2 and D_{1,k^*}, which is the same with a traditional OMA scheme. Therefore, we only focus on the performance of D_2 and D_{1,k^*} in this chapter. We assume that D_2 is located at the origin of a disc with a radius of R_D. K relays are uniformly distributed in that disc. Wireless links are assumed to follow independent non-selective block Rayleigh fading [107–112] and are corrupted by additive white Gaussian noise with a power value of N_0. $h_{1,k} = \frac{h}{\sqrt{1+d_{1,k}^{\alpha}}}$ and $h_{2,k} = \frac{h'}{\sqrt{1+r_{2,k}^{\alpha}}}$ [54], respectively, represent the channel coefficients of $D_{1,k} \rightarrow$ BS and $D_2 \rightarrow D_{1,k}$ links, where $d_{1,k}$ is the distance between $D_{1,k}$ and the BS, and $r_{2,k}$ is the distance between D_2 and $D_{1,k}$. h and h' are independent Rayleigh fading channel gains and α represents the path loss exponent. We assume that $d_{1,k} \gg r_{2,k}$ [54]. Moreover, $d_{1,k} = \sqrt{d_{D_2,BS}^2 + r_{2,k}^2 - 2d_{D_2,BS} r_{2,k} \cos(\theta_k)}$, where $d_{D_2,BS}$ is the distance between D_2 and the BS and θ_k denotes the angle $\angle D_{1,k} D_2$ BS. For the sake of practicality, we assume that residual loop self-interference (LI) exists at $D_{1,k}$. The LI signal is assumed to be additive Gaussian signal with zero mean [113] [114]. The assumption of a Gaussian distribution might hold in reality because of the various sources of imperfections in the cancellation process based on the central limit theorem. Moreover, the variance of this Gaussian LI signal is $\Omega_{LI} P_r$ based on [115] and [116], where P_r is the normalized transmit power of each relay and Ω_{LI} is its LI cancellation coefficient. $x_{1,k}$ and x_2 are messages transmitted by $D_{1,k}$ and D_2. In this chapter, we consider the case that $x_{1,k}$ and x_2 form a NOMA group, as the two-user NOMA case is reasonably followed in [54] [49] [79–81] and [106]. Such case is also investigated in the Third Generation Partnership Project. In fact, the subsequent analysis can be extended for a multiple-user scenario by clustering.

To prepare for the proposal of TRSPA, we take an arbitrary user relay $D_{1,k}$ as an example to describe how a user relay assists D_2 in the FD CNOMA scheme proposed in Chapter 3. D_2 appears and disappears randomly. $D_{1,k}$ detects the received signal and determines whether D_2 exists or not. If $D_{1,k}$'s detection result shows the existence

of D_2, $D_{1,k}$ will then try to decode x_2. After $D_{1,k}$ has successfully obtained x_2, $D_{1,k}$ transmits a superimposed NOMA signal consisting of x_2 and $x_{1,k}$ to the BS. Based on SIC [117], the BS will successively decode messages of D_2 and $D_{1,k}$. Otherwise, if the detection result claims D_2 does not exist, $D_{1,k}$ will directly transmit its own message using full power. BS then directly decodes $x_{1,k}$.

4.2.2 Signal Model

The signal received by $D_{1,k}$ is $y^r_{D_{1,k}}[l] = \begin{cases} \sqrt{P_s}h_{2,k}x_2[l] + \varpi_1 x_{LI,k}[l] + n_{D_{1,k}}[l], & H_1 \\ \varpi_1 x_{LI,k}[l] + n_{D_{1,k}}[l], & H_0 \end{cases}$, where $x_{LI,k}$ denotes the LI signal at $D_{1,k}$ and $n_{D_{1,k}}$ is the noise signal, during the l-th time slot. P_s is the normalized transmit power of D_2. In the following analysis, we assume that $P_r = P_s$[1] [79–81, 106]. H_1 and H_0 refer to the hypotheses that D_2 exists or not, respectively. ϖ_1 is an indicator variable, where $\varpi_1 = 1$ denotes the relay working in FD mode. For comparison, we will also study HD and OMA modes where $\varpi_1 = 0$.

Recalling the FD CNOMA scheme illustrated in Section 4.2.1, if $D_{1,k}$ claims the existence of D_2, $D_{1,k}$ will decode x_2 from its received signal with the signal-to-interference-plus-noise ratio (SINR) of

$$\gamma_{D_2 \to D_{1,k}} = \frac{|h_{2,k}|^2 \rho}{\varpi_1 \Omega_{LI} \rho + 1} \tag{4.1}$$

where $\frac{P_r}{N_0} = \frac{P_s}{N_0} \triangleq \rho$ is the transmit SNR. We first consider the case that $D_{1,k}$ correctly decodes D_2. $D_{1,k}$ transmits the superimposed NOMA signal $y^t_{D_{1,k}}[l] = \sqrt{P_r a_{1,k}}x_{1,k}[l] + \sqrt{P_r a_{2,k}}x_2[l-\tau]$, where τ represents the processing delay at $D_{1,k}$ with an integer $\tau \geq 1$. $a_{1,k}$ and $a_{2,k}$ are power allocation coefficients for $x_{1,k}$ and x_2, respectively, where $a_{1,k} + a_{2,k} = 1$. The received signal at the BS is $y^r_{BS}[l] = h_{1,k}y^t_{D_{1,k}}[l] + n_{BS}[l]$, where n_{BS} denotes the noise signal at the BS. Similar to [54] [47] and [49], D_2 and $D_{1,k}$ are sorted based on their QoS priority during SIC. D_2 should access the spectrum band with a high priority, as discussed in Chapter 1. Therefore, during SIC, the BS first decodes x_2

[1] This is assumed to simplify the derivation process. A similar technique can be applied when $P_r \neq P_s$.

with the SINR value of

$$\gamma_{D_2 \to D_{1,k} \to BS} = \frac{a_{2,k}\left|h_{1,k}\right|^2 \rho}{a_{1,k}\left|h_{1,k}\right|^2 \rho + 1}. \tag{4.2}$$

After decoding x_2 and subtracting it from y_{BS}^r, the BS will decode $x_{1,k}$ with a SNR value of

$$\gamma_{D_{1,k} \to BS} = a_{1,k}\left|h_{1,k}\right|^2 \rho. \tag{4.3}$$

We then consider the case that $D_{1,k}$ fails to detect and obtain x_2. It will directly send its own message to the BS with full power so that the power resource is sufficiently utilized. Under such condition, the received SNR value at the BS when it decodes $x_{1,k}$ is given by

$$\hat{\gamma}_{D_{1,k} \to BS} = \left|h_{1,k}\right|^2 \rho. \tag{4.4}$$

4.2.3 Relay Selection Strategy

In this subsection, both our proposed TRSPA strategy and other relay selection benchmarks with various relaying modes are presented to prepare for subsequent comparison.

4.2.3.1 Three-Stage Relay Selection with Power Allocation (TRSPA)

In the first stage, all relays sense the spectrum band to determine whether D_2 exists or not and then relays with positive sensing results further decode x_2. Therefore, the following subset $\mathcal{S}_1$ ($\mathcal{S}_1 \subseteq \mathcal{S}$) is built.

$$\begin{aligned} \mathcal{S}_1 = \{ & D_{1,k} : \ 1 \le k \le K, \\ & T_{ED,k} \ge \lambda, \ \log\left(1 + \gamma_{D_2 \to D_{1,k}}\right) \ge R_2 \} \end{aligned} \tag{4.5}$$

where R_2 is the target data rate of x_2; $T_{ED,k} = \frac{1}{L}\sum_{l=1}^{L}\left(y_{D_{1,k}}^r[l]\right)^2$ represents the test statistic of energy detection (ED) by $D_{1,k}$; L represents the sampling number; λ is the detection threshold of ED, which is determined by the preset false alarm probability

P_f^{pre}. As stated in Chapter 3, FD CNOMA adopts the widely used ED, since it is efficient and simple to be implemented in hardware.

In the second stage, we intend to find out all relays within $\mathcal{S}_1$ which are able to successfully forward x_2 to the BS. If the BS fails to decode x_2 even when $a_{1,k} = 0$, then the corresponding $D_{1,k}$ will by no means succeed. Therefore, we substitute $a_{1,k} = 0$ into (4.2) and get the maximum value of $\gamma_{D_2 \to D_{1,k} \to BS}$, i.e., $\gamma_{D_2 \to D_{1,k} \to BS,MAX} = \left|h_{1,k}\right|^2 \rho$. As long as $\log\left(1 + \left|h_{1,k}\right|^2 \rho\right) \geq R_2$, $D_{1,k}$ is likely to realize the successful transmission of x_2. In conclusion, the second stage is to build the following subset $\mathcal{S}_2$ ($\mathcal{S}_2 \subseteq \mathcal{S}_1$) to enable the BS to decode x_2 correctly.

$$\mathcal{S}_2 = \left\{ D_{1,k} : \ D_{1,k} \in \mathcal{S}_1, \ \log\left(1 + \left|h_{1,k}\right|^2 \rho\right) \geq R_2 \right\}. \tag{4.6}$$

For the third stage, we select the relay D_{1,k^*} by (4.7).

$$k^* = \underset{k \in \{1,2,\cdots,K\}}{\arg} \max \left|h_{1,k}\right|^2 \quad \text{s.t.} \quad D_{1,k} \in \mathcal{S}_2. \tag{4.7}$$

According to [49], the relay with maximum $\left|h_{1,k}\right|^2$ can be found out by a virtual timer. Each relay $D_{1,k}$ ($D_{1,k} \in \mathcal{S}_2$) starts a virtual timer initiated by $t_n = t_0 \exp\left(-\left|h_{1,k}\right|^2\right)$, where t_0 is a constant. The timer of $D_{1,k}$ with the best channel condition to the BS (i.e., the selected relay D_{1,k^*}) will expire first. Then D_{1,k^*} broadcasts a flag message signaling its presence and other relays back off. Moreover, the optimal power allocation coefficient is dynamically worked out based on CSI as shown in (4.8).

$$a_{1,k} = \frac{\left|h_{1,k}\right|^2 \rho - T_2}{\left|h_{1,k}\right|^2 \rho (1 + T_2)} \tag{4.8}$$

where $T_2 = 2^{R_2} - 1$ is the target SNR when decoding x_2. The purpose of our proposed relay selection strategy TRSPA is to find out the best user relay in order to maximize the ergodic rate of that selected relay on the condition of guaranteeing successful trans-

missions of D_2's signal, which means x_2 is successfully decoded by the BS. Here we claim that the power allocation coefficient given by (4.8) is optimal and relevant proofs will be presented in Theorem 2 and Theorem 3 by illustrating (4.8) indeed enables TRSPA to achieve that goal.

It is noted that if $|\mathcal{S}_1| = 0$ or $|\mathcal{S}_2| = 0$, where $|\mathcal{S}_1|$ and $|\mathcal{S}_2|$ refer to the sizes of $\mathcal{S}_1$ and $\mathcal{S}_2$, respectively, it is impossible for any relay to realize the successful transmission of x_2. Similar to the case of (4.4), relays will then directly transmit their own messages with full power. In order to achieve the largest data transmission rate, the selected relay is given by

$$\begin{aligned} k^* &= \underset{k\in\{12\cdots K\}}{\arg\max}\, \hat{\gamma}_{D_{1,k}\to BS} \text{ s.t. } D_{1,k} \in \mathcal{S} \\ &= \underset{k\in\{12\cdots K\}}{\arg\max}\, \left|h_{1,k}\right|^2 \text{ s.t. } D_{1,k} \in \mathcal{S}. \end{aligned} \tag{4.9}$$

Combining the above descriptions, the implementation procedure of our proposed TRSPA strategy in a practical system can be illustrated as Table 4.1. Accordingly, only CSI between the BS and relay nodes is required while CSI between relays and D_2 is not needed. Another conclusion is that the proposed TRSPA strategy is distributed.

Theorem 2. *For a FD CNOMA scheme, the power allocation coefficient given by* (4.8) *enables the proposed TRSPA strategy to minimize the outage probability of* D_2.

Proof. As above-stated, the premise is to ensure successful transmissions of D_2's signal. Therefore, in this proof, we aim to illustrate that with the power allocation coefficient given by (4.8), our proposed TRSPA scheme achieves the optimal outage performance, i.e., the smallest outage probability of D_2, among all possible relay selection results with any possible power allocation coefficient. In order to illustrate the superiority of our proposed TRSPA scheme and the power allocation method (4.8), we assume that the system may adopt any other relay selection strategy with any other power allocation coefficient and consider it as the control group. By proving that the outage performance of our proposed method is better than an arbitrary control group, the superiority of our method could be validated.

Table 4.1: Implementation of Three-Stage Relay Selection Strategy With Dynamic Power Allocation

Step	Implementation
1	According to practical service requirements, D_2 randomly appears and disappears. No one knows beforehand for sure the spectrum resource occupation situation. Each relay executes spectrum sensing to figure out whether D_2 is transmitting signals to the BS or not at the present. As to an arbitrary relay, if its sensing results claims the existence of D_2, it will then try to decode and finally obtain the signal x_2. In other words, we need to build the set $\mathcal{S}_1$ ($\mathcal{S}_1 \subseteq \mathcal{S}$) based on (4.5).
2	The BS broadcasts a training signal to relay nodes. Based on the training symbol, each relay node estimates $h_{1,l}$.
3	Each relay determines whether it belongs to the set $\mathcal{S}_1$ or not. If it does, this relay needs to further determine whether it belongs to $\mathcal{S}_2$, based on (4.6), so that the set $\mathcal{S}_2$ is built.
4	Each relay broadcasts a flag message 'Success' or Failure' to other relays, according to whether it belongs to $\mathcal{S}_2$ or not.
5	According to the broadcasted messages, if the set $\mathcal{S}_2$ is not empty, the virtual timer process of each relay within this set will be started by setting $t_l = t_0 \exp\left(-\left\|h_{1,l}\right\|^2\right)$, where t_0 is a constant. According to (4.7), the initial value of relay D_{1,l^*}'s timer is the smallest and thus it will expire first. Other relays in $\mathcal{S}_2$ will back off. Power allocation coefficients adopted by this relay are given by (4.8). D_{1,l^*} broadcasts a flag message 'Optimal relay' signaling its presence. As soon as receiving this flag message, other relays will stop their virtual timers. The relay selection process is now completed. On the other hand, if the set $\mathcal{S}_2$ is empty according to the broadcasted messages, D_2's signal transmission will be interrupted. In such case, in order to sufficiently utilize system resources, the optimal relay selection strategy is to find out the relay within the set $\mathcal{S}$, which has the best channel condition to the BS, as shown in (4.9). To be specific, each relay within $\mathcal{S}$ starts a virtual timer initiated by $t_l = t_0 \exp\left(-\left\|h_{1,l}\right\|^2\right)$. The initial value of the relay in $\mathcal{S}$, which has the largest $\left\|h_{1,l}\right\|^2$, is the smallest and thus it will expire first. At this moment, this relay needs to broadcast a flag message 'Optimal relay' signaling its presence. As soon as receiving this flag message, other relays will back off and stop their virtual timers. The relay selection process is now completed.

To be specific, the control group is set as follows. An arbitrary relay $D_{1,\tilde{k}}$ with a channel coefficient of $h_{1,\tilde{k}}$ between itself and the BS is chosen by any other RS strategy with power coefficients $a_{1,\tilde{k}}$ and $a_{2,\tilde{k}}$. If x_2 is successfully decoded by the BS with the

assistance of $D_{1,\tilde{k}}$, then $\frac{a_{2,\tilde{k}}|h_{1,\tilde{k}}|^2\rho}{a_{1,\tilde{k}}|h_{1,\tilde{k}}|^2\rho+1} \geq T_2$ must be true based on (4.2). We also learn that $|\mathcal{S}_1| \neq 0$, since at least $D_{1,\tilde{k}}$ obtains x_2. Moreover, based on $\frac{a_{2,\tilde{k}}|h_{1,\tilde{k}}|^2\rho}{a_{1,\tilde{k}}|h_{1,\tilde{k}}|^2\rho+1} \geq T_2$, we have $0 \leq a_{1,\tilde{k}}\left|h_{1,\tilde{k}}\right|^2\rho \leq \frac{|h_{1,\tilde{k}}|^2\rho-T_2}{1+T_2}$, which means $T_2 \leq \left|h_{1,\tilde{k}}\right|^2\rho$. Thus, $D_{1,\tilde{k}} \in \mathcal{S}_2$ according to (4.6) and we get $|\mathcal{S}_2| \neq 0$. Since $|\mathcal{S}_1| \neq 0$ and $|\mathcal{S}_2| \neq 0$, the selected relay by TRSPA is $k^* = \underset{k\in\{1,2,\cdots,K\}}{\arg\max}\left|h_{1,k}\right|^2$ s.t. $D_{1,k} \in \mathcal{S}_2$ and the corresponding power coefficient is $a_{1,k^*} = \frac{|h_{1,k^*}|^2\rho-T_2}{|h_{1,k^*}|^2\rho(1+T_2)}$ based on (4.7) and (4.8). In such case, $\gamma_{D_2\to D_{1,k}\to BS} = \frac{a_{2,k^*}|h_{1,k^*}|^2\rho}{a_{1,k^*}|h_{1,k^*}|^2\rho+1} = T_2$, which means x_2 can also be correctly decoded by the BS with the assistance of the selected D_{1,k^*} by our proposed TRSPA strategy. In conclusion, as long as there exists any RS strategy with any power allocation coefficient, which realizes successful decoding, our proposed TRSPA will be capable of doing so as well. Therefore, our proposed power allocation method (4.8) enables TRSPA to realize the smallest outage probability among all possible relay selection strategies with any possible power allocation coefficient. In other words, from the perspective of outage performance for D_2, the power allocation coefficient (4.8) is proved to be optimal, which completes the proof. □

Theorem 3. *The power allocation coefficient given by* (4.8) *enables the proposed TRSPA to achieve the largest ergodic rate for the selected user relay when x_2 is successfully decoded by the BS.*

Proof. As above-stated, our purpose is to find out the best user relay to maximize its ergodic rate on the condition of guaranteeing successful transmissions of D_2's signal. Therefore, in this proof, we aim to illustrate that with the power allocation coefficient given by (4.8), our proposed TRSPA scheme achieves the largest ergodic rate for the selected user relay when x_2 is successfully decoded by the BS.

We continue with the proof of Theorem 2. When x_2 is successfully decoded by the BS, we have $\frac{a_{2,\tilde{k}}|h_{1,\tilde{k}}|^2\rho}{a_{1,\tilde{k}}|h_{1,\tilde{k}}|^2\rho+1} \geq T_2$. Therefore, $a_{1,\tilde{k}}\left|h_{1,\tilde{k}}\right|^2\rho \leq \frac{|h_{1,\tilde{k}}|^2\rho-T_2}{1+T_2} \leq \frac{|h_{1,k}|^2_{MAX}\rho-T_2}{1+T_2}$, where $\left|h_{1,k}\right|^2_{MAX}$ represents the largest channel power gain among all relays within

$\mathcal{S}_2$ ($|\mathcal{S}_2| \neq 0$ based on Theorem 2). According to (4.7) and (4.8), the selected relay by our proposed TRSPA strategy satisfies $a_{1,k^*}\left|h_{1,k^*}\right|^2\rho = \frac{\left|h_{1,k}\right|^2_{MAX}\rho - T_2}{1+T_2}$. Therefore, $\log\left(1 + a_{1,\tilde{k}}\left|h_{1,\tilde{k}}\right|^2\rho\right) \leq \log\left(1 + a_{1,k^*}\left|h_{1,k^*}\right|^2\rho\right)$, i.e., $\gamma_{D_{1,\tilde{k}}\to BS} \leq \gamma_{D_{1,k^*}\to BS}$. That is to say our proposed power allocation method (4.8) enables TRSPA to realize the largest ergodic rate of the selected relay among all possible relay selection strategies with any possible power allocation coefficient. In other words, from the perspective of ergodic rate for the selected user relay, the power allocation coefficient (4.8) is proved to be optimal, which completes the proof. □

In conclusion, the proposed power allocation coefficient (4.8) is proved to achieve the optimal outage performance, on which basis, the largest ergodic rate, among all possible methods. Considering the above-mentioned purpose of our relay selection strategy, (4.8) indeed enables the proposed TRSPA to maximize the ergodic rate of the selected relay on the condition of guaranteeing successful transmissions of D_2's signal. Therefore, the power allocation coefficient given by (4.8) is proved to be optimal.

However, superior performance may come along with the increase of implementation cost, since TRSPA requires all relay nodes to sense the existence of D_2. It needs to be first pointed out that the widely used energy detection is employed, because it is simple and easy to be implemented in hardware with low computation complexity. Additionally, spectrum sensing brings the following benefits. First, relays perform spectrum sensing to identify idle spectrum resources so that they may obtain the additional opportunity to access the licensed spectrum band of D_2. Second, relay candidate set is narrowed after spectrum sensing so that the calculation complexity is decreased. Third, CSI from D_2 to relays is no longer necessary for TRSPA. Corresponding training signals and control channels are not necessary, either. To sum up, the low-complexity energy detection to sense the existence of D_2 indeed leads to implementation cost to a certain extent. Nevertheless, it also brings obvious advantages in the sufficient utilization of wireless resources. On one side is the progressive data processing and operating

speed, but on the other side is the limited and scarce communication resources. Therefore, we believe that the implementation cost of energy detection is acceptable.

So far, we have explained our proposed TRSPA relay selection strategy. Next, other relay selection benchmarks with various relaying modes will be presented to prepare for subsequent comparison.

4.2.3.2 Max-Min Relay Selection

Based on [118], Max-Min relay selection strategy chooses the relay

$$k^*_{Max-Min} = \arg\max_k \left\{ \min \left[\left|h_{1,k}\right|^2, \left|h_{2,k}\right|^2 \right] : \ D_{1,k} \in \mathcal{S} \right\}.$$

4.2.3.3 Single-Stage Relay Selection (SRS)

Based on [54], SRS strategy chooses the relay

$$k^*_{SRS} = \arg\max_k \left\{ \min \left[\log\left(1 + \frac{\left|h_{2,k}\right|^2 \rho}{\varpi_1 \Omega_{LI} \rho + 1}\right), \log\left(1 + \frac{a^{SRS}_{2,k} \left|h_{1,k}\right|^2 \rho}{a^{SRS}_{1,k} \left|h_{1,k}\right|^2 \rho + 1}\right) \right] \right\},$$

where $a^{SRS}_{1,k}$ and $a^{SRS}_{2,k}$ are the predefined power coefficients for the user relay and the weak user.

4.2.3.4 Two-Stage Relay Selection (TRS)

According to the reference [47], TRS first builds a subset

$$\mathcal{S}_{TRS} = \left\{ D_{1,k} : \ 1 \le k \le K, \ \log\left(1 + \frac{\left|h_{2,k}\right|^2 \rho}{\varpi_1 \Omega_{LI} \rho + 1}\right) \ge R_2, \ \log\left(1 + \frac{a^{TRS}_{2,k} \left|h_{1,k}\right|^2 \rho}{a^{TRS}_{1,k} \left|h_{1,k}\right|^2 \rho + 1}\right) \ge R_2 \right\},$$

where $a^{TRS}_{1,k}$ and $a^{TRS}_{2,k}$ are the predefined power coefficients. For comparison fairness, we assume that relays in a TRS strategy also have the capability of spectrum sensing. Then the second stage is to select a relay $D_{1,k^*_{TRS}}$ within $\mathcal{S}_{TRS}$ where $k^*_{TRS} =$

$$\arg\max_{k} \left\{ \log\left(1 + a_{1,k}^{TRS} \left|h_{1,k}\right|^2 \rho\right) : \ D_{1,k} \in \mathcal{S}_{TRS} \right\}.$$

4.2.3.5 HD CNOMA

The critical difference between the HD counterpart (i.e., HD CNOMA) and FD CNOMA is whether user relays work in HD or FD relaying modes.

4.2.3.6 COMA

Inspired by [79], the COMA counterpart is improved as follows for comparison fairness. In the first slot, the user relay determines whether D_2 exists or not by spectrum sensing. If the detection result claims the existence of D_2, the relay will decode x_2 and then successively transmit $x_{1,k}$ and x_2 in the next two slots. Otherwise, it will only transmit $x_{1,k}$ in the next two slots.

4.3 Performance Analysis

4.3.1 Outage Probability

4.3.1.1 Outage Probability and Diversity Analysis of D_2 under H_1

Denote φ_1 as the event that all relays fail to detect and decode x_2 correctively. If there exist some relays (e.g. j relays, $1 \leq j \leq K$) successfully obtaining x_2, we denote φ_2 as the event that none of them are capable of forwarding x_2 to the BS. The outage event of x_2 is then expressed as $\varphi = \varphi_1 \cup \varphi_2$, and thus the outage probability of D_2 for TRSPA

in a FD CNOMA scheme (i.e., TRSPA-FD) is

$$\begin{aligned} P_{D_2}^{TRSPA-FD} &= \Pr(\varphi_1) + \Pr(\varphi_2) = \Pr(|\mathcal{S}_1| = 0) \\ &+ \sum_{j=1}^{K} \Pr(|\mathcal{S}_2| = 0 | |\mathcal{S}_1| = j) = \left(1 - P_{sd}^{FD}\right)^K \\ &+ \sum_{j=1}^{K} C_K^j \left(P_{sd}^{FD}\right)^j \left(1 - P_{sd}^{FD}\right)^{K-j} \left(1 - J_d^{FD}\right)^j \\ &= \left(\left(1 - P_{sd}^{FD}\right) + P_{sd}^{FD}\left(1 - J_d^{FD}\right)\right)^K \end{aligned} \tag{4.10}$$

where P_{sd}^{FD} is the probability for an arbitrary relay to successfully detect and decode x_2; J_d^{FD} represents the probability for the BS to correctly decode x_2 forwarded by an arbitrary relay; and $C_K^j = \frac{K!}{j!(K-j)!}$. P_{sd}^{FD} and J_d^{FD} are formulated as

$$\begin{aligned} P_{sd}^{FD} &= \int_0^{\infty} P_d^{FD}(x) \Pr\left(\gamma_{D_2 \to D_{1,k}} > T_2\right) f_X(x)\, dx \\ &= \int_{\frac{\varpi_1 \Omega_{LI} \rho + 1}{\rho} T_2}^{\infty} P_d^{FD}(x) f_X(x)\, dx \end{aligned} \tag{4.11}$$

$$\begin{aligned} J_d^{FD} &= \Pr\left(\gamma_{D_2 \to D_{1,k} \to BS, MAX} > T_2\right) \\ &= \Pr\left(\left|h_{1,k}\right|^2 \rho > T_2\right) \approx e^{-\left(1 + d_{D_2,BS}^{\alpha}\right)\frac{T_2}{\rho}} \end{aligned} \tag{4.12}$$

where $P_d^{FD}(x)$ is the detection probability of ED by $D_{1,k}$ to detect x_2. It is a function associated with $\left|h_{2,k}\right|^2$, which is denoted as x. $f_X(x)$ is the probability density function (PDF) of x.

Theorem 4. *P_{sd}^{FD} can be worked out as*

$$\begin{aligned} P_{sd}^{FD} &= \frac{\pi}{4N} \sum_{n=1}^{N} \left(\sqrt{1 - \phi_n^2}\,(\phi_n + 1)\, e^{-p_n T_2} \right) - \frac{\sqrt{\pi}}{2N} \frac{p_n}{c_n} \\ &\times \sum_{\psi=0}^{\infty} \sum_{n=1}^{N} \frac{(-1)^{\psi} \left(\frac{1}{\sqrt{2}}\right)^{2\psi+1}}{(\psi!)(2\psi+1)} \sqrt{1 - \phi_n^2}\,(\phi_n + 1)\, c_n e^{p_n} \Theta_{n,\psi} \end{aligned} \tag{4.13}$$

$$\begin{aligned} &\Theta_{n,\psi} \\ &= \left(-\sqrt{\frac{L}{2}}\right)^{2\psi+1} \frac{e^{-p_n(T_2+1)}}{p_n} + \sum_{\xi=1}^{2\psi+1} C_{2\psi+1}^{\xi} \left(-\sqrt{\frac{L}{2}}\right)^{2\psi+1-\xi} \\ &\times B^{\xi} \left(\frac{(-1)^{\xi} p_n^{\xi-1} \mathrm{Ei}(-p_n u)}{(\xi-1)!} + \frac{e^{-p_n u}}{u^{\xi-1}} \sum_{\omega=0}^{\xi-2} \frac{(-1)^{\omega} p_n^{\omega} u^{\omega}}{(\xi-1)(\xi-2)\cdots(\xi-\omega-1)} \right) \end{aligned} \tag{4.14}$$

where $B = \frac{Q^{-1}\left(P_f^{pre}\right)\sqrt{2/L}+1}{\sqrt{2/L}}$, $u = T_2 + 1$, $p_n = c_n \frac{\varpi_1 \Omega_{LI}\rho+1}{\rho}$, $c_n = 1 + \left(\frac{R_D}{2}(\phi_n + 1)\right)^{\alpha}$ *and* $\phi_n = \cos\left(\frac{2n-1}{2N}\pi\right)$. $\mathrm{Ei}(\cdot)$ *is the exponential integral function.*

Proof. See Appendix 4. □

Substituting J_d^{FD} and P_{sd}^{FD} obtained from (4.12), (4.13) and (4.14) into (4.10), we get the outage probability $P_{D_2}^{TRS\,PA-FD}$.

Corollary 7. *On the basis of the derivation result* (4.10) *for TRSPA-FD, we make the following changes to obtain the outage probabilities* $P_{D_2}^{TRS\,PA-HD}$ *and* $P_{D_2}^{TRS\,PA-OMA}$ *of* D_2 *for TRSPA-HD and TRSPA-OMA, which respectively refer to TRSPA working in HD CNOMA and COMA schemes: i) substitute* $\varpi_1 = 0$ *into* (4.10) *since HD CNOMA and COMA are not affected by LI; and ii) change* T_2 *into* $\phi_{HD,2} = 2^{2R_2} - 1$ *and* $\phi_{OMA,2} = 2^{3R_2} - 1$ *which are the target SNRs during decoding* x_2 *in HD CNOMA and COMA schemes, respectively, since each of their entire transmission processes finish in two or three time slots based on Section 4.2.3.*

We further analyze the diversity order for D_2 which is defined as

$$d_{D_2}^{TRS\,PA-FD} = -\lim_{\rho\to\infty} \frac{\lg\left(P_{D_2}^{TRS\,PA-FD}\right)}{\lg\rho}. \tag{4.15}$$

When $\rho \to \infty$, we get $\lim_{\rho\to\infty} J_d^{FD} \triangleq J_d^{FD,\infty} \approx 1$ based on (4.12) and $e^{-\frac{1}{\rho}} \approx 1 - \frac{1}{\rho}$. With $\lim_{\rho\to\infty} \frac{\varpi_1\Omega_{LI}\rho+1}{\rho} = \varpi_1\Omega_{LI}$, we obtain the asymptotic value of P_{sd}^{FD}, i.e., $\lim_{\rho\to\infty} P_{sd}^{FD} = P_{sd}^{FD,\infty} \triangleq P_{SD}^{FD}$. Given (4.10), the asymptotic outage probability of D_2 for TRSPA-FD is

$$\lim_{\rho\to\infty} P_{D_2}^{TRS\,PA-FD} \triangleq P_{D_2}^{TRS\,PA-FD,\infty} = \left(1 - P_{SD}^{FD}\right)^K. \tag{4.16}$$

Substituting (4.16) into (4.15), we learn that D_2's diversity order equals zero, i.e., $d_{D_2}^{TRS\,PA-FD} = 0$.

Remark 4. *The diversity order of TRSPA-FD is zero due to the effect of residual LI. Therefore, a floor exists for* D_2*'s outage probability.*

As to TRSPA-HD, according to (4.11), its successful detecting and decoding probability P_{sd}^{HD} when $\rho \to \infty$ is approximated as $P_{sd}^{HD,\infty} = \lim_{\rho\to\infty} \int_{\frac{\phi_{HD,2}}{\rho}}^{\infty} P_d^{HD}(x) f_X(x)\, dx$, where $P_d^{HD}(x)$ is the detection probability of an arbitrary relay in a TRSPA-HD system. $\lim_{\rho\to\infty} P_d^{HD}(x) = Q\left(\frac{Q^{-1}\left(P_f^{pre}\right)\sqrt{2/L}-\rho x}{\sqrt{2/L}(1+\rho x)}\right) = Q\left(-\sqrt{\frac{L}{2}}\right)$ according to (4.40). Therefore, $P_{sd}^{HD,\infty}$ is further written as $P_{sd}^{HD,\infty} = \lim_{\rho\to\infty} \int_{\frac{\phi_{HD,2}}{\rho}}^{\infty} f_X(x)dx = 1 - \lim_{\rho\to\infty} F_X\left(\frac{\phi_{HD,2}}{\rho}\right)$. According to (4.41), $\lim_{\rho\to\infty} F_X\left(\frac{\phi_{HD,2}}{\rho}\right)$ is approximated as $\lim_{\rho\to\infty} \frac{\phi_{HD,2}}{\rho} \int_0^{R_D} \left(1 + r_{2,k}^{\alpha}\right)\frac{2r_{2,k}}{R_D^2} dr_{2,k}$. Let $R = \int_0^{R_D} \left(1 + r_{2,k}^{\alpha}\right)\frac{2r_{2,k}}{R_D^2} dr_{2,k} = 1 + \frac{2}{\alpha+2} R_D^{\alpha}$ and we get $\lim_{\rho\to\infty} F_X\left(\frac{\phi_{HD,2}}{\rho}\right) \approx \lim_{\rho\to\infty} R\frac{\phi_{HD,2}}{\rho}$. Then $P_{sd}^{HD,\infty} = 1 - \lim_{\rho\to\infty} F_X\left(\frac{\phi_{HD,2}}{\rho}\right) \approx 1 - \lim_{\rho\to\infty} R\frac{\phi_{HD,2}}{\rho}$. Based on (4.10), the asymptotic outage probability of D_2 for TRSPA-HD when $\rho \to \infty$ is

$$P_{D_2}^{TRSPA-HD,\infty} = \left(\left(1 + d_{D_2,BS}^{\alpha}\right)\phi_{HD,2} + R\phi_{HD,2}\right)^K \left(\frac{1}{\rho}\right)^K. \tag{4.17}$$

Substituting (4.17) into (4.15), we get $d_{D_2}^{TRSPA-HD} = K$.

Similarly, we also work out the asymptotic outage probability of D_2 for TRSPA-OMA:

$$\begin{aligned} &P_{D_2}^{TRSPA-OMA,\infty} \\ &= \left(\left(1 + d_{D_2,BS}^{\alpha}\right)\phi_{OMA,2} + R\phi_{OMA,2}\right)^K \left(\frac{1}{\rho}\right)^K. \end{aligned} \tag{4.18}$$

Substituting (4.18) into (4.15), we learn that the diversity order for TRSPA-OMA equals K.

Remark 5. *Diversity orders of TRSPA for HD CNOMA and COMA schemes both equal* K.

4.3.1.2 Outage Probability and Diversity Analysis of D_2 under H_0

D_2 does not exist herein.

4.3.2 Ergodic Rate

4.3.2.1 Ergodic Rate and Spatial Multiplexing Gain of D_{1,k^*} under H_1

The CDF $F_Y(y)$ of the received SNR (i.e., Y) at the BS when decoding x_{1,k^*} is a critical parameter when deriving D_{1,k^*}'s ergodic rate. We next work out $F_Y(y)$ in three independent cases.

The first case $E_{1,j}$ refers to $|\mathcal{S}_1| = j \neq 0$ and $|\mathcal{S}_2| = 0$, which means none of the j relays within $\mathcal{S}_1$ could enable the BS to successfully decode x_2 even if they allocate all power to x_2. $k^* = \arg\max_k \left\{ \left|h_{1,k}\right|^2 : D_{1,k} \in \mathcal{S} \right\}$ according to Section 4.2.3.1. Then the received SINR at the BS to decode x_{1,k^*} is $\hat{\gamma}_{D_{1,k^*}\to BS} \big| E_{1,j} = \max_{k\in\mathcal{S}} \left|h_{1,k}\right|^2 \rho \triangleq Y | E_{1,j}$. In the second case $E_{2,i,j}$ when $|\mathcal{S}_1| = j \neq 0$ and $|\mathcal{S}_2| = i \neq 0$, $k^* = \arg\max_k \left\{ \left|h_{1,k}\right|^2 : D_{1,k} \in \mathcal{S}_2 \right\}$ according to (4.7) and $a_{1,k^*} = \frac{\left|h_{1,k^*}\right|^2\rho - T_2}{\left|h_{1,k^*}\right|^2\rho(1+T_2)}$ according to (4.8). Then the received SINR value under $E_{2,i,j}$ at the BS to decode x_{1,k^*} is $\gamma_{D_{1,k^*}\to BS} \big| E_{2,i,j} = \max_{k\in\mathcal{S}_2} a_{1,k} \left|h_{1,k}\right|^2 \rho = \max_{k\in\mathcal{S}_2} \frac{\left|h_{1,k}\right|^2\rho - T_2}{1+T_2} \triangleq Y | E_{2,i,j}$. As to the third case E_3 when $|\mathcal{S}_1| = 0$, similar with $E_{1,j}$, $k^* = \arg\max_k \left\{ \left|h_{1,k}\right|^2 : D_{1,k} \in \mathcal{S} \right\}$ according to Section 4.2.3.1. Then the received SINR under E_3 at the BS to decode x_{1,k^*} is $\hat{\gamma}_{D_{1,k^*}\to BS} \big| E_3 = \max_{k\in\mathcal{S}} \left|h_{1,k}\right|^2 \rho \triangleq Y | E_3$.

Given the fact that the outage probability of a practical system is usually extremely small to guarantee the reliability and robustness [83] [119], the CDF of Y can be formulated as (4.19) by combining all these three cases.

$$
\begin{aligned}
F_Y(y) &= \sum_{j=1}^{K} \Pr\left(|\mathcal{S}_1| = j \neq 0,\ |\mathcal{S}_2| = 0\right) \Pr\left(\left(\hat{\gamma}_{D_{1,k^*}\to BS} \big| E_{1,j}\right) < y\right) + \Pr\left(|\mathcal{S}_1| = 0\right) \Pr\left(\left(\hat{\gamma}_{D_{1,k^*}\to BS} \big| E_3\right) < y\right) \\
&+ \sum_{j=1}^{K} \sum_{i=1}^{j} \Pr\left(|\mathcal{S}_1| = j \neq 0,\ |\mathcal{S}_2| = i \neq 0\right) \Pr\left(\left(\gamma_{D_{1,k^*}\to BS} \big| E_{2,i,j}\right) < y\right) \\
&= \sum_{j=1}^{K} C_K^j \left(P_{sd}^{FD}\right)^j \left(1 - P_{sd}^{FD}\right)^{K-j} \left(1 - J_d^{FD}\right)^j \left(1 - e^{-\left(1+d_{D_2,BS}^{\alpha}\right)\frac{y}{\rho}}\right)^K + \left(1 - P_{sd}^{FD}\right)^K \left(1 - e^{-\left(1+d_{D_2,BS}^{\alpha}\right)\frac{y}{\rho}}\right)^K \\
&+ \sum_{j=1}^{K} C_K^j \left(P_{sd}^{FD}\right)^j \left(1 - P_{sd}^{FD}\right)^{K-j} \left(\sum_{i=1}^{j} C_j^i \left(J_d^{FD}\right)^i \left(1 - J_d^{FD}\right)^{j-i} \left(1 - e^{-\left(1+d_{D_2,BS}^{\alpha}\right)\frac{(1+T_2)y+T_2}{\rho}}\right)^i \right)
\end{aligned}
\tag{4.19}
$$

The achievable rate of D_{1,k^*} is $R_{D_{1,k^*}}^{TRS\,PA-FD}|H_1 = \log(1+Y)$. Then the ergodic rate under H_1 is $E\left[R_{D_1}^{TRS\,PA-FD}|H_1\right] = E\left[\log(1+Y)\right] = \frac{1}{\ln 2}\int_0^\infty \frac{1}{1+y}\left(1 - F_Y(y)\right) dy$ [79] [106]. According to $\int_0^\infty \frac{1}{1+y} e^{-\left(1+d_{D_2,BS}^{\alpha}\right)\frac{y}{\rho}m} dy = -e^{\left(1+d_{D_2,BS}^{\alpha}\right)\frac{m}{\rho}} \mathrm{Ei}\left(-\left(1 + d_{D_2,BS}^{\alpha}\right)\frac{m}{\rho}\right)$ [120]

and (4.19), we have

$$E\left[R_{D_{1,k^*}}^{TRS\,PA-FD}|H_1\right] = J_1 + J_2 + J_3 \tag{4.20}$$

where

$$\begin{aligned} J_1 = {} & \tfrac{1}{\ln 2}\sum_{j=1}^{K} C_K^j \left(P_{sd}^{FD}\right)^j \left(1-P_{sd}^{FD}\right)^{K-j}\left(1-J_d^{FD}\right)^j \\ & \times\left(\sum_{m=1}^{K} C_K^m(-1)^m e^{\left(1+d_{D_2,BS}^{\alpha}\right)\frac{m}{\rho}}\mathrm{Ei}\left(-\frac{\left(1+d_{D_2,BS}^{\alpha}\right)m}{\rho}\right)\right) \end{aligned} \tag{4.21}$$

$$\begin{aligned} J_2 = {} & \tfrac{1}{\ln 2}\sum_{j=1}^{K} C_K^j \left(P_{sd}^{FD}\right)^j \left(1-P_{sd}^{FD}\right)^{K-j}\sum_{i=1}^{j} C_j^i \left(J_d^{FD}\right)^i \\ & \times\left(1-J_d^{FD}\right)^{j-i}\sum_{m=1}^{i} C_i^m(-1)^m e^{\frac{\left(1+d_{D_2,BS}^{\alpha}\right)(1+2T_2)m}{\rho}} \\ & \times\mathrm{Ei}\left(-\frac{\left(1+d_{D_2,BS}^{\alpha}\right)(1+T_2)m}{\rho}\right) \end{aligned} \tag{4.22}$$

$$\begin{aligned} J_3 = {} & \tfrac{1}{\ln 2}\left(1-P_{sd}^{FD}\right)^K \\ & \times\sum_{m=1}^{K} C_K^m(-1)^m e^{\left(1+d_{D_2,BS}^{\alpha}\right)\frac{m}{\rho}}\mathrm{Ei}\left(-\frac{\left(1+d_{D_2,BS}^{\alpha}\right)m}{\rho}\right). \end{aligned} \tag{4.23}$$

Corollary 8. *Based on* (4.20) *for TRSPA-FD, we make the following changes to obtain the ergodic rate of TRSPA-HD: i) let* $\varpi_1 = 0$*; ii) change* T_2 *into* $\phi_{HD,2} = 2^{2R_2} - 1$*; and iii) rewrite* (4.20) *into* $E\left[R_{D_{1,k^*}}^{TRS\,PA-HD}|H_1\right] = \frac{1}{2}(J_1 + J_2 + J_3)$*. As to TRSPA-OMA, besides assigning* $\varpi_1 = 0$*, changing* T_2 *into* $\phi_{OMA,2} = 2^{3R_2} - 1$*, and rewriting* (4.20) *into* $E\left[R_{D_{1,k^*}}^{TRS\,PA-OMA}|H_1\right] = \frac{2}{3}J_1 + \frac{1}{3}J_2 + \frac{2}{3}J_3$*,* J_2 *also needs to be modified into* $J_{OMA,2}$ *as* (4.24)*,*

$$\begin{aligned} J_{OMA,2} = {} & \tfrac{1}{\ln 2}\sum_{j=1}^{K} C_K^j \left(P_{sd}^{OMA}\right)^j \left(1-P_{sd}^{OMA}\right)^{K-j} \\ & \times\sum_{i=1}^{j} C_j^i \left(J_d^{OMA}\right)^i \left(1-J_d^{OMA}\right)^{j-i}\sum_{m=1}^{i} C_i^m(-1)^m e^{\left(1+d_{D_2,BS}^{\alpha}\right)\frac{m}{\rho}}\mathrm{Ei}\left(-\frac{\left(1+d_{D_2,BS}^{\alpha}\right)m}{\rho}\right) \end{aligned} \tag{4.24}$$

where the parameters P_{sd}^{OMA} *and* J_d^{OMA} *are defined in a TRSPA-OMA scheme with the same physical meanings as* P_{sd}^{FD} *and* J_d^{FD} *in* (4.11) *and* (4.12)*.*

Then we evaluate the slope of the ergodic rate curve in the high SNR region. Its

physical meaning is spatial multiplexing gain [121]. It is defined as

$$S_{D_{1,k^*}}^{TRS\,PA-FD}|H_1 = \lim_{\rho\to\infty} \frac{E\left[R_{D_{1,k^*}}^{TRS\,PA-FD}\middle|H_1\right]}{\log\rho}. \tag{4.25}$$

Using $\mathrm{Ei}\left(-\frac{1}{\rho}\right) \to \ln\frac{1}{\rho} + C_E$ where C_E is the Euler constant, the asymptotic ergodic rate of D_{1,k^*} for TRSPA-FD when $\rho \to \infty$ can be written as (4.26)-(4.29) according to (4.20)-(4.23).

$$E\left[R_{D_{1,k^*}}^{TRS\,PA-FD,\infty}|H_1\right] = J_1^{\infty} + J_2^{\infty} + J_3^{\infty} \tag{4.26}$$

where J_1, J_2 and J_3 are approximated as J_1^{∞}, J_2^{∞} and J_3^{∞} when $\rho \to \infty$, respectively.

$$J_1^{\infty} = 0. \tag{4.27}$$

$$\begin{aligned} J_2^{\infty} = {} & \tfrac{1}{\ln 2}\sum_{j=1}^{K} C_K^j\left(P_{SD}^{FD}\right)^j\left(1-P_{SD}^{FD}\right)^{K-j}\sum_{i=1}^{j} C_j^i \\ & \times\left(\left(1+d_{D_2,BS}^{\alpha}\right)\tfrac{T_2}{\rho}\right)^{j-i}\sum_{m=1}^{i} C_i^m(-1)^m \\ & \times\left(\ln\frac{\left(1+d_{D_2,BS}^{\alpha}\right)(1+T_2)m}{\rho}+C_E\right). \end{aligned} \tag{4.28}$$

$$\begin{aligned} J_3^{\infty} = {} & \tfrac{1}{\ln 2}\left(1-P_{SD}^{FD}\right)^{K} \\ & \times\sum_{m=1}^{K} C_K^m(-1)^m\left(\ln\frac{\left(1+d_{D_2,BS}^{\alpha}\right)m}{\rho}+C_E\right). \end{aligned} \tag{4.29}$$

Accordingly, substituting (4.27), $\lim_{\rho\to\infty}\frac{J_2^{\infty}}{\log\rho} = \sum_{j=1}^{K} C_K^j\left(P_{SD}^{FD}\right)^j\left(1-P_{SD}^{FD}\right)^{K-j}\left(\sum_{m=1}^{j} C_i^m(-1)^{m+1}\right)$ and $\lim_{\rho\to\infty}\frac{J_3^{\infty}}{\log\rho} = \left(1-P_{SD}^{FD}\right)^{K}\sum_{m=1}^{K} C_K^m(-1)^{m+1}$ into (4.26), we work out the spatial multiplexing gain in (4.30) for TRSPA-FD.

$$\begin{aligned} & S_{D_{1,k^*}}^{TRS\,PA-FD}|H_1 = \sum_{j=1}^{K} C_K^j\left(P_{SD}^{FD}\right)^j\left(1-P_{SD}^{FD}\right)^{L-j} \\ & \times\sum_{m=1}^{j} C_i^m(-1)^{m+1} + \left(1-P_{SD}^{FD}\right)^{K}\sum_{m=1}^{K} C_K^m(-1)^{m+1} = 1. \end{aligned} \tag{4.30}$$

Similarly, we also obtain the spatial multiplexing gains $S_{D_{1,k^*}}^{TRS\,PA-HD}|H_1 = \frac{1}{2}$ and $S_{D_{1,k^*}}^{TRS\,PA-OMA}|H_1 = \frac{1}{3}$.

In a system with A_1 transmit antennas and A_2 receive antennas, the maximum spatial multiplexing gain is $\min(A_1, A_2)$ [122]. Given the investigated system model in Section 4.2.1, the maximum spatial multiplexing gain of D_{1,k^*} is 1.

Remark 6. *The spatial multiplexing gain for D_{1,k^*} in a TRSPA-FD system under H_1 is* 1 *and it is the achievable maximum value in the considered system. As to TRSPA-HD and TRSPA-OMA, their spatial multiplexing gains are only $\frac{1}{2}$ and $\frac{1}{3}$.*

4.3.2.2 Ergodic Rate and Spatial Multiplexing Gain of D_{1,k^*} under H_0

Under H_0, all relays cannot obtain D_2's message since D_2 does not exist. According to (4.9), $k^* = \arg\max_k \left\{ \left|h_{1,k}\right|^2 : \ D_{1,k} \in \mathcal{S} \right\}$. Then D_{1,k^*}'s data rate is $R^{TRS\,PA-FD}_{D_{1,k^*}}|H_0 = \log\left(1 + \hat{\gamma}_{D_{1,k^*}\to BS}\right) = \log\left(1 + \left|h_{1,k^*}\right|^2\rho\right)$. Therefore, the ergodic rate of D_{1,k^*} is $E\left[R^{TRS\,PA-FD}_{D_{1,k^*}}|H_0\right] = E\left[\log\left(1 + \underbrace{\max\left|h_{1,k}\right|^2\rho}_{\hat{Y}}\right)\right] = \frac{1}{\ln 2}\int_0^\infty \frac{1}{1+\hat{y}}\left(1 - F_{\hat{Y}}(\hat{y})\right)d\hat{y}$, where $F_{\hat{Y}}(\hat{y})$ is the CDF of $\hat{Y}$. We know that $F_{\hat{Y}}(\hat{y}) = \Pr\left(\max\left|h_{1,k}\right|^2\rho < \hat{y}\right) = \left(1 - e^{-\left(1+d^\alpha_{D_2,BS}\right)\frac{\hat{y}}{\rho}}\right)^K$. The ergodic rate of D_{1,k^*} under H_0 is thus written as $E\left[R^{TRS\,PA-FD}_{D_{1,k^*}}|H_0\right] = \frac{1}{\ln 2}\int_0^\infty \frac{1}{1+\hat{y}}\left(\sum_{j=1}^{K} C_K^j(-1)^j e^{-\left(1+d^\alpha_{D_2,BS}\right)\frac{\hat{y}}{\rho}j}\right)d\hat{y}$. According to [120], we further get

$$\begin{aligned} E\left[R^{TRS\,PA-FD}_{D_{1,k^*}}|H_0\right] &= \frac{1}{\ln 2}\sum_{j=1}^{K} C_K^j(-1)^j \\ &\times\left(-e^{\left(1+d^\alpha_{D_2,BS}\right)\frac{j}{\rho}}\mathrm{Ei}\left(-\left(1+d^\alpha_{D_2,BS}\right)\frac{j}{\rho}\right)\right). \end{aligned} \tag{4.31}$$

Corollary 9. *Ergodic rates of D_{1,k^*} under H_0 for TRSPA-HD and TRSPA-OMA are written as*

$$\begin{aligned} E\left[R^{TRS\,PA-HD}_{D_{1,k^*}}|H_0\right] &= \frac{1}{2\ln 2}\sum_{j=1}^{K} C_K^j(-1)^j \\ &\times\left(-e^{\left(1+d^\alpha_{D_2,BS}\right)\frac{j}{\rho}}\mathrm{Ei}\left(-\left(1+d^\alpha_{D_2,BS}\right)\frac{j}{\rho}\right)\right) \end{aligned} \tag{4.32}$$

$$\begin{aligned} E\left[R^{TRS\,PA-OMA}_{D_{1,k^*}}|H_0\right] &= \frac{2}{3\ln 2}\sum_{j=1}^{K} C_K^j(-1)^j \\ &\times\left(-e^{\left(1+d^\alpha_{D_2,BS}\right)\frac{j}{\rho}}\mathrm{Ei}\left(-\left(1+d^\alpha_{D_2,BS}\right)\frac{j}{\rho}\right)\right). \end{aligned} \tag{4.33}$$

We know that $\mathrm{Ei}\left(-\frac{1}{\rho}\right) \approx \ln\frac{1}{\rho} + C_E$ and $e^{-\frac{1}{\rho}} \approx 1 - \frac{1}{\rho}$ when $\rho \to \infty$. Based on (4.31), the asymptotic ergodic rate of D_{1,k^*} under H_0 for TRSPA-FD is written as

$$\begin{aligned} &E\left[R_{D_{1,k^*}}^{TRSPA-FD,\infty}|H_0\right] \\ &= \frac{-1}{\ln 2}\sum_{j=1}^{K} C_K^j(-1)^j\left(\ln\frac{\left(1+d_{D_2,BS}^{\alpha}\right)^j}{\rho} + C_E\right). \end{aligned} \tag{4.34}$$

Substituting (4.34) into (4.25), the spatial multiplexing gain of TRSPA-FD is worked out to be 1, i.e., $S_{D_{1,k^*}}^{TRSPA-FD}\Big| H_0 = 1$. Similarly, spatial multiplexing gains of TRSPA-HD and TRSPA-OMA are $\frac{1}{2}$ and $\frac{2}{3}$, i.e., $S_{D_{1,k^*}}^{TRSPA-HD}\Big| H_0 = \frac{1}{2}$ and $S_{D_{1,k^*}}^{TRSPA-OMA}\Big| H_0 = \frac{2}{3}$.

Remark 7. *The spatial multiplexing gain for D_{1,k^*} in a TRSPA-FD system under H_0 is* 1 *and it is the achievable maximum value of our considered system. As to TRSPA-HD and TRSPA-OMA, their spatial multiplexing gains are only $\frac{1}{2}$ and $\frac{2}{3}$.*

4.4 Performance Comparison

The above section already considers the impact of residual LI caused by the practical assumption of imperfect self-interference cancellation. According to Remarks 4–7 and research findings associated with CNOMA, FD CNOMA outperforms HD CNOMA and COMA in the low SNR region. However, it gradually loses its advantage as SNR increases, since LI gets stronger in the high SNR region. The intensity of LI seems to be the dominant factor of performance comparison result. Motivated by this, we further presents comparison results under the consideration of reasonable LI intensity to explicitly answer the question which relaying mode the proposed TRSPA strategy should choose in practice.

4.4.1 Outage Probability

The general comparison result of FD-relaying-related research works [79] [80] [81] is that FD performs better than HD and OMA in the low SNR region but it will be out-

performed in the high SNR region. It is of great practical significance to compare the results of TRSPA-FD, TRSPA-HD and TRSPA-OMA with reasonable SI suppression capabilities, especially in the high SNR region.

Based on [115] and [116], existing SI suppression techniques are able to reduce the intensity of LI to the same level as noise floor, i.e., $\Omega_{LI}P_r = N_0$. Substituting $\Omega_{LI}P_r = N_0$ into (4.11) and (4.40), when $\rho \to \infty$, P_{sd}^{FD} of TRSPA-FD is approximated as

$$\begin{aligned} P_{sd,\,LI=noi}^{FD,\infty} &= \lim_{\rho\to\infty} \int_{\frac{2T_2}{\rho}}^{\infty} P_d^{FD}(x) f_X(x)\, dx \\ &\approx 1 - \lim_{\rho\to\infty} F_X\left(\tfrac{2T_2}{\rho}\right) = 1 - \lim_{\rho\to\infty} R\tfrac{2T_2}{\rho}. \end{aligned} \tag{4.35}$$

The asymptotic outage probability of TRSPA-FD in (4.16) becomes

$$P_{D_2,\,LI=noi}^{TRSPA-FD,\infty} = \left(\left(1 + d_{D_2,BS}^{\alpha}\right) T_2 + 2RT_2\right)^K \left(\tfrac{1}{\rho}\right)^K. \tag{4.36}$$

Substituting (4.36) into (4.15), the corresponding diversity order is worked out as $d_{D_2,\,LI=noi}^{TRSPA-FD} = -\lim\limits_{\rho\to\infty} \frac{\lg\left(P_{D_2,\,LI=noi}^{TRSPA-FD,\infty}\right)}{\lg\rho} = K$ in a practical scenario. The outage probability of TRSPA-FD therefore decreases at the same rate as TRSPA-HD and TRSPA-OMA as ρ gets larger. Also, their performance comparison result will not fluctuate with the change of ρ. The one with a better performance is always better. We next need to further demonstrate that FD is the best one.

We define the outage performance gain of TRSPA-FD over TRSPA-HD as $G_{FD,\,HD} = -10\lg \frac{P_{D_2,\,LI=noi}^{TRSPA-FD,\infty}}{P_{D_2}^{TRSPA-HD,\infty}}$. According to (4.36) and (4.17), $G_{FD,\,HD}$ is calculated as

$$G_{FD,\,HD} = -10K \lg \frac{\left(\left(1+d_{D_2,BS}^{\alpha}\right)T_2 + 2RT_2\right)}{\left(\left(1+d_{D_2,BS}^{\alpha}\right)\phi_{HD,2} + R\phi_{HD,2}\right)}. \tag{4.37}$$

Since $\phi_{HD,2} - T_2 = \left(2^{R_2} - 1\right)^2 > 0$ is true for any positive number R_2, we have $\phi_{HD,2} > 2T_2 > T_2$. Thus, $G_{FD,\,HD}$ is positive, verifying that TRSPA-FD achieves a better outage performance than TRSPA-HD. The outage performance gain of TRSPA-FD compared

to TRSPA-OMA is

$$G_{FD,\,OMA} = -10K \lg \frac{\left(\left(1+d_{D_2,BS}^{\alpha}\right)T_2+2RT_2\right)}{\left(\left(1+d_{D_2,BS}^{\alpha}\right)\phi_{OMA,2}+R\phi_{OMA,2}\right)}. \tag{4.38}$$

Since $\phi_{OMA,2} > \phi_{HD,2} > 2T_2 > T_2$, $G_{FD,\,OMA}$ must be a positive constant.

Remark 8. *Given reasonable SI suppression capabilities, TRSPA-FD always achieves better outage performance than TRSPA-HD and TRSPA-OMA and it will never be exceeded no matter how large the SNR is. Therefore, different from the general conclusion of other researchers, we confirm that FD is the outage-optimal choice when designing a practical TRSPA system.*

4.4.2 Ergodic Rate

We substitute $\Omega_{LI}P_r = N_0$ into (4.27), (4.28) and (4.29). By using (4.35), they become $J_{1,\,LI=noi}^{\infty} = 0$, $J_{2,\,LI=noi}^{\infty} = \frac{1}{\ln 2}\sum_{j=1}^{K} C_K^j \left(P_{sd,\,LI=noi}^{FD}\right)^j \times \left(1 - P_{sd,\,LI=noi}^{FD}\right)^{K-j} \sum_{i=1}^{j} C_j^i \left(\frac{\left(1+d_{D_2,BS}^{\alpha}\right)T_2}{\rho}\right)^{j-i}$ $\times \sum_{m=1}^{i} C_i^m (-1)^m \ln\left(\frac{\left(1+d_{D_2,BS}^{\alpha}\right)(1+T_2)m}{\rho} + C_E\right)$ and $J_{3,\,LI=noi}^{\infty} = 0$. Furthermore, we have

$$\lim_{\rho\to\infty} \frac{J_{1,\,LI=noi}^{\infty} + J_{2,\,LI=noi}^{\infty} + J_{3,\,LI=noi}^{\infty}}{\log\rho} = \lim_{\rho\to\infty} \sum_{i=1}^{K} C_K^i \left(\left(1 + d_{D_2,BS}^{\alpha}\right)\frac{T_2}{\rho}\right)^{K-i} = 1.$$

According to (4.25) and (4.26), the spatial multiplexing gain of D_{1,k^*} for TRSPA-FD in practical scenarios is equal to 1, which is the same as Remark 6.

Remark 9. *Given reasonable SI suppression capabilities of FD user relays, the spatial multiplexing gain of TRSPA-FD still achieves* 1*, which is the same as Remark 6. It is the maximum achievable value, and is larger than those of TRSPA-HD and TRSPA-OMA.*

However, there is only one concern about the superiority illustration of TRSPA-FD in terms of ergodic rate. According to Section 4.4.1, TRSPA-HD and TRSPA-OMA

always achieve worse outage performance than TRSPA-FD. Their user relays are more likely to fail to obtain x_2. So they tend to allocate more power to relays in order to fully utilize the power resources according to the proposed TRSPA stated in Section 4.2.3.1. In such cases, these benchmarks may achieve larger ergodic rates than TRSPA-FD, however, at the cost of worse outage performance. As stated in Chapter 1, the transmissions of user relays' messages are executed on the condition that D_2's QoS requirement is satisfied. Such a sacrifice of outage performance is not allowed. Moreover, the ergodic rate comparison under unequal premises of outage probabilities is not fair. Motivated by these, we next compare TRSPA-FD's ergodic rate with the benchmarks under the same constraint of predetermined outage performance requirement.

Given the preset outage performance requirement P_{out}^{req}, the outage probability obtained from (4.18) is directly set to be P_{out}^{req}. Then the required transmit SNR by TRSPA-OMA is

$$\rho_{req} = \left(1 + d_{D_2,BS}^{\alpha} + R\right)\left(2^{3R_2} - 1\right)\Big/(P_{out}^{req})^{\frac{1}{K}}. \tag{4.39}$$

According to $E\left[R_{D_{1,k^*}}^{TRS\,PA-OMA,\infty}|H_1\right] = \frac{1}{3\ln 2}\sum_{m=1}^{K} C_K^m(-1)^{m+1}\left(\ln\frac{\left(1+d_{SB}^{\alpha}\right)m}{\rho_{req}} + C_E\right)$, the derivative function $\frac{d\left(E\left[R_{D_{1,k^*}}^{TRS\,PA-OMA,\infty}|H_1\right]\right)}{d\left(\log\rho_{req}\right)} = \frac{1}{3}$ is obtained. We know from (4.39) that ρ_{req} is determined by R_2 and it increases with R_2. Thus, we need to further work out the derivative function with respect to the independent variable R_2. Let $W = \left(1 + d_{D_2,BS}^{\alpha} + R\right)\Big/(P_{out}^{req})^{\frac{1}{K}}$. Then ρ_{req} can be written as $W\left(2^{3R_2} - 1\right)$ based on (4.39). Accordingly, the derivative of $\log\rho_{req}$ with respect to R_2 is approximated as $\frac{d\left(\log\rho_{req}\right)}{d(R_2)} \approx 3$. Therefore, under the restriction of P_{out}^{req}, $E\left[R_{D_{1,k^*}}^{TRS\,PA-OMA,\infty}|H_1\right]$ rises at a rate of $\frac{d\left(E\left[R_{D_{1,k^*}}^{TRS\,PA-OMA,\infty}|H_1\right]\right)}{d(R_2)} \approx \frac{1}{3}\times 3 = 1$ regarding R_2.

As to TRSPA-FD, its SNR is ρ_{req} as well for comparison fairness. We substitute $\Omega_{LI}P_r = N_0$ and $T_2 = \left(\frac{\rho_{req}}{W} + 1\right)^{\frac{1}{3}} - 1$ into (4.27), (4.28) and (4.29). Then by using (4.35), they become $J_{1,\,LI=noi}^{\infty} = 0$, $J_{2,\,LI=noi}^{\infty} = \frac{1}{\ln 2}\sum_{m=1}^{K} C_K^m(-1)^m\left(\ln\frac{\left(1+d_{D_2,BS}^{\alpha}\right)\left(\frac{\rho_{req}}{W}+1\right)^{\frac{1}{3}}m}{\rho_{req}} + C_E\right)$ and $J_{3,\,LI=noi}^{\infty} = 0$, respectively. Therefore, we get $\lim_{\rho\to\infty}\frac{J_{1,\,LI=noi}^{\infty}+J_{2,\,LI=noi}^{\infty}+J_{3,\,LI=noi}^{\infty}}{\log\rho} = \frac{2}{3}$. According

to (4.26), we learn that $\lim_{\rho\to\infty} \frac{E\left[R_{D_{1,k^*}}^{TRSPA-FD,\infty}|H_1\right]}{\log\rho} = \frac{2}{3}$ in this case. $E\left[R_{D_{1,k^*}}^{TRSPA-FD,\infty}|H_1\right]$ increases at a rate of $\frac{d\left(E\left[R_{D_{1,k^*}}^{TRSPA-FD,\infty}|H_1\right]\right)}{d(R_2)} = \frac{d\left(E\left[R_{D_{1,k^*}}^{TRSPA-FD,\infty}|H_1\right]\right)}{d\left(\log\rho_{req}\right)} \frac{d\left(\log\rho_{req}\right)}{d(R_2)} \approx \frac{2}{3}\times 3 = 2$. Similarly, as R_2 rises, the ergodic rate for TRSPA-HD rises at a rate of $\frac{d\left(E\left[R_{D_{1,k^*}}^{TRSPA-HD,\infty}|H_1\right]\right)}{d(R_2)} \approx \frac{1}{6}\times 3 = \frac{1}{2}$.

Noted that TRSPA-OMA's outage probability is set to be P_{out}^{req} as shown in (4.39). We learn from (4.37) and (4.38) that the outage probabilities for TRSPA-FD and TRSPA-HD are actually smaller than that of TRSPA-OMA, i.e., P_{out}^{req}, when they consume the same transmit power ρ_{req}. That is to say, all of these three schemes satisfy the predetermined outage performance requirement. So we summarize Remark 10.

Remark 10. *Under the same restriction of the preset outage performance requirement, as R_2 increases (i.e., the required SNR ρ_{req} gets larger correspondingly), the ergodic rates of TRSPA-FD, TRSPA-HD and TRSPA-OMA increase at rates of 2, $\frac{1}{2}$ and 1, respectively.*

In conclusion, on the premise that the outage performance requirement is guaranteed, TRSPA-FD's ergodic rate rises the most rapidly in the high SNR region. Together with its superior performance presented in subsequent simulation comparison where SNR rises from a small value, we confirm that FD is always the ergodic-rate-optimal choice for a TRSPA system, regardless of the value of SNR.

4.5 Numerical Results

We present numerical simulation results to i) validate the derived expressions in Section 4.3; ii) compare the performance of our proposed TRSPA with various benchmarks introduced in Section 4.2.3, including Max-Min [118], SRS [54] and TRS [47], and iii) verify the superiority of TRSPA-FD over TRSPA-HD and TRSPA-OMA, where TRSPA-FD, TRSPA-HD and TRSPA-OMA refer to the proposed TRSPA strategy

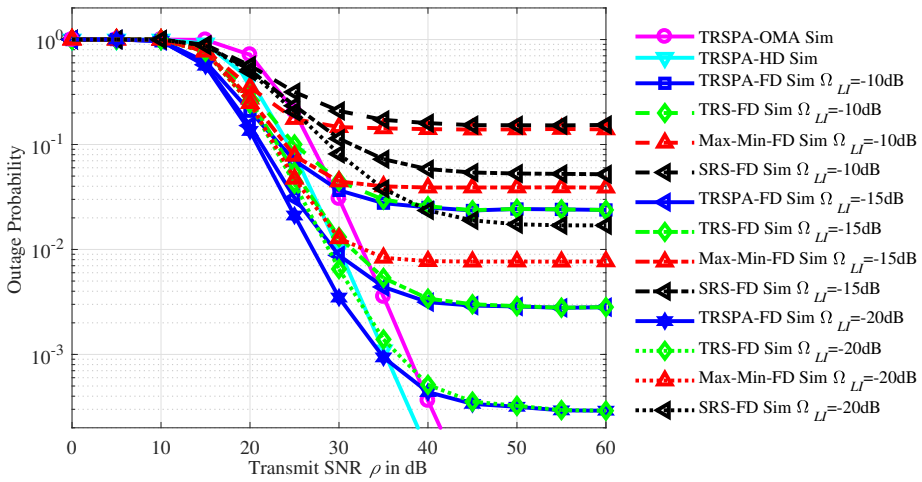

Figure 4.2: Simulated outage probabilities of D_2 versus transmit SNR for TRSPA-FD and benchmarks with different Ω_{LI}s under the hypothesis of H_1.

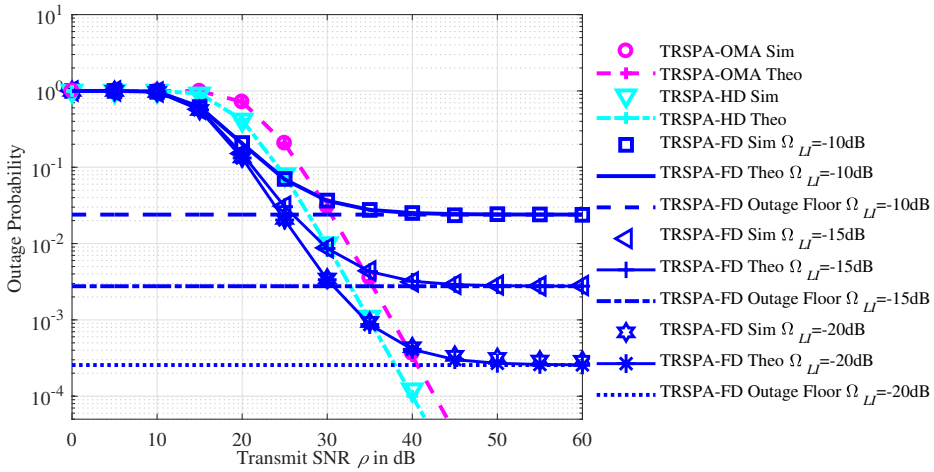

Figure 4.3: Exact and simulated outage probabilities of D_2 versus transmit SNR for TRSPA-FD and benchmarks with different Ω_{LI}s under the hypothesis of H_1.

working in the FD CNOMA scheme proposed in Chapter 3, HD CNOMA [123] and COMA [79] schemes, respectively. Unless otherwise stated, the simulation parameters are summarized as follows: α= 2, R_D = 2 m, $d_{D_2,BS}$ = 10 m, N = 15 and K = 2 [54], L = 30 and P_f^{pre} = 0.1 [113]; power coefficients of relays for benchmarks are $a_{1,k}^{Max-Min} = a_{1,k}^{SRS} = a_{1,k}^{TRS} = 0.25$ [47]; R_2 = 0.5 bit per channel user (BPCU) and $\Omega_{LI} = -15$ dB [79].

We compare the simulated outage performance of D_2 versus transmit SNR for the proposed TRSPA-FD scheme with different Ω_{LI}s and other benchmarks under H_1 in

Fig. 4.2. Corresponding theoretical derivation results are presented in Fig. 4.3 to validate the correctness. In Fig. 4.3, the exact results of TRSPA-FD, TRSPA-HD and TRSPA-OMA are worked out based on (4.10) and Corollary 7, respectively. Outage floor of TRSPA-FD is obtained from (4.16). The well-matched simulation and exact results and the well-approximated simulation results and outage floors validate these derived results. An outage floor for TRSPA-FD exists in Fig. 4.3 due to effects of residual LI in a FD relaying mode, verifying Remark 4. When it comes to the performance comparison, it is observed from Fig. 4.2 that the proposed TRSPA strategy with proper power allocation coefficients always achieves better outage performance than other RS strategies, verifying Theorem 2. As to TRSPA applied to different relaying modes, TRSPA-FD outperforms TRSPA-HD and TRSPA-OMA in the low SNR region, since TRSPA-FD completes each transmission process of D_2 in one time slot while TRSPA-HD and TRSPA-OMA, respectively, need two and three time slots. However, as SNR gets larger, over 30 dB in the case of $\Omega_{LI} = -15$ dB, the outage performance of TRSPA-FD is outperformed by benchmarks, since the intensity of LI gradually becomes stronger, limiting the outage performance of FD mode. This conclusion is consistent with those in [79], [80] and [81]. We also learn from Fig. 4.2 that a smaller LI cancellation coefficient leads to a better outage performance.

According to [115] and [116], existing SI suppression techniques are capable of reducing the intensity of LI to the same level as noise floor, which means $\Omega_{LI}P_r = N_0$. Therefore, we will take a step further than existing works [79], [80] and [81]. We compare the performance of TRSPA when applied to different relaying modes with reasonable SI suppression capabilities. Fig. 4.4 compares the simulated outage performance of TRSPA-FD with TRSPA-HD and TRSPA-OMA in such case, while Fig. 4.5 presents their simulated, exact and asymptotic values. Fig. 4.4 illustrates the superior performance of TRSPA-FD in practical scenarios regardless of the SNR being high or low. The achieved diversity order of TRSPA-FD is equal to K in Fig. 4.4, instead of zero. This observation verifies Remark 8 and is the most critical difference

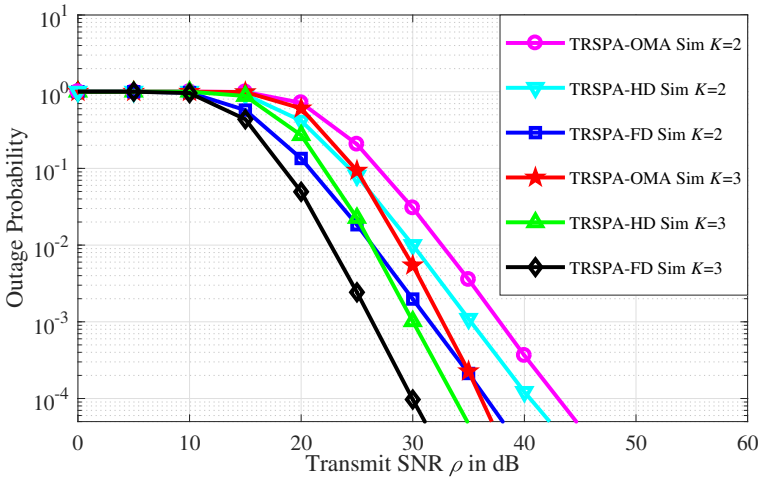

Figure 4.4: Simulated outage probabilities of D_2 versus transmit SNR for TRSPA-FD with reasonable SI suppression capabilities, TRSPA-HD and TRSPA-OMA with different relay numbers Ks under the hypothesis of H_1.

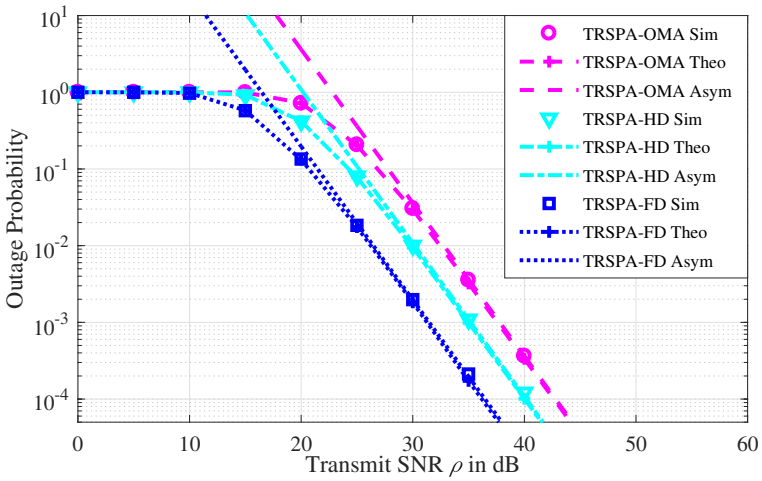

Figure 4.5: Simulated, exact and asymptotic outage probabilities of D_2 when $K = 2$ versus transmit SNR for TRSPA-FD with reasonable SI suppression capabilities, TRSPA-HD and TRSPA-OMA under the hypothesis of H_1.

from Figs. 4.2 and 4.3. Also, the outage performance of TRSPA-FD is not limited by any floor in practical scenarios. TRSPA-FD always achieves the best outage performance throughout the entire SNR range. Additionally, we learn that more relays lead to smaller outage probabilities due to higher diversity gains. Finally, the well-approximated curves in Fig. 4.5 validate derivation results (4.17) (4.18) and (4.36).

Figure 4.6 presents the simulated ergodic rates of D_{1,k^*} for TRSPA-FD and other benchmarks versus transmit SNR under H_1. We assume that $R_2 = 0.1$ BPCU [54].

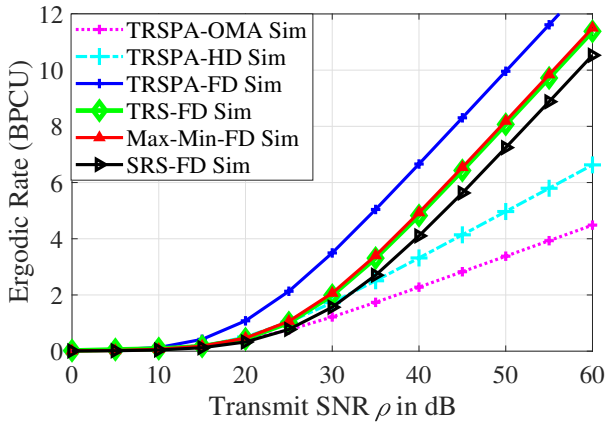

Figure 4.6: Simulated ergodic rates of D_{1,k^*} versus transmit SNR for TRSPA and benchmarks under the hypothesis of H_1.

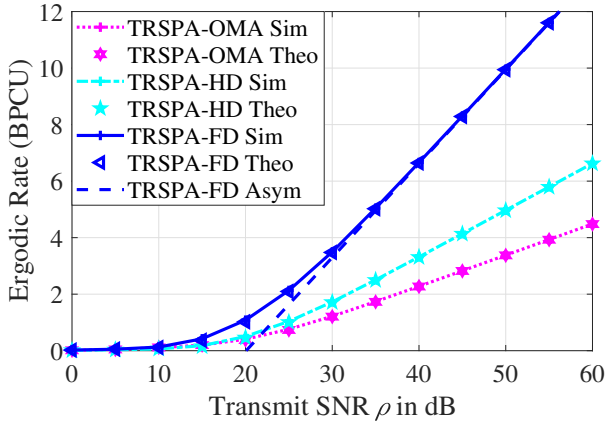

Figure 4.7: Simulated, exact and asymptotic ergodic rates of D_{1,k^*} versus transmit SNR for TRSPA and benchmarks under the hypothesis of H_1.

Their exact and asymptotic results are presented in Fig. 4.7 which are obtained from (4.20), Corollary 8 and (4.26). Well-matched results validate these expressions. Using the two points (40 dB, 5.64BPCU) and (50 dB, 8.96BPCU) on the asymptotic curve of TRSPA-FD in Fig. 4.7, we can compute the slope which is $3.32/10 = 0.332$. The result verifies Remark 6 because $0.332 \times 10 \lg 2 = 1$. When it comes to the performance comparison, according to Fig. 4.6, the proposed TRSPA-FD scheme achieves a larger ergodic rate for D_{1,k^*} compared with other RS strategies and relaying modes, because of i) its dynamic power allocation method, and ii) its feature of allowing D_{1,k^*} to transmit all the time. We know that D_{1,k^*} has to wait for its turn in TRSPA-HD and TRSPA-OMA schemes.

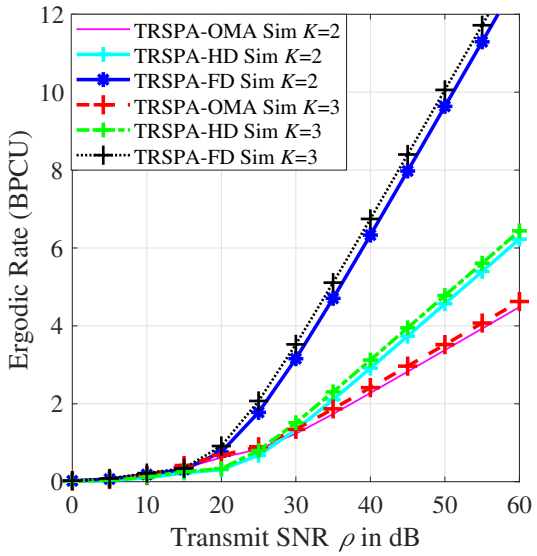

Figure 4.8: Simulated ergodic rates of D_{1,k^*} versus transmit SNR for TRSPA-FD with reasonable SI suppression capabilities, TRSPA-HD and TRSPA-OMA with different relay numbers Ks under the hypothesis of H_1.

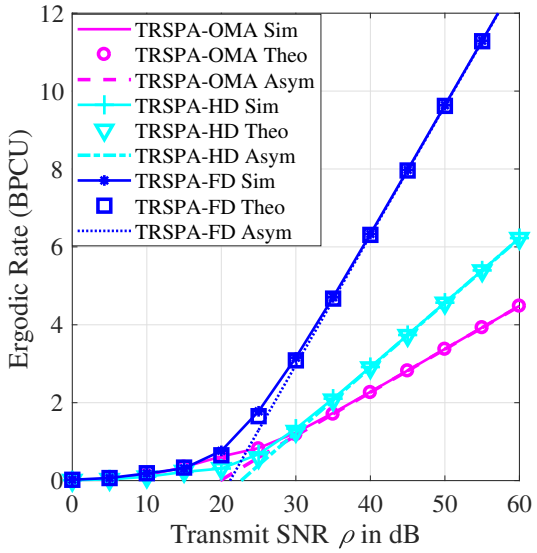

Figure 4.9: Simulated, exact and asymptotic ergodic rates of D_{1,k^*} when $K = 2$ versus transmit SNR for TRSPA-FD with reasonable SI suppression capabilities, TRSPA-HD and TRSPA-OMA under the hypothesis of H_1.

We present the simulated ergodic rate results under different numbers of relays for TRSPA-FD with reasonable SI suppression capabilities, TRSPA-HD and TRSPA-OMA in Fig. 4.8. Fig. 4.9 further presents their exact and asymptotic curves. In a similar method with Fig. 4.7, the slopes of the ergodic rate curves in Fig. 4.9 at the

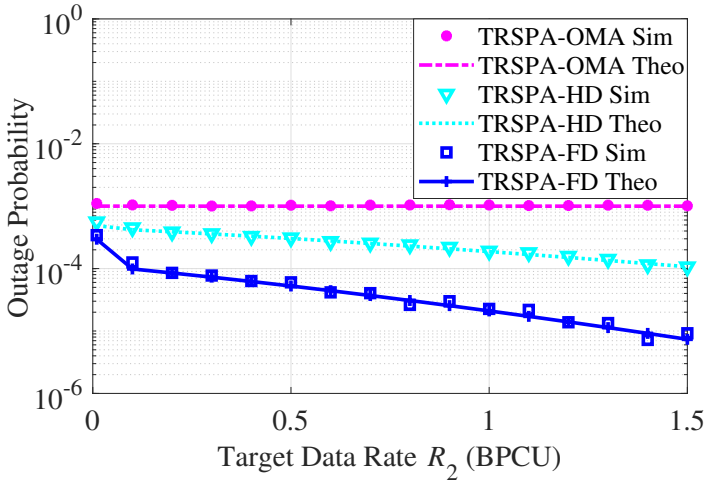

Figure 4.10: Simulated and exact outage probabilities of D_2 versus R_2 for TRSPA-FD with reasonable SI suppression capabilities, TRSPA-HD and TRSPA-OMA constrained by the predetermined outage performance requirement under the hypothesis of H_1.

high SNR region for TRSPA-FD, TRSPA-HD and TRSPA-OMA are found to be 1, $\frac{1}{2}$, and $\frac{1}{3}$, respectively. The results verify Remark 6 and Remark 9. When it comes to performance comparison, we learn from Fig. 4.8 that $K = 3$ achieves a larger ergodic rate than $K = 2$ due to a larger spatial diversity gain. It is observed that the ergodic rate of TRSPA-FD with reasonable SI suppression capabilities is larger than those of benchmarks due to simultaneously receiving and transmitting. However, there exists an exception. By careful observation on Fig. 4.8, the ergodic rate of TRSPA-FD is found to be slightly exceeded by that of TRSPA-OMA when the transmit SNR is 15 dB. Such a phenomenon is already analyzed theoretically in Section 4.4. Based on Section 4.4, TRSPA-OMA's larger ergodic rate is obtained at the cost of worse outage performance. For the sake of practicality and fairness, we will further compare their achieved ergodic rates under the same outage performance requirement.

We compare TRSPA-FD with reasonable SI suppression capabilities, TRSPA-HD and TRDPA-OMA in Figs. 4.10 and 4.11 under the same outage performance requirement P_{out}^{req}. Assume that $P_{out}^{req} = 0.001$ and $d_{D_2,BS} = 20$ m. As R_2 increases, the required transmit SNR by TRSPA-OMA is worked out based on (4.10) and Corollary 7 in a numerical method. Note that $P_{D_2}^{TRSPA-OMA} = P_{out}^{req}$ is used when working out that SNR

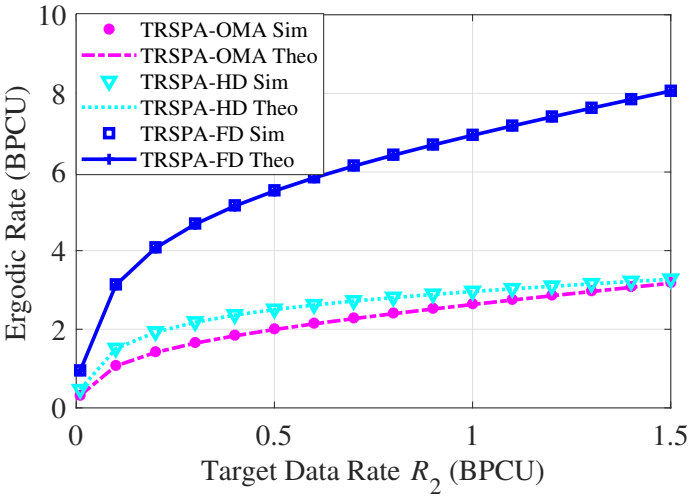

Figure 4.11: Simulated and exact ergodic rates of D_{1,k^*} versus R_2 for TRSPA-FD with reasonable SI suppression capabilities, TRSPA-HD and TRSPA-OMA constrained by the predetermined outage performance requirement under the hypothesis of H_1.

value to guarantee the outage performance requirement. With the same SNR value for comparison fairness, we also plot the outage probability curves of TRSPA-FD and TRSPA-HD in Fig. 4.10. As the x-axis increases from a small value, which implies that the transmit SNR rises from small as well according to (4.39), TRSPA-FD achieves the best outage performance. When R_2 continues to increase, TRSPA-FD continues to outperform other benchmarks. In summary, its outage probability is the lowest regardless of the SNR being large or small. It is shown in Fig. 4.10 that the outage probabilities of all schemes are no larger than P_{out}^{req}. Therefore they indeed satisfy the preset QoS requirement, which is the premise of the ergodic rate comparison in Fig. 4.11.

Under the outage probabilities shown in Fig. 4.10, we compare the achieved ergodic rates of TRSPA-FD and benchmarks in Fig. 4.11. When R_2 increases (i.e., the corresponding SNR increases) from a small value, TRSPA-FD achieves the largest ergodic rate compared with benchmarks. As R_2 keeps increasing, the ergodic rate of TRSPA-FD rises at a rate of 2, which is larger than those of TRSPA-HD and TRSPA-OMA. The observation verifies Remark 10. Therefore, TRSPA-FD always achieves the largest ergodic rate at all SNR values. Given the comparison results in Fig. 4.10, we can conclude that TRSPA-FD always outperforms other benchmarks in terms of

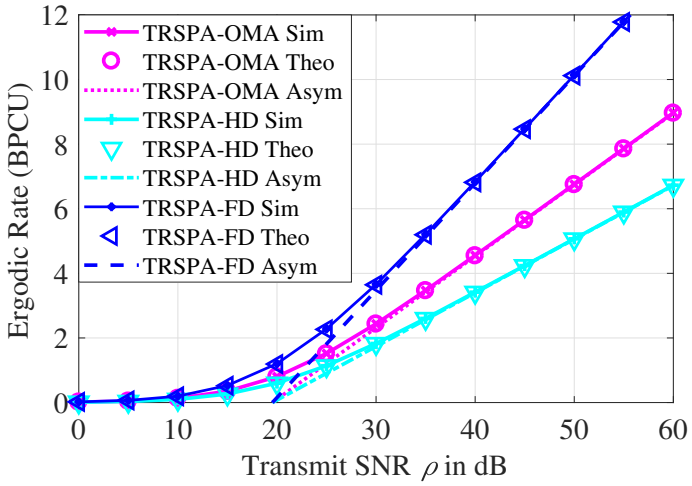

Figure 4.12: Simulated, exact and asymptotic ergodic rates of D_{1,k^*} versus transmit SNR for TRSPA-FD and various benchmarks under the hypothesis of H_0.

ergodic rate, regardless of the value of SNR, under the practical restriction of outage performance requirement.

Figure 4.12 shows the ergodic rates of D_{1,k^*} for TRSPA-FD and benchmarks under H_0. The exact and asymptotic values are worked out by (4.31)-(4.34). From Fig. 4.12, we find that the slopes of ergodic rate curves for TRSPA-FD, TRSPA-HD and TRSPA-OMA in the high SNR region are respectively 1, $\frac{1}{2}$ and $\frac{2}{3}$. These values verify Remark 7. TRSPA-FD always obtains the largest ergodic rate under H_0 due to the benefit of using FD mode. Moreover, all RS strategies achieve larger ergodic rates under H_0 than H_1 (see Fig. 4.8). It is because D_{1,k^*} transmits its signal using full power under H_0 but it allocates partial power to forward D_2's signal under H_1.

4.6 Summary

This chapter has proposed a power-allocation-based relay selection strategy TRSPA for the FD CNOMA scheme based on spectrum sensing, where strong secondary user relays assist a weak primary user to transmit signals to the BS. Owing to optimal power allocations, TRSPA maximizes the ergodic rate of the selected SU relay on the condition of PU's successful transmissions. Uniform distribution has been employed

for practically modelling the locations of relays. Exact and asymptotic expressions of outage probability and ergodic rate have been worked out. Accordingly, the diversity order is calculated to be zero, which means imperfectly cancelled LI severely restricts the outage performance. The spatial multiplexing gain is calculated to be one, which achieves its maximum achievable value. We then insightfully exploit the performance of TRSPA for FD CNOMA with reasonable SI suppression capabilities, and compare it with TRSPA-HD and TRSPA-OMA. It is concluded that FD relaying mode is both outage optimal and ergodic-rate optimal for a practical TRSPA system. Finally, simulation results illustrate that our derivations are correct and that TRSPA is superior to other relay selection strategies including Max-Min, SRS and TRS. Even though LI impairs the advantages of the FD mode, current SI suppression techniques already enable TRSPA applied in the FD mode to achieve better performance than other relaying modes, that is TRSPA-HD and TRSPA-OMA.

In the next chapter, we exploit a novel two-way relaying FD CNOMA scheme, where users intend to exchange signals via a FD two-way relay. This scheme can be considered as an extension of the proposed one-way relaying CNOMA schemes in the previous three chapters.

Appendix 4: Proof of Theorem 4

On the condition of $d_{1,k} = \sqrt{d_{D_2,BS}^2 + r_{2,k}^2 - 2d_{D_2,BS} r_{2,k} \cos(\theta_k)}$ and $d_{1,k} \gg r_{2,k}$ as stated in Section 4.2.1, the distance between $D_{1,k}$ and the BS is approximated as the distance between the BS and D_2, i.e., $d_{1,k} \approx d_{D_2,BS}$ [54]. According to the central limit theorem, the detection probability $P_d^{FD}(x)$ is

$$P_d^{FD}(x) = Q\left(\frac{Q^{-1}\left(P_f^{pre}\right)\sqrt{\frac{2}{L}}(1+\varpi_1\Omega_{LI}\rho)-\rho x}{\sqrt{2/L}(1+\varpi_1\Omega_{LI}\rho+\rho x)}\right) \tag{4.40}$$

where $Q(\cdot)$ is the Marcum Q-function. Moreover, relays are uniformly distributed within the disc around D_2. Thus, the PDF of $r_{2,k}$ is $f_R(r_{2,k}) = \frac{2r_{2,k}}{R_D^2}$. Given $h_{2,k} = \frac{h'}{\sqrt{1+r_{2,k}^{\alpha}}}$, the cumulative distribution function (CDF) of $\left|h_{2,k}\right|^2$ is expressed as

$$F_X(x) = \int_0^{R_D} \left(1 - e^{-\left(1+r_{2,k}^{\alpha}\right)x}\right) \frac{2r_{2,k}}{R_D^2} dr_{2,k}. \tag{4.41}$$

According to Gaussian-Chebyshev quadrature [124], $F_X(x)$ is further calculated as $F_X(x) \approx \frac{\pi}{2N} \sum_{n=1}^{N} \sqrt{1-\phi_n^2}\,(1 - e^{-c_n x})\,(\phi_n + 1)$, where $c_n = 1 + \left(\frac{R_D}{2}(\phi_n + 1)\right)^{\alpha}$ and $\phi_n = \cos\left(\frac{2n-1}{2N}\pi\right)$ [54]. N is the complexity-vs-accuracy tradeoff parameter. Therefore, the PDF of $\left|h_{2,k}\right|^2$ is

$$f_X(x) \approx \frac{\pi}{2N} \sum_{n=1}^{N} \sqrt{1-\phi_n^2}\,(\phi_n + 1)\, c_n e^{-c_n x}. \tag{4.42}$$

Substituting (4.40) and (4.42) into (4.11), the expression of P_{sd}^{FD} can be obtained as shown in (4.13) and (4.14) after tedious algebraic manipulations and integral calculations. The proof is completed.

Chapter 5

Two-Way Relaying Full-Duplex Cooperative NOMA Scheme

5.1 Introduction

In this chapter, we investigate a two-way relaying FD CNOMA scheme and then further evaluate its performance. To be specific, we first introduce the system model of the considered FD CNOMA scheme where two users exchange information via the assistance of a two-way FD relay and then explain the signal transmission process of our proposed two-way relaying FD CNOMA scheme. Afterwards, the closed-form expressions for the outage probabilities, diversity orders, ergodic rates, and system throughputs in delay-limited and delay-tolerant transmission modes are derived. It is noted that, to present the comprehensive performance evaluation, both perfect and imperfect SICs are taken into consideration. Finally, simulation results are presented to validate these derived closed-form expressions and to compare the performance of the proposed FD CNOMA system with benchmarks, i.e., HD CNOMA and cooperative OMA for bi-directional communication.

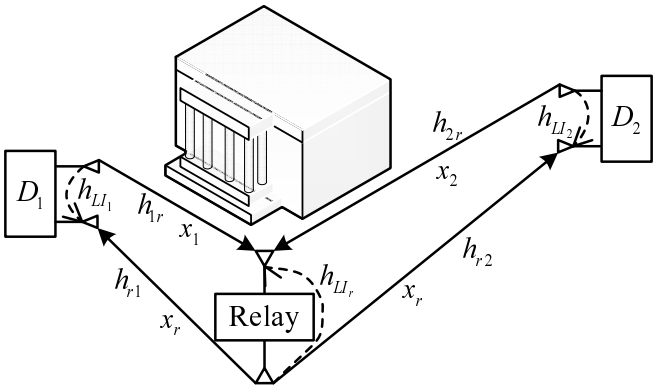

Figure 5.1: FD CNOMA system model.

5.2 System Model

We consider a FD CNOMA system consisting of two users (D_1 and D_2) and a dedicated relay. We assume that D_2 is farther away from the relay than D_1, as shown in Fig. 5.1. Like [125] and [126], this chapter assumes that no direct link exists between the two users because of severe shadowing effects caused by physical obstacles. The two users exchange information via the assistance of the dedicated relay. To enable FD transmission, D_1, D_2 and the relay are individually equipped with one transmitting antenna and one receiving antenna. As indicated in Chapter 1, one of the main motivations of this chapter is to present the comprehensive performance analysis. Therefore, we choose the above-described scenario which is a general model. Then our derivation approaches and corresponding remarks in this chapter will be of more reference significance to better provide the theoretical foundation for future diversified application systems.

We assume that all of the wireless links suffer from independent non-selective block Rayleigh fading and are disturbed by additive white Gaussian noise (AWGN) with mean power N_0. Denote h_{1r}, h_{r1}, h_{2r} and h_{r2} as the channel coefficients of the following links, $D_1 \rightarrow$ relay, relay $\rightarrow D_1$, $D_2 \rightarrow$ relay and relay $\rightarrow D_2$. We also assume that the corresponding channel power gains, i.e., $|h_{1r}|^2$, $|h_{r1}|^2$, $|h_{2r}|^2$ and $|h_{r2}|^2$, are exponentially distributed random variables with mean values Ω_κ, $\kappa \in \{1r,\ r1,\ 2r,\ r2\}$

[25, 26]. The channels are reciprocal, and thus we assume $\Omega_{1r} = \Omega_{r1} \triangleq \Omega_1$ and $\Omega_{2r} = \Omega_{r2} \triangleq \Omega_2$. Additionally, ipSIC at the relay and D_1 is considered in this chapter to evaluate the impact of error propagation on FD CNOMA. According to [66], the residual IS caused by ipSIC is modeled as a Rayleigh fading channel. g_r and g_D respectively denote the IS channel coefficients at the relay and D_1. Ω_g is the mean value of $|g_r|^2$ and $|g_D|^2$. Note that perfect channel state information of these links is available for signal decoding. When the FD mode is employed, we assume that an imperfect self-interference cancellation scheme is adopted at the users and the relay [16, 17] and hence the residual loop self-interference (LI)[1] exists. We model the attenuations (h_{LI_1}, h_{LI_2} and h_{LI_r}) at D_1, D_2 and the relay caused by imperfect self-interference cancellation as Rayleigh distributions with Ω_{LI_1}, Ω_{LI_2} and Ω_{LI_r} being the mean values of $\left|h_{LI_1}\right|^2$, $\left|h_{LI_2}\right|^2$ and $\left|h_{LI_r}\right|^2$ [127]. For simplicity, we assume that $\Omega_{LI_1} = \Omega_{LI_2} = \Omega_{LI_r} \triangleq \Omega_{LI}$.[2]

We denote x_1 and x_2 as the normalized transmitted signals by D_1 and D_2 with unity power, i.e., $E\left[x_1^2\right] = E\left[x_2^2\right] = 1$. The entire transmission process is divided into a series of time slots. During the k-th time slot, D_1 and D_2 respectively transmit $x_1[k]$ and $x_2[k]$ with the power of P_s while the relay transmits the superimposed NOMA signal $x_r[k]$ with the power of P_r. Note that efficient power control is capable of enhancing the performance of the considered system, which is beyond the scope of this chapter. Therefore, the signal received by the relay at the k-th time slot is given by $y_r[k] = h_{1r}\sqrt{P_s}x_1[k] + h_{2r}\sqrt{P_s}x_2[k] + x_{LI_r}[k] + n_r[k]$, where $x_{LI_r}[k]$ represents the LI signal and $n_r[k]$ is a Gaussian noise signal with zero mean. Moreover, according to the NOMA protocol, $x_r[k]$ is a weighted sum of $x_1[k]$ and $x_2[k]$ (a superimposed signal) with time delay τ. That is to say $x_r[k] = \sqrt{P_r a_1}x_1[k-\tau] + \sqrt{P_r a_2}x_2[k-\tau]$, where τ is an integer larger than or equal to 1, $P_r a_i$ is the transmission power for the signal $x_i[k-\tau]$ ($i = 1, 2$), and $a_1 + a_2 = 1$ [128]. In particular, to ensure the fairness between D_1 and

[1]Loop self-interference represents the signal which is transmitted by a FD device such as a relay or user equipment, and it is simultaneously looped back to the device's receiver.

[2]When the mean square values are different, the derivation and analysis are similar but the expressions become more complex.

D_2, a higher power should be allocated to the distant user D_2 who has worse channel conditions. Hence, we assume that $a_1 > a_2$ which is also assumed in [19, 26–28]. In this way, more power is allocated to x_1. Note that the fixed power allocation coefficients for two NOMA users are considered. Relaxing this assumption will further improve the performance of systems and should be concluded in our future work. Moreover, the received signal at D_i $(i = 1, 2)$ is given by $y_{D_i}[k] = h_{ri}x_r[k] + x_{LI_i}[k] + n_{D_i}[k]$, where $x_{LI_i}[k]$ is the LI signal at D_i and $n_{D_i}[k]$ denotes the AWGN signal. We assume that the power values of the relay and the sources are equal to simplify the analysis, i.e., $P_s = P_r = \hat{P}$. Such assumption is also made in [66] and [129].

Applying the NOMA protocol and SIC technique [13, 28], the relay first decodes the transmitted signal x_1 by the nearby user which has better channel conditions. The signal-to-interference-plus-noise ratio (SINR) at the relay equals

$$\gamma_{D_1 \to r} = \frac{|h_{1r}|^2 \rho}{|h_{2r}|^2 \rho + \left|h_{LI_r}\right|^2 \rho + 1} \tag{5.1}$$

where $\rho = \frac{\hat{P}}{N_0}$ is defined as the common signal-to-noise ratio without fading [130]. After decoding x_1 and then subtracting x_1 from the received signal, x_2 is subsequently decoded by the relay with a SINR value of

$$\gamma_{D_2 \to r} = \frac{|h_{2r}|^2 \rho}{\varepsilon |g_r|^2 \rho + \left|h_{LI_r}\right|^2 \rho + 1} \tag{5.2}$$

where $\varepsilon = 0$ and $\varepsilon = 1$ respectively denote the situations of pSIC and ipSIC.

In the superimposed signals y_{D_i} $(i = 1, 2)$ which are received by D_1 and D_2, the intensity of x_1 is higher than that of x_2 because $a_1 > a_2$. Then x_1 will be directly detected by D_2, with a SINR value of

$$\gamma_{D_2, x_1} = \frac{|h_{r2}|^2 \rho a_1}{|h_{r2}|^2 \rho a_2 + \left|h_{LI_2}\right|^2 \rho + 1}. \tag{5.3}$$

According to NOMA, SIC is adopted at D_1. The component x_1 which has a SINR value of

$$\gamma_{D_1, x_1} = \frac{|h_{r1}|^2 \rho a_1}{|h_{r1}|^2 \rho a_2 + \left|h_{LI_1}\right|^2 \rho + 1} \tag{5.4}$$

is first detected by D_1 and subtracted from $y_{D_1}[k]$. As to x_2, it is then detected by D_1

with the SINR value of

$$\gamma_{D_1,x_2} = \frac{|h_{r1}|^2 \rho a_2}{\varepsilon |g_D|^2 \rho + \left|h_{LI_1}\right|^2 \rho + 1}. \tag{5.5}$$

5.3 Performance Analysis

In this chapter, we consider two types of transmission modes, namely the delay-limited and the delay-tolerant transmission modes [131]. In the former mode, each user has a target data rate and the rate is determined by its QoS requirement. The message of each user is sent at a fixed rate. Outage probability is an important metric for performance evaluation. Delay-tolerant transmission refers to the situation where no time delay constraints are imposed on the decoding period. Users' target rates are allocated opportunistically and the transmitted data rates are adaptively determined according to these users' channel conditions. The codeword can be designed arbitrarily long, spanning over all of the fading states. Then it will be decoded until it is received in full length. The user always decodes messages correctly during SIC. The metric for performance evaluation in this mode is ergodic rate. Therefore, the ergodic rate should be calculated on the condition of successful decoding during SIC.

5.3.1 Outage Probability

5.3.1.1 Outage Probability of the $D_1 \rightarrow$ relay $\rightarrow D_2$ Link

Considering the NOMA protocol, the complementary event of outage communication for the $D_1 \rightarrow$ relay $\rightarrow D_2$ link can be described as follows. The relay successfully detects x_1 and D_2 also successfully detects x_1. R_2 denotes the target rate of this link and $T_2 = 2^{R_2} - 1$ is the corresponding target SNR. Then the probability of the complementary event is expressed as $\Pr\left(\gamma_{D_1 \rightarrow r} > T_2,\ \gamma_{D_2,x_1} > T_2\right)$, where $\Pr(\cdot)$ represents the probability function. It is noted whether the relay can successfully decode x_2 or not after it decodes and subtracts x_1 has nothing to do with the outage probability for the

$D_1 \rightarrow$ relay $\rightarrow D_2$ link, since D_2 directly detects x_1. It is the outage probability of the $D_2 \rightarrow$ relay $\rightarrow D_1$ link that the decoding result of x_2 by the relay really affects, which we will discuss later. Based on (5.1) and (5.3), the outage probabilities with pSIC and ipSIC for the $D_1 \rightarrow$ relay $\rightarrow D_2$ link are the same with each other and they can be written as

$$\begin{aligned} P_{D_2}^{FD,pSIC} &= P_{D_2}^{FD,ipSIC} \\ &= 1 - \Pr\left(\gamma_{D_1 \rightarrow r} > T_2,\ \gamma_{D_2,x_1} > T_2\right). \end{aligned} \tag{5.6}$$

Theorem 5. *The closed-form expression for the outage probability of the $D_1 \rightarrow$ relay $\rightarrow$ D_2 link with pSIC/ipSIC in the proposed FD CNOMA scheme is*

$$P_{D_2}^{FD,pSIC} = P_{D_2}^{FD,ipSIC} = 1 - \frac{\Omega_1}{\Omega_2 T_2 + \Omega_1} \frac{\Omega_1}{\Omega_{LI} T_2 + \Omega_1} e^{-\frac{T_2}{\Omega_1 \rho}} \frac{\Omega_2 (a_1 - a_2 T_2)}{T_2 \Omega_{LI} + \Omega_2 (a_1 - a_2 T_2)} e^{-\frac{T_2}{\Omega_2 \rho (a_1 - a_2 T_2)}} \tag{5.7}$$

if $a_1 > a_2 T_2$. Otherwise, $P_{D_2}^{FD,pSIC} = P_{D_2}^{FD,ipSIC} = 1$.

Proof. First, we note that $\gamma_{D_1 \rightarrow r} > T_2$ and $\gamma_{D_2,x_1} > T_2$ are independent events. Thus,

$$\begin{aligned} &\Pr\left(\gamma_{D_1 \rightarrow r} > T_2, \gamma_{D_2,x_1} > T_2\right) \\ &\quad = \Pr\left(\gamma_{D_1 \rightarrow r} > T_2\right) \times \Pr\left(\gamma_{D_2,x_1} > T_2\right). \end{aligned} \tag{5.8}$$

Let I_1 represent $\Pr\left(\gamma_{D_1 \rightarrow r} > T_2\right)$ and let x, y and z be $|h_{1r}|^2$, $|h_{2r}|^2$ and $\left|h_{LI_r}\right|^2$, respectively.

$$I_1 = \int_0^\infty \left(\int_0^\infty \left(\int_{T_2 y + T_2 z + \frac{T_2}{\rho}}^\infty f_X(x)\, dx \right) f_Y(y)\, dy \right) f_Z(z)\, dz = \frac{\Omega_1}{\Omega_2 T_2 + \Omega_1} \frac{\Omega_1}{\Omega_{LI} T_2 + \Omega_1} e^{-\frac{T_2}{\Omega_1 \rho}}. \tag{5.9}$$

Let I_2 represent $\Pr\left(\gamma_{D_2,x_1} > T_2\right)$. Also, x and y refer to $|h_{r2}|^2$ and $\left|h_{LI_2}\right|^2$, respectively. Then

$$\begin{aligned} I_2 &\overset{a_1 > a_2 T_2}{=} \int_0^\infty \left(\int_{\frac{T_2}{a_1 - a_2 T_2} y + \frac{T_2}{\rho (a_1 - a_2 T_2)}}^\infty f_X(x)\, dx \right) f_Y(y)\, dy \\ &= \frac{\Omega_2 (a_1 - a_2 T_2)}{T_2 \Omega_{LI} + \Omega_2 (a_1 - a_2 T_2)} e^{-\frac{T_2}{\Omega_2 \rho (a_1 - a_2 T_2)}}. \end{aligned} \tag{5.10}$$

Note that the first equality in (5.10) holds if $a_1 > a_2 T_2$. Otherwise, I_2 equals 0. After substituting (5.9) and (5.10) into $P_{D_2}^{FD,pSIC} = P_{D_2}^{FD,ipSIC} = 1 - I_1 I_2$, (5.7) can be obtained.

□

For comparison, in this section we also show the derivation results of the CNOMA system where HD devices (i.e., D_1, D_2 and relay) are adopted. Closed-form expressions for HD CNOMA are obtained from similar procedures of FD CNOMA, and thus

we directly present their eventual results as corollaries of corresponding derivation results of FD CNOMA for simplicity.

Corollary 10. *Defining the target SNR* $\phi_2 = 2^{2R_2} - 1$ *where* R_2 *is the target rate of the* $D_1 \rightarrow$ relay $\rightarrow D_2$ *link, the outage probability of this link for HD CNOMA with pSIC/ipSIC is*

$$\begin{aligned} P_{D_2}^{HD,pSIC} &= P_{D_2}^{HD,ipSIC} \\ &= 1 - \frac{\Omega_1}{\Omega_2\phi_2+\Omega_1} e^{-\frac{\phi_2}{\Omega_1\rho} - \frac{\phi_2}{\Omega_2\rho(a_1-a_2\phi_2)}} \end{aligned} \tag{5.11}$$

if $a_1 > a_2\phi_2$. *Otherwise,* $P_{D_2}^{HD,pSIC/ipSIC} = 1$.

5.3.1.2 Outage Probability of the $D_2 \rightarrow$ relay $\rightarrow D_1$ Link

The complementary event of outage for the $D_2 \rightarrow$ relay $\rightarrow D_1$ link is explained as follows. The relay first detects x_1 and then x_2 successfully, and D_1 also detects x_1 as well as x_2 successfully. Denoting the target rate of the link as R_1 and defining the corresponding target SNR as $T_1 = 2^{R_1} - 1$, the probability of the complementary event is expressed as $\Pr(\gamma_{D_1\rightarrow r} > T_2,\ \gamma_{D_2\rightarrow r} > T_1,\ \gamma_{D_1,x_1} > T_2,\ \gamma_{D_1,x_2} > T_1)$. Therefore, the outage probability of the $D_2 \rightarrow$ relay $\rightarrow D_1$ link for FD CNOMA with ipSIC is

$$P_{D_1}^{FD,ipSIC} = 1 - \Pr(\gamma_{D_1\rightarrow r} > T_2, \gamma_{D_2\rightarrow r} > T_1, \gamma_{D_1,x_1} > T_2, \gamma_{D_1,x_2} > T_1) \tag{5.12}$$

where $\varepsilon = 1$.

Theorem 6. *The closed-form expression of the outage probability for the* $D_2 \rightarrow$ relay $\rightarrow$ D_1 *link with ipSIC in the proposed FD CNOMA scheme is given by*

$$\begin{aligned} P_{D_1}^{FD,ipSIC} = 1 &- \left(\frac{1}{Q_8\Omega_{LI}} \frac{\Omega_1\Omega_2}{\Omega_g\Omega_1 T_1+\Omega_g\Omega_2 T_1 T_2+\Omega_1\Omega_2} e^{-\frac{T_1}{\rho\Omega_2} - \frac{Q_7}{\rho\Omega_1}} - \frac{1}{\Omega_{LI}\Omega_1 Q_9 Q_{10}} \frac{1}{Q_9\Omega_g T_1 T_2+1} e^{\frac{1}{\Omega_2\rho} - \frac{Q_7 Q_9}{\rho}} \right) \\ &\times \Bigg(U(Q_2 - Q_1) \frac{1}{\Omega_{LI} Q_4} \frac{\Omega_1}{\Omega_1+\Omega_g\rho Q_2} e^{-\frac{1}{\Omega_1} Q_2} \\ &+ U(Q_1 - Q_2) \frac{1}{\Omega_{LI} Q_3} \frac{Q_5}{Q_5+\Omega_g Q_3} e^{-\frac{1}{\Omega_1} Q_1 - \frac{Q_5}{\rho\Omega_g}} + U(Q_1 - Q_2) \frac{1}{\Omega_{LI} Q_3} e^{-\frac{Q_1}{\Omega_1}} \left(1 - e^{-\frac{Q_5}{\rho\Omega_g}}\right) \\ &+ U(Q_1 - Q_2) \left(\frac{1}{\Omega_{LI}\Omega_g Q_4 Q_{11}} e^{-\frac{Q_2}{\Omega_1} - \frac{1}{\rho} Q_5 Q_{11}} - \frac{1}{\Omega_{LI}\Omega_g Q_4 Q_6} e^{-\frac{Q_2}{\Omega_1} - \frac{1}{\rho} Q_5 Q_6 + \frac{1}{\rho} Q_4} \right) \Bigg) \end{aligned} \tag{5.13}$$

where $Q_1 = \frac{T_2}{\rho(a_1 - a_2 T_2)}$, $Q_2 = \frac{T_1}{\rho a_2}$, $Q_3 = \frac{1}{\Omega_{LI}} + \frac{1}{\Omega_1} Q_1\rho$, $Q_4 = \frac{1}{\Omega_{LI}} + \frac{1}{\Omega_1} Q_2\rho$, $Q_5 = \frac{Q_1 - Q_2}{Q_2}$, $Q_6 = \frac{1}{\Omega_1} Q_2\rho + \frac{1}{\Omega_g} + \frac{Q_4}{Q_5}$, $Q_7 = (1 + T_1) T_2$, $Q_8 = \frac{T_1}{\Omega_2} + \frac{Q_7}{\Omega_1} + \frac{1}{\Omega_{LI}}$, $Q_9 = \frac{1}{\Omega_2 T_2} + \frac{1}{\Omega_1}$,

$Q_{10} = Q_9 Q_7 + \frac{1}{\Omega_{LI}} - \frac{1}{\Omega_2}$, *and* $Q_{11} = \frac{1}{\Omega_g} + \frac{1}{\Omega_1} Q_2 \rho$. $U(x) = 1$ *when* $x \geq 0$, *or otherwise,* $U(x) = 0$.

Proof. See Appendix 5. □

Corollary 11. *Based on* (5.13)*, for the special case* $\varepsilon = 0$*, the outage probability of the* $D_2 \rightarrow$ relay $\rightarrow D_1$ *link with pSIC in the proposed FD CNOMA scheme is*

$$\begin{aligned} P_{D_1}^{FD,pSIC} = \\ 1 - \frac{\Omega_1}{\theta_{FD}\rho\Omega_{LI}+\Omega_1} \frac{\Omega_1\Omega_2}{\Omega_1\Omega_{LI}T_1+\Omega_2\Omega_{LI}A+\Omega_1\Omega_2} e^{-\frac{\theta_{FD}}{\Omega_1} - \frac{1}{\Omega_2}\frac{T_1}{\rho} - \frac{1}{\Omega_1}B} \\ - \frac{\Omega_1}{\theta_{FD}\rho\Omega_{LI}+\Omega_1} \frac{\Omega_2 T_2}{\Omega_1+\Omega_2 T_2} \frac{1}{A'\Omega_{LI}-1} e^{B' - \frac{\theta_{FD}}{\Omega_1}} \end{aligned} \tag{5.14}$$

where $A = T_2(T_1+1)$, $B = \frac{1}{\rho}(T_1+1)T_2$, $A' = \frac{1}{\Omega_2} + A\left(-\frac{1}{\Omega_2}\frac{1}{T_2} - \frac{1}{\Omega_1}\right)$, $B' = \frac{1}{\Omega_2}\frac{1}{\rho} + \left(-\frac{1}{\Omega_2}\frac{1}{T_2} - \frac{1}{\Omega_1}\right)B$ *and* $\theta_{FD} = \max\left(\frac{T_2}{\rho(a_1 - a_2 T_2)}, \frac{T_1}{\rho a_2}\right)$.

Corollary 12. *Define* $\phi_1 = 2^{2R_1} - 1$ *where* R_1 *is the target rate of the* $D_2 \rightarrow$ relay $\rightarrow D_1$ *link. The outage probabilities in the HD CNOMA scheme with ipSIC and pSIC are respectively*

$$\begin{aligned} P_{D_1}^{HD,ipSIC} &= 1 - \frac{1}{\Omega_g\Omega_2 Q_4^{HD} Q_5^{HD}} e^{-\frac{1}{\Omega_1}\frac{1}{\rho}\phi_2 - \frac{1}{\rho}Q_4^{HD}\phi_1} \\ &\times \left(U\left(Q_2^{HD} - Q_1^{HD}\right) \frac{1}{\Omega_g Q_3^{HD}} e^{-\frac{Q_2^{HD}}{\Omega_1}} + U\left(Q_1^{HD} - Q_2^{HD}\right) \left(e^{-\frac{Q_1^{HD}}{\Omega_1}} - e^{-\frac{a_2\left(Q_1^{HD} - Q_2^{HD}\right)}{\Omega_g\phi_1} - \frac{Q_1^{HD}}{\Omega_1}} \right) \right. \\ &\left. + U\left(Q_1^{HD} - Q_2^{HD}\right) \frac{1}{\Omega_g Q_3^{HD}} e^{-\frac{Q_2^{HD}}{\Omega_1} - Q_3^{HD}\left(Q_1^{HD} - Q_2^{HD}\right)\frac{a_2}{\phi_1}} \right) \end{aligned} \tag{5.15}$$

$$P_{D_1}^{HD,pSIC} = 1 - \frac{\Omega_1}{\Omega_2\phi_2 + \Omega_1} e^{-\frac{1}{\Omega_1}\theta_{HD} - \frac{\phi_2}{\Omega_1\rho} - \frac{\phi_1\phi_2}{\Omega_1\rho} - \frac{\phi_1}{\Omega_2\rho}} \tag{5.16}$$

where $Q_1^{HD} = \frac{\phi_2}{\rho(a_1 - a_2\phi_2)}$, $Q_2^{HD} = \frac{\phi_1}{\rho a_2}$, $Q_3^{HD} = \frac{1}{\Omega_g} + \frac{1}{\Omega_1}\frac{\phi_1}{a_2}$, $Q_4^{HD} = \frac{1}{\Omega_2} + \frac{1}{\Omega_1}\phi_2$, $Q_5^{HD} = \frac{1}{\Omega_g} + \phi_1 Q_4^{HD}$ *and* $\theta_{HD} = \max\left(\frac{\phi_2}{\rho(a_1 - a_2\phi_2)}, \frac{\phi_1}{\rho a_2}\right)$.

5.3.2 Diversity Analysis

For more insights, we analyze the diversity order as defined in (5.17), by investigating the slope of the outage probability curves in the high SNR region.

$$d_{D_i}^{FD,pSIC/ipSIC} = -\lim_{\rho\to\infty} \frac{\log_{10} P_{D_i}^{FD,pSIC/ipSIC}(\rho)}{\log_{10}\rho};\ i = 1, 2. \tag{5.17}$$

5.3.2.1 Diversity Order of the $D_1 \rightarrow$ relay $\rightarrow D_2$ Link

Using (5.7) and $e^{-x} \approx 1 - x$, it can be readily shown that

$$\begin{aligned} \lim_{\rho\to\infty} P_{D_2}^{FD,pSIC} &= \lim_{\rho\to\infty} P_{D_2}^{FD,ipSIC} \\ &= 1 - \frac{\Omega_1}{\Omega_2 T_2+\Omega_1}\frac{\Omega_1}{\Omega_{LI} T_2+\Omega_1}\frac{\Omega_2(a_1-a_2T_2)}{T_2\Omega_{LI}+\Omega_2(a_1-a_2T_2)}. \end{aligned} \tag{5.18}$$

After substituting (5.18) into (5.17), we learn that the diversity orders of the $D_1 \rightarrow$ relay $\rightarrow D_2$ link with pSIC and ipSIC for FD CNOMA are zeros, i.e., $d_{D_2}^{FD,pSIC} = d_{D_2}^{FD,ipSIC} = 0$. Therefore, no matter whether the SIC is perfect or not, the diversity order of the $D_1 \rightarrow$ relay $\rightarrow D_2$ link is always equal to zero. That is to say pSIC cannot solve the zero diversity order issue. According to (5.1) and (5.3), we have $\lim_{\rho\to\infty} \gamma_{D_1\to r} = \frac{|h_{1r}|^2}{|h_{2r}|^2+|h_{LI_r}|^2}$ and $\lim_{\rho\to\infty} \gamma_{D_2,x_1} = \frac{|h_{r2}|^2 a_1}{|h_{r2}|^2 a_2+|h_{LI_2}|^2}$. When $\rho \rightarrow \infty$, these SINR values approximate to constants which are not related with ρ. Terms in their denominators are corresponding to the inter-user interference among superimposed NOMA signals and the residual LI caused by imperfect self-interference cancellation. Accordingly, the outage probability of the proposed FD CNOMA in (5.6) could not keep decreasing when $\rho \rightarrow \infty$. This means the effects of the increasing power are offset by these interference signals since the interference power values also get larger. Adopting pSIC or ipSIC makes no difference on the above analysis. Therefore based on (5.17), neither pSIC nor ipSIC can solve the zero diversity order issue caused by the inter-user interference and the residual LI.

Based on (5.11), the asymptotic outage probability of $D_1 \rightarrow$ relay $\rightarrow D_2$ for HD CNOMA is

$$\lim_{\rho\to\infty} P_{D_2}^{HDpSIC/ipSIC} = \frac{\Omega_2\phi_2}{\Omega_2\phi_2 + \Omega_1}. \tag{5.19}$$

Similary, after substituting (5.19) into (5.17), we learn that the diversity orders with both pSIC and ipSIC are zeros, i.e., $d_{D_2}^{HD,pSIC} = d_{D_2}^{HD,ipSIC} = 0$.

5.3.2.2 Diversity Order of the $D_2 \rightarrow$ relay $\rightarrow D_1$ Link

Using (5.13), the asymptotic outage probability expression of $P_{D_1}^{FD,ipSIC}$ as $\rho \rightarrow \infty$ is shown in (5.20).

$$\lim_{\rho\to\infty} P_{D_1}^{FD,ipSIC} = 1 - \left(\frac{1}{Q_8\Omega_{LI}} \frac{\Omega_1\Omega_2}{\Omega_g\Omega_1 T_1+\Omega_g\Omega_2 T_1 T_2+\Omega_1\Omega_2} - \frac{1}{\Omega_{LI}\Omega_1 Q_9 Q_{10}} \frac{1}{Q_9\Omega_g T_1 T_2+1}\right) \times \left(U\left(Q_2-Q_1\right) \frac{1}{\Omega_{LI}Q_4} \frac{\Omega_1}{\Omega_1+\Omega_g\rho Q_2} + U\left(Q_1-Q_2\right)\left(\frac{1}{\Omega_{LI}Q_3} \frac{Q_5}{Q_5+\Omega_g Q_3} + \frac{1}{\Omega_{LI}\Omega_g Q_4 Q_{11}} - \frac{1}{\Omega_{LI}\Omega_g Q_4 Q_6}\right)\right). \tag{5.20}$$

After substituting (5.20) into (5.17), we have $d_{D_1}^{FD,ipSIC} = 0$.

For the pSIC scheme, the asymptotic outage probability of $P_{D_1}^{FD,pSIC}$ when $\rho \rightarrow \infty$ is worked out based on (5.14), as presented in (5.21).

$$\lim_{\rho\to\infty} P_{D_1}^{FD,pSIC} = 1 - \left(\frac{\Omega_1\Omega_2}{\Omega_1\Omega_{LI}T_1+\Omega_2\Omega_{LI}A+\Omega_1\Omega_2} + \frac{\Omega_2 T_2}{\Omega_1+\Omega_2 T_2} \frac{1}{A'\Omega_{LI}-1}\right) \frac{\Omega_1}{\theta_{FD}\rho\Omega_{LI}+\Omega_1} \tag{5.21}$$

After substituting (5.21) into (5.17), we have $d_{D_1}^{FD,pSIC} = 0$. Therefore, the diversity order of the $D_2 \rightarrow$ relay $\rightarrow D_1$ link with pSIC or ipSIC is always equal to zero. According to (5.1), (5.2), (5.4) and (5.5), we have $\lim_{\rho\to\infty} \gamma_{D_1\rightarrow r} = \frac{|h_{1r}|^2}{|h_{2r}|^2+\left|h_{LI_r}\right|^2}$, $\lim_{\rho\to\infty} \gamma_{D_2\rightarrow r} = \frac{|h_{2r}|^2}{\varepsilon|g_r|^2+\left|h_{LI_r}\right|^2}$, $\lim_{\rho\to\infty} \gamma_{D_1,x_1} = \frac{|h_{r1}|^2 a_1}{|h_{r1}|^2 a_2+\left|h_{LI_1}\right|^2}$ and $\lim_{\rho\to\infty} \gamma_{D_1,x_2} = \frac{|h_{r1}|^2 a_2}{\varepsilon|g_D|^2+\left|h_{LI_1}\right|^2}$. These SINR values approximate to constants which are not related with ρ when $\rho \rightarrow \infty$. Terms in their denominators are corresponding to the inter-user interference, the residual LI and the residual IS caused by ipSIC. Accordingly, the outage probability of the proposed FD CNOMA in (5.12) cannot keep decreasing when $\rho \rightarrow \infty$. Even if pSIC is adopted, the above analysis still holds due to the unavoidable interference signals. Therefore based on (5.17), pSIC and ipSIC make no differences on the zero diversity order issue caused by the inter-user interference and the residual LI.

Based on (5.15) and (5.16), the asymptotic outage probabilities of the $D_2 \rightarrow$ relay $\rightarrow D_1$ link with ipSIC and pSIC for HD CNOMA respectively equal

$$\lim_{\rho\to\infty} P_{D_1}^{HD,ipSIC} = 1 - \frac{1}{\Omega_8^2\Omega_2 Q_3^{HD} Q_4^{HD} Q_5^{HD}} \tag{5.22}$$

$$\lim_{\rho\to\infty} P_{D_1}^{HD,pSIC} = \frac{\Omega_2\phi_2}{\Omega_2\phi_2+\Omega_1}. \tag{5.23}$$

After substituting (5.22) and (5.23) into (5.17), we learn that the diversity orders for

HD CNOMA of the $D_2 \rightarrow$ relay $\rightarrow D_1$ link with ipSIC and pSIC are zeros, i.e., $d_{D_1}^{HD,ipSIC} = d_{D_1}^{HD,pSIC} = 0$.

Remark 11. *The diversity orders of outage probabilities of both links with pSIC and ipSIC for FD CNOMA and HD CNOMA are equal to zeros. Therefore, outage probability floors exist for these outage probability curves. Considering the NOMA protocol, a node suffers from the interference from other signals when it first decodes the signal with larger power. Such interference is defined as the inter-user interference in this chapter. The use of pSIC is incapable of overcoming the zero diversity order issue since the inter-user interference is unavoidable in a NOMA scheme.*

5.3.3 Throughput in Delay-Limited Transmission Mode

The two users D_1 and D_2 are supposed to receive information at target rates R_1 and R_2, respectively. Under the delay-limited transmission mode [30, 31], the system throughput of our proposed FD CNOMA system is subject to the impact of outage. Thus, the throughput of the proposed FD CNOMA system with pSIC and ipSIC can be written as

$$\begin{aligned} &R_l^{FD,pSIC/ipSIC} = \\ &\left(1 - P_{D_1}^{FD,pSIC/ipSIC}\right) R_1 + \left(1 - P_{D_2}^{FD,pSIC/ipSIC}\right) R_2 \end{aligned} \tag{5.24}$$

where $P_{D_2}^{FD,pSIC/ipSIC}$ and $P_{D_1}^{FD,pSIC/ipSIC}$ are obtained from (5.7), (5.13) and (5.14). Similarly, the throughput for HD CNOMA with pSIC/ipSIC under the delay-limited transmission mode is

$$\begin{aligned} &R_l^{HD,pSIC/ipSIC} = \\ &\left(1 - P_{D_1}^{HD,pSIC/ipSIC}\right) R_1 + \left(1 - P_{D_2}^{HD,pSIC/ipSIC}\right) R_2 \end{aligned} \tag{5.25}$$

where $P_{D_2}^{HD,pSIC/ipSIC}$ and $P_{D_1}^{HD,pSIC/ipSIC}$ are obtained from (5.11), (5.15) and (5.16).

5.3.4 Ergodic Rate

5.3.4.1 Ergodic Rate of the $D_1 \rightarrow$ relay $\rightarrow D_2$ Link

Based on (5.1) and (5.3), the ergodic rates of the $D_1 \rightarrow$ relay $\rightarrow D_2$ link with pSIC and ipSIC are the same. Since the signal x_1 should be detected both by the relay and by D_2, the achievable rates of the $D_1 \rightarrow$ relay $\rightarrow D_2$ link in our FD CNOMA scheme with both pSIC and ipSIC can be expressed as

$$R_{D_2}^{FD,pSIC} = R_{D_2}^{FD,ipSIC} = \log\left(1 + \min\left(\gamma_{D_1 \rightarrow r}, \gamma_{D_2,x_1}\right)\right). \tag{5.26}$$

Thus the corresponding ergodic achievable rates are given by

$$\begin{aligned} &E\left[R_{D_2}^{FD,pSIC}\right] = E\left[R_{D_2}^{FD,ipSIC}\right] = \\ &E\left[\log\left(1 + \underbrace{\min\left(\gamma_{D_1 \rightarrow r}, \gamma_{D_2,x_1}\right)}_{Z}\right)\right] = \frac{1}{\ln 2}\int_0^{\infty} \frac{1-F_Z(z)}{1+z} dz \end{aligned} \tag{5.27}$$

where $Z = \min\left(\gamma_{D_1 \rightarrow r},\ \gamma_{D_2,x_1}\right)$ and $F_Z(z)$ denotes the CDF of Z. Obviously, it is difficult to work out $F_Z(z)$. Considering the subsequent even more complicated derivation based on $F_Z(z)$ to derive $E\left[R_{D_2}^{FD,pSIC/ipSIC}\right]$, similarly with [129], this chapter focuses on the high SNR region and presents the high SNR approximation $E\left[R_{D_2}^{FD,pSIC/ipSIC,\infty}\right]$. In this way, we manage to derive a closed-form expression for this ergodic rate to make the performance evaluation possible.

When $\rho \rightarrow \infty$, we have $\lim\limits_{\rho\rightarrow\infty} \gamma_{D_1 \rightarrow r} = \frac{|h_{1r}|^2}{|h_{2r}|^2 + \left|h_{LI_r}\right|^2}$ and $\lim\limits_{\rho\rightarrow\infty} \gamma_{D_2,x_1} = \frac{|h_{r2}|^2 a_1}{|h_{r2}|^2 a_2 + \left|h_{LI_2}\right|^2}$. Thus,

$$\begin{aligned} &\lim_{\rho\rightarrow\infty} \min\left(\gamma_{D_1 \rightarrow r}, \gamma_{D_2,x_1}\right) \\ &= \underbrace{\min\left(\frac{|h_{1r}|^2}{|h_{2r}|^2 + \left|h_{LI_r}\right|^2}, \frac{|h_{r2}|^2 a_1}{|h_{r2}|^2 a_2 + \left|h_{LI_2}\right|^2}\right)}_{Y}. \end{aligned} \tag{5.28}$$

$$\begin{aligned} &F_Y(y) = \\ &1 - \Pr\left(\frac{|h_{1r}|^2}{|h_{2r}|^2 + \left|h_{LI_r}\right|^2} > y\right) \Pr\left(\frac{|h_{r2}|^2 a_1}{|h_{r2}|^2 a_2 + \left|h_{LI_2}\right|^2} > y\right). \end{aligned} \tag{5.29}$$

Theorem 7. *The asymptotic ergodic achievable rate of the $D_1 \rightarrow$ relay $\rightarrow D_2$ link with*

pSIC/ipSIC for our FD CNOMA scheme in the high SNR region is given by

$$\begin{aligned}\lim_{\rho\to\infty} E\left[R_{D_2}^{FD,pSIC/ipSIC}\right] &\triangleq E\left[R_{D_2}^{FD,pSIC/ipSIC,\infty}\right]\\ &= \tfrac{A_1}{\ln 2}\ln\left(1+\tfrac{a_1}{a_2}\right)+\tfrac{1}{\ln 2}\tfrac{B_1}{\Omega_{LI}-a_2\Omega_2}\ln\left(1+\tfrac{\Omega_{LI}-a_2\Omega_2}{a_2\Omega_2}\right)\\ &+\tfrac{1}{\ln 2}\tfrac{N_1}{\Omega_2}\ln\left(1+\tfrac{a_1\Omega_2}{a_2\Omega_1}\right)+\tfrac{1}{\ln 2}\tfrac{M_1}{\Omega_{LI}}\ln\left(1+\tfrac{a_1\Omega_{LI}}{a_2\Omega_1}\right)\end{aligned} \tag{5.30}$$

where $A_1 = \frac{\Omega_1^2\Omega_2}{(\Omega_1-\Omega_2)(\Omega_2-\Omega_{LI})(\Omega_1-\Omega_{LI})}$, $B_1 = \frac{a_1\Omega_{LI}\Omega_1^2\Omega_2(\Omega_{LI}-a_2\Omega_2)^2}{(\Omega_{LI}-\Omega_2)\left(\Omega_{LI}\Omega_1-a_1\Omega_2^2-a_2\Omega_1\Omega_2\right)(\Omega_{LI}\Omega_1-a_1\Omega_{LI}\Omega_2-a_2\Omega_1\Omega_2)}$, $M_1 = \frac{(a_1\Omega_{LI}+a_2\Omega_1)\Omega_{LI}^2\Omega_1\Omega_2}{(\Omega_{LI}-\Omega_1)(a_1\Omega_{LI}\Omega_2+a_2\Omega_1\Omega_2-\Omega_{LI}\Omega_1)(\Omega_{LI}-\Omega_2)}$ *and* $N_1 = \frac{(a_1\Omega_2+a_2\Omega_1)\Omega_1\Omega_2^3}{(\Omega_2-\Omega_1)\left(a_1\Omega_2^2+a_2\Omega_1\Omega_2-\Omega_{LI}\Omega_1\right)(\Omega_2-\Omega_{LI})}$.

Proof. See Appendix 5. □

Corollary 13. *The asymptotic ergodic achievable rate of the* $D_1 \to$ relay $\to D_2$ *link for HD CNOMA with pSIC/ipSIC in the high SNR region is given by*

$$\begin{aligned}E\left[R_{D_2}^{HD,pSIC,\infty}\right] &= E\left[R_{D_2}^{HD,ipSIC,\infty}\right]\\ &= \tfrac{A_2}{2\ln 2}\ln\left(1+\tfrac{a_1}{a_2}\right)+\tfrac{B_2}{2\ln 2}\tfrac{1}{\Omega_2}\ln\left(1+\tfrac{a_1\Omega_2}{a_2\Omega_1}\right)\end{aligned} \tag{5.31}$$

where $A_2 = \frac{\Omega_1}{\Omega_1-\Omega_2}$ *and* $B_2 = \frac{\Omega_1\Omega_2}{\Omega_2-\Omega_1}$.

5.3.4.2 Ergodic Rate of the $D_2 \to$ relay $\to D_1$ Link

In this subsection, we assume that both the relay and D_1 successfully detect x_1 according to the inherent definition of ergodic rate at the beginning of this section. Then the achievable rate of the $D_2 \to$ relay $\to D_1$ link is

$$R_{D_1}^{FD} = \log\left(1+\min\left(\gamma_{D_2\to r},\gamma_{D_1,x_2}\right)\right). \tag{5.32}$$

Theorem 8. *The ergodic achievable rate of the* $D_2 \to$ relay $\to D_1$ *link for FD CNOMA with ipSIC when* $\varepsilon = 1$ *is given by*

$$\begin{aligned}E\left[R_{D_1}^{FD,ipSIC}\right] &= -\tfrac{F_1}{\ln 2}e^{\mu}\mathrm{Ei}\left(-\mu\right)\\ &-\tfrac{F_2}{\ln 2}e^{\frac{\Omega_2}{\Omega_{LI}}\mu}\mathrm{Ei}\left(-\tfrac{\Omega_2}{\Omega_{LI}}\mu\right)-\tfrac{F_3}{\ln 2}e^{\frac{\Omega_2}{\Omega_g}\mu}\mathrm{Ei}\left(-\tfrac{\Omega_2}{\Omega_g}\mu\right)\\ &-\tfrac{F_4}{\ln 2}e^{\frac{\Omega_1 a_2}{\Omega_{LI}}\mu}\mathrm{Ei}\left(-\tfrac{\Omega_1 a_2}{\Omega_{LI}}\mu\right)-\tfrac{F_5}{\ln 2}e^{\frac{\Omega_1 a_2}{\Omega_g}\mu}\mathrm{Ei}\left(-\tfrac{\Omega_1 a_2}{\Omega_g}\mu\right)\end{aligned} \tag{5.33}$$

where $\mathrm{Ei}(\cdot)$ *represents the exponential integral function [132].* $\mu = \frac{1}{\Omega_2}\frac{1}{\rho}+\frac{1}{\Omega_1}\frac{1}{\rho a_2}$, $F_1 = \frac{\Omega_2^2a_2^2\Omega_1^2}{\Omega_2-\Omega_{LI}}\times\frac{1}{(\Omega_2-\Omega_g)(\Omega_1a_2-\Omega_{LI})(\Omega_1a_2-\Omega_g)}$, $F_2 = \frac{\Omega_2^2a_2^2\Omega_1^2\Omega_{LI}^2}{(\Omega_{LI}-\Omega_2)(\Omega_2\Omega_{LI}-\Omega_g\Omega_2)(\Omega_1a_2-\Omega_2)(\Omega_{LI}\Omega_1a_2-\Omega_g\Omega_2)}$, $F_3 = \frac{\Omega_2^2a_2^2\Omega_1^2\Omega_g^2}{\Omega_g-\Omega_2}\times\frac{1}{(\Omega_2\Omega_g-\Omega_{LI}\Omega_2)(\Omega_1\Omega_ga_2-\Omega_{LI}\Omega_2)(\Omega_1a_2-\Omega_2)}$, $F_4 = \frac{\Omega_2^2a_2^2\Omega_1^2\Omega_{LI}^2}{(\Omega_{LI}-\Omega_1a_2)(\Omega_2-\Omega_1a_2)(\Omega_2\Omega_{LI}-\Omega_g\Omega_1a_2)(\Omega_1\Omega_{LI}a_2-\Omega_g\Omega_1a_2)}$ *and* $F_5 = \frac{\Omega_2^2a_2^2\Omega_1^2\Omega_g^2}{(\Omega_g-\Omega_1a_2)(\Omega_2\Omega_g-\Omega_{LI}\Omega_1a_2)(\Omega_2-\Omega_1a_2)(\Omega_1\Omega_ga_2-\Omega_{LI}\Omega_1a_2)}$.

Proof. See Appendix 5. □

Corollary 14. *For the special case $\varepsilon = 0$, the ergodic rate of the $D_2 \rightarrow$ relay $\rightarrow D_1$ link with pSIC in the proposed FD CNOMA scheme is*

$$\begin{aligned} & E\left[R_{D_1}^{FD,pSIC}\right] \\ &= \tfrac{A_3}{\ln 2}\left(-e^{\mu}\mathrm{Ei}\left(-\mu\right)\right) + \tfrac{B_3}{\ln 2}\left(-e^{\frac{a_2\Omega_1}{\Omega_{LI}}\mu}\mathrm{Ei}\left(-\tfrac{a_2\Omega_1}{\Omega_{LI}}\mu\right)\right) \\ &+ \tfrac{C_3}{\ln 2}\left(-e^{\frac{\Omega_2}{\Omega_{LI}}\mu}\mathrm{Ei}\left(-\tfrac{\Omega_2}{\Omega_{LI}}\mu\right)\right) \end{aligned} \tag{5.34}$$

where $A_3 = \frac{a_2\Omega_1\Omega_2}{(a_2\Omega_1-\Omega_{LI})(\Omega_2-\Omega_{LI})}$, $B_3 = \frac{a_2\Omega_1\Omega_2}{(\Omega_{LI}-a_2\Omega_1)(\Omega_2-a_2\Omega_1)}$ *and* $C_3 = \frac{a_2\Omega_1\Omega_2}{(\Omega_{LI}-\Omega_2)(a_2\Omega_1-\Omega_2)}$.

Corollary 15. *The ergodic achievable rates of the $D_2 \rightarrow$ relay $\rightarrow D_1$ link for HD CNOMA with ipSIC and pSIC are respectively given by*

$$\begin{aligned} E\left[R_{D_1}^{HD,ipSIC}\right] &= -\tfrac{F_6}{2\ln 2}e^{\mu}\mathrm{Ei}\left(-\mu\right) \\ &-\tfrac{F_7}{2\ln 2}e^{\frac{\Omega_2}{\Omega_g}\mu}\mathrm{Ei}\left(-\tfrac{\Omega_2}{\Omega_g}\mu\right) - \tfrac{F_8}{2\ln 2}e^{\frac{\Omega_1 a_2}{\Omega_g}\mu}\mathrm{Ei}\left(-\tfrac{\Omega_1 a_2}{\Omega_g}\mu\right) \end{aligned} \tag{5.35}$$

$$E\left[R_{D_1}^{HD,pSIC}\right] = -\tfrac{1}{2\ln 2}e^{\mu}\mathrm{Ei}\left(-\mu\right). \tag{5.36}$$

where $F_6 = \frac{\Omega_2 a_2\Omega_1}{(\Omega_2-\Omega_g)(\Omega_1 a_2-\Omega_g)}$, $F_7 = \frac{\Omega_2 a_2\Omega_1}{(\Omega_g-\Omega_2)(\Omega_1 a_2-\Omega_2)}$ *and* $F_8 = \frac{\Omega_2 a_2\Omega_1}{(\Omega_g-\Omega_1 a_2)(\Omega_2-\Omega_1 a_2)}$.

5.3.5 Spatial Multiplexing Gain

According to Chapter 4, we evaluate the slope of the ergodic rate curve in the high SNR region. Its physical meaning is spatial multiplexing gain. The slope of ergodic rate for FD CNOMA in high SNR region is

$$S_{D_i}^{FD,pSIC/ipSIC} \triangleq \lim_{\rho\to\infty}\frac{E\left[R_{D_i}^{FD,pSIC/ipSIC}(\rho)\right]}{\log_{10}\rho}; \quad i = 1, 2. \tag{5.37}$$

5.3.5.1 Spatial Multiplexing Gain of the $D_1 \rightarrow$ relay $\rightarrow D_2$ Link

According to (5.30) and (5.37), we have $S_{D_2}^{FD,pSIC/ipSIC} = 0$. Similarly, we have $S_{D_2}^{HD,pSIC} = S_{D_2}^{HD,ipSIC} = 0$ based on (5.31).

5.3.5.2 Spatial Multiplexing Gain of the $D_2 \rightarrow$ relay $\rightarrow D_1$ Link

In the high SNR region where ρ is very large, μ of (5.33) becomes very small. We apply the approximation $\mathrm{Ei}(-v) \approx \ln(v) + C_E$ where v is very small to (5.33) and C_E is the Euler constant [132]. Then on the basis of (5.33), the asymptotic ergodic achievable rate with ipSIC of the $D_2 \rightarrow$ relay $\rightarrow D_1$ link for FD CNOMA is given by

$$\begin{aligned}
&\lim_{\rho\to\infty} E\left[R_{D_1}^{FD,ipSIC}\right] \triangleq E\left[R_{D_1}^{FD,ipSIC,\infty}\right] \\
&= -\tfrac{F_1}{\ln 2}\left(\ln(\mu) + C_E\right) - \tfrac{F_2}{\ln 2}\left(\ln\left(\tfrac{\Omega_2}{\Omega_{LI}}\mu\right) + C_E\right) \\
&\quad - \tfrac{F_3}{\ln 2}\left(\ln\left(\tfrac{\Omega_2}{\Omega_g}\mu\right) + C_E\right) - \tfrac{F_4}{\ln 2}\left(\ln\left(\tfrac{\Omega_1 a_2}{\Omega_{LI}}\mu\right) + C_E\right) \\
&\quad - \tfrac{F_5}{\ln 2}\left(\ln\left(\tfrac{\Omega_1 a_2}{\Omega_g}\mu\right) + C_E\right).
\end{aligned} \tag{5.38}$$

After substituting (5.38) into (5.37), we obtain

$$\begin{aligned}
S_{D_1}^{FD,ipSIC} &= \lim_{\rho\to\infty} \frac{E\left[R_{D_1}^{FD,ipSIC,\infty}(\rho)\right]}{\log_{10}\rho} \\
&= (F_1 + F_2 + F_3 + F_4 + F_5)\log 10 = 0.
\end{aligned} \tag{5.39}$$

For the situation of pSIC, the asymptotic ergodic rate of the $D_2 \rightarrow$ relay $\rightarrow D_1$ link when $\rho \rightarrow \infty$ for FD CNOMA is written as (5.40), according to (5.34).

$$\begin{aligned}
&\lim_{\rho\to\infty} E\left[R_{D_1}^{FD,pSIC}\right] \triangleq E\left[R_{D_1}^{FD,pSIC,\infty}\right] \\
&= -\tfrac{A_3(\ln(\mu)+C_E)}{\ln 2} - \tfrac{B_3(\ln(\frac{a_2\Omega_1\mu}{\Omega_{LI}})+C_E)}{\ln 2} - \tfrac{C_3(\ln(\frac{\Omega_2\mu}{\Omega_{LI}})+C_E)}{\ln 2}.
\end{aligned} \tag{5.40}$$

After substituting (5.40) into (5.37), we obtain

$$\begin{aligned}
S_{D_1}^{FD,pSIC} &= \lim_{\rho\to\infty} \frac{E\left[R_{D_1}^{FD,pSIC,\infty}(\rho)\right]}{\log_{10}\rho} \\
&= \tfrac{\ln 10}{\ln 2}(A_3 + B_3 + C_3) = 0.
\end{aligned} \tag{5.41}$$

Similarly, asymptotic ergodic achievable rates for HD CNOMA with ipSIC and pSIC in the high SNR region respectively equal

$$\begin{aligned}
&E\left[R_{D_1}^{HD,ipSIC,\infty}\right] = -\tfrac{F_6}{2\ln 2}\left(\ln(\mu) + C_E\right) \\
&-\tfrac{F_7}{2\ln 2}\left(\ln\left(\tfrac{\Omega_2}{\Omega_g}\mu\right) + C_E\right) - \tfrac{F_8}{2\ln 2}\left(\ln\left(\tfrac{\Omega_1 a_2}{\Omega_g}\mu\right) + C_E\right)
\end{aligned} \tag{5.42}$$

$$E\left[R_{D_1}^{HD,pSIC,\infty}\right] = -\frac{1}{2\ln 2}\left(\ln\mu + C_E\right). \tag{5.43}$$

By substituting (5.42) and (5.43) into (5.37), we learn that

$$S_{D_1}^{HD,ipSIC} = \frac{1}{2}(F_6 + F_7 + F_8)\log 10 = 0 \tag{5.44}$$

$$S_{D_1}^{HD,pSIC} = \lim_{\rho\to\infty} \frac{-\frac{1}{2\ln 2}(\ln\mu + C_E)}{\log_{10}\rho} = \frac{\ln 10}{2\ln 2} = 1.66. \tag{5.45}$$

Remark 12. *According to the calculation results* $S_{D_2}^{FD,pSIC/ipSIC} = S_{D_1}^{FD,pSIC} = S_{D_1}^{FD,ipSIC} = 0$*, the ergodic achievable rates of the* $D_1 \rightarrow$ relay $\rightarrow D_2$ *and* $D_2 \rightarrow$ relay $\rightarrow D_1$ *links for FD CNOMA converge to ergodic rate ceilings in the high SNR region due to the residual LI and the inter-user interference. Also, pSIC is incapable of overcoming the ergodic rate ceiling issue, since the realistic assumption of imperfect self-interference cancellation is considered in this chapter and thus the residual LI always exists.*

Remark 13. *For the* $D_2 \rightarrow$ relay $\rightarrow D_1$ *link in a HD CNOMA scheme with pSIC,* $\gamma_{D_2 \rightarrow r} = |h_{2r}|^2 \rho$ *and* $\gamma_{D_1,x_2} = |h_{r1}|^2 \rho a_2$ *which are both linear with* ρ*. According to* (5.32)*, the ergodic rate keeps getting larger as* ρ *increases. Thus compared with ipSIC, the situation of pSIC overcomes the ergodic rate ceiling issue of the* $D_2 \rightarrow$ relay $\rightarrow D_1$ *link for HD CNOMA.*

5.3.6 Throughput in Delay-Tolerant Transmission Mode

The system throughput of the FD CNOMA scheme in the delay-tolerant transmission mode is determined by evaluating the ergodic rates. Based on (5.30), (5.33) and (5.34), the throughput of the FD CNOMA scheme with pSIC/ipSIC is given by

$$\begin{aligned} &R_t^{FD,pSIC/ipSIC} = \\ &E\left[R_{D_1}^{FD,pSIC/ipSIC}\right] + E\left[R_{D_2}^{FD,pSIC/ipSIC}\right]. \end{aligned} \tag{5.46}$$

Similarly, the throughput in the delay-tolerant transmission mode of the HD CNOMA system with pSIC/ipSIC is given by (5.47) based on (5.31), (5.35) and (5.36).

$$\begin{aligned} &R_t^{HD,pSIC/ipSIC} = \\ &E\left[R_{D_1}^{HD,pSIC/ipSIC}\right] + E\left[R_{D_2}^{HD,pSIC/ipSIC}\right]. \end{aligned} \tag{5.47}$$

5.4 Numerical Results

We compare the performance of our proposed FD CNOMA scheme with the benchmarks, namely HD CNOMA and COMA, for bi-directional communication. In the case of COMA, the entire information exchange process is divided into four time slots.

Table 5.1: Simulation Parameters

Parameter	Value
Distance between D_1 and relay	$d = 0.3$ [129]
Target rate of the $D_2 \rightarrow$ relay $\rightarrow D_1$ link	$R_1 = 3$ BPCU [129]
Target rate of the $D_1 \rightarrow$ relay $\rightarrow D_2$ link	$R_2 = 1$ BPCU [129]
Mean values of the LI and IS channel power gains	$\Omega_{LI} = -15$ dB [129], $\Omega_g = -20$ dB [66]
Power allocation coefficients	$a_1 = 0.8$, $a_2 = 0.2$ [66]
Path-loss exponent	$\alpha = 4$ [133]

Both HD CNOMA and COMA systems are not affected by LI. In the following simulation figures, "FD", "HD" and "OMA" are used to denote the proposed FD CNOMA scheme and the two benchmarks. Link #1 denotes the $D_1 \rightarrow$ relay $\rightarrow D_2$ link and Link #2 denotes the $D_2 \rightarrow$ relay $\rightarrow D_1$ link. Without loss of generality, the D_1—relay—D_2 distance is normalized to unity. We then denote the D_1—relay distance as d and the relay—D_2 distance as $1 - d$. We also assume that the mean values of channel power gains $\Omega_{1r} = \Omega_{r1} = \Omega_1 = d^{-\alpha}$ and $\Omega_{2r} = \Omega_{r2} = \Omega_2 = (1-d)^{-\alpha}$, where α is the path-loss exponent. Unless otherwise stated, all simulation parameters are summarized in Table 5.1.

5.4.1 Outage Probability

Figure 5.2 plots the analytical and simulated outage probabilities of the transmission links (Link #1 and Link #2) with both pSIC and ipSIC versus the transmit SNR for our proposed FD CNOMA system and HD CNOMA. As stated in the performance analysis section, the outage probability of Link #1 is not affected by ipSIC. And the analytical outage probabilities of the two links for FD CNOMA with pSIC and ipSIC are plotted based on (5.7), (5.13) and (5.14), respectively. Those for the HD CNOMA scheme with pSIC and ipSIC are plotted based on (5.11), (5.15) and (5.16), respectively. First, all of the analytical and the simulated results match each other very closely. Second, the FD CNOMA scheme always outperforms HD CNOMA in this experiment. On

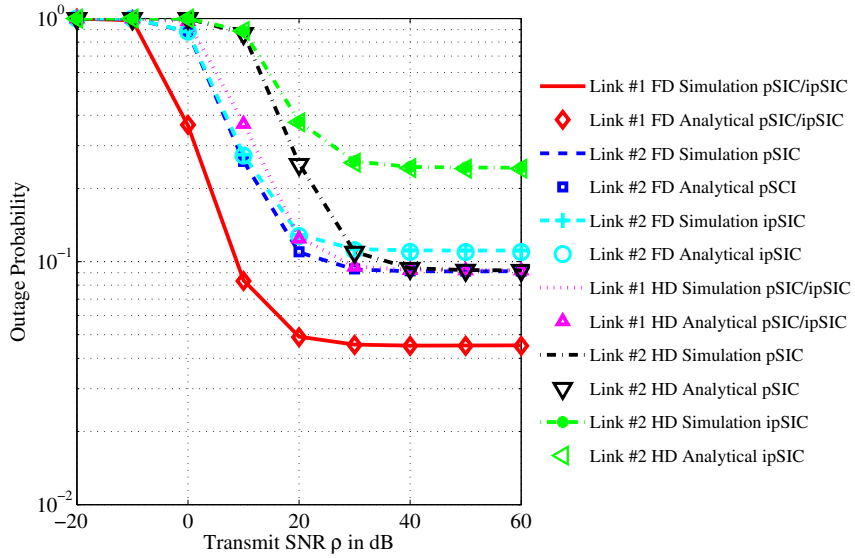

Figure 5.2: Analytical and simulated outage probabilities of the two transmission links versus transmit SNR (ρ) for the FD CNOMA system and the HD CNOMA system with pSIC/ipSIC.

the one hand, FD CNOMA suffers from LI but HD CNOMA does not. On the other hand, the required SNR value corresponding to a given target rate is smaller for FD CNOMA compared with HD CNOMA, since FD CNOMA only requires one time slot to complete each information exchange process while HD CNOMA requires two. The overall effect gives FD CNOMA an advantage over HD CNOMA in terms of outage probability. Third, we learn that pSIC is capable of improving the outage performance of FD CNOMA and HD CNOMA, compared with ipSIC.

Figure 5.3 plots the asymptotic outage probabilities and the simulated outage probabilities of Link #1 and Link #2 with both pSIC and ipSIC for FD CNOMA and HD CNOMA. Link #1 is still not affected by ipSIC. The asymptotic outage probabilities of the two links for FD CNOMA with pSIC and ipSIC are plotted based on (5.18), (5.20) and (5.21). Those in the HD CNOMA scheme with pSIC and ipSIC are plotted based on (5.19), (5.22) and (5.23). We can observe that the asymptotic outage probabilities closely match the simulated outage probabilities in the high SNR region. Also, outage probability floors always exist in both links for both FD CNOMA and HD CNOMA with pSIC and ipSIC. Therefore, the corresponding diversity orders are zeros. Such

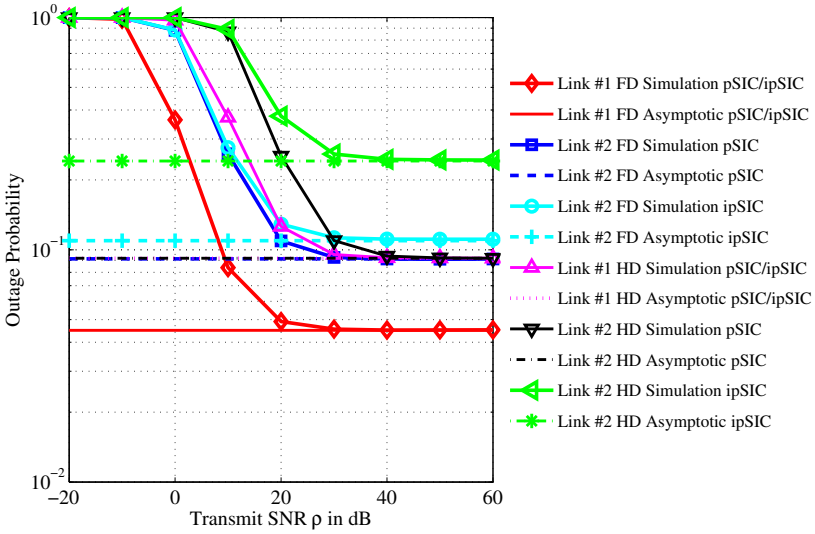

Figure 5.3: Asymptotic and simulated outage probabilities of the two transmission links versus transmit SNR (ρ) for the FD CNOMA system and the HD CNOMA system with pSIC/ipSIC.

phenomenon is caused by the following three factors, namely the residual interference caused by ipSIC, the residual LI in FD CNOMA systems caused by imperfect SIS techniques and the inter-user interference. It is noted that even if the considered system adopts HD CNOMA where LI does not exist, or it employs pSIC where residual IS does not exist, the outage probability still has a floor since the inter-user interference is unavoidable in NOMA.

Figure 5.4 plots the simulated outage probabilities of the two links for FD CNOMA, HD CNOMA and COMA. Since 4 time slots are used, COMA requires the largest SNR value to achieve the same target rate compared with HD CNOMA and FD CNOMA. In the meanwhile, FD CNOMA requires the lowest SNR value and HD CNOMA requires the second lowest. Figure 5.4 shows when the transmit SNR (ρ) is below 19 dB, the effect of the above-explained different levels of "required SNR" dominates. Hence, FD CNOMA obtains the lowest outage probability and HD CNOMA outperforms COMA. When the transmit SNR becomes very large, the performance of HD CNOMA is limited by the inter-user interference, and that of FD CNOMA is limited by the inter-user interference and LI. Under the condition of ipSIC, they are also limited by the residual

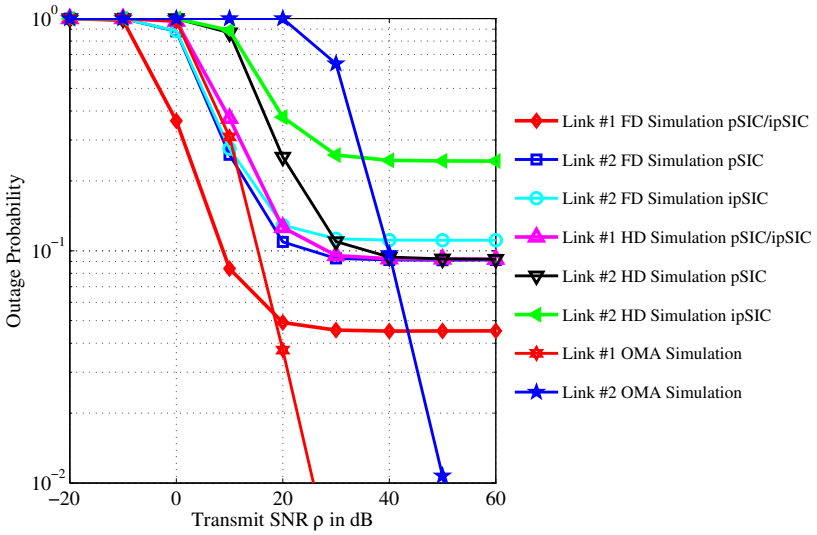

Figure 5.4: Simulated outage probabilities of the two transmission links versus transmit SNR (ρ) for the FD CNOMA system, HD CNOMA system, and COMA system with pSIC/ipSIC.

IS. Since COMA only suffers from the noise signal, its outage probability continues to decrease as the transmit SNR increases. Eventually, COMA will outperform FD CNOMA and HD CNOMA in the very high SNR region. Therefore, the outage performance of FD CNOMA is exceeded by COMA in the high SNR region (beyond 19 dB).

It is noted that even though outage probability curves of the FD CNOMA system in Fig. 5.4 have error floors, this does not mean FD CNOMA performs poorer than COMA. As stated in the simulation section of Chapter 3, LI signal can be suppressed to the same level with the noise floor according to [92, 93] and [96]. Current self-interference suppression techniques are capable of reducing the LI's power $\Omega_{LI}P_r$ to N_0, which means $\Omega_{LI} = \frac{1}{\rho}$. In Fig. 5.4, (15 dB, 0.07) meets the above-mentioned relationship between Ω_{LI} and ρ in real-world scenarios and it belongs to the FD CNOMA curve corresponding to $\Omega_{LI} = -15$ dB. FD CNOMA performs the best and has the lowest outage probability at this point. Therefore, in this experiment, FD CNOMA is already superior to HD CNOMA and COMA with existing self-interference suppression techniques. Given the rapid development of suppression techniques, the superior-

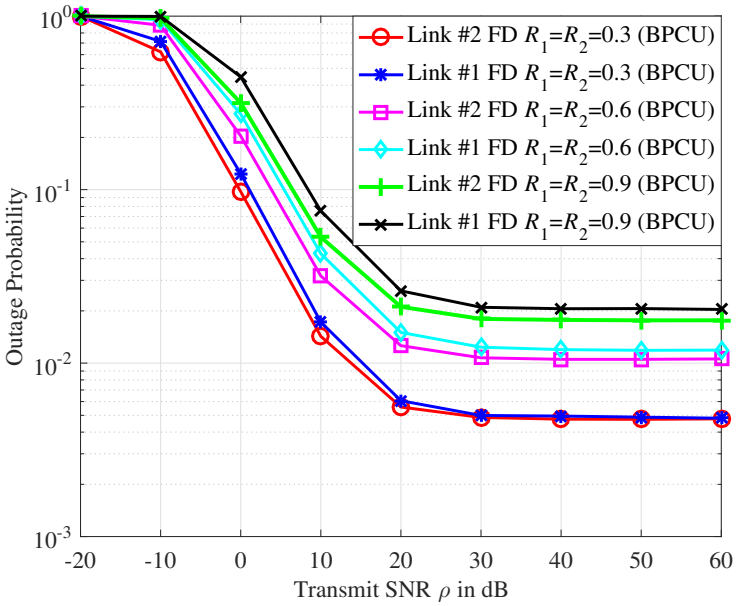

Figure 5.5: Simulated outage probabilities of the two transmission links versus transmit SNR (ρ) for the FD CNOMA system in case of ipSIC with different values of R_1 and R_2, where $d = 0.2$.

ity of FD CNOMA will be even more and more obvious.

Figure 5.5 presents the simulated outage probabilities of Link #1 and Link #2 with ipSIC versus the transmit SNR for our proposed FD CNOMA system, where target data transmission rates R_1 and R_2 are equal to 0.3 BPCU, 0.6 BPCU and 0.9 BPCU, respectively. It can be observed that an error floor exists in each outage probability curve for the FD CNOMA system. Another observation is that smaller target rate leads to better outage performance for both transmission links. When the target rate is smaller, it will be easier for the received SNR during decoding to be realized with a relatively small transmit SNR, so the successful communication probability gets larger and thus the outage probability gets smaller. The outage probability can be improved by properly changing parameter settings.

5.4.2 System Throughput in Delay-Limited Transmission Mode

Figure 5.6 plots the system throughput with both pSIC and ipSIC under the delay-limited transmission mode for FD CNOMA, HD CNOMA and COMA systems. For

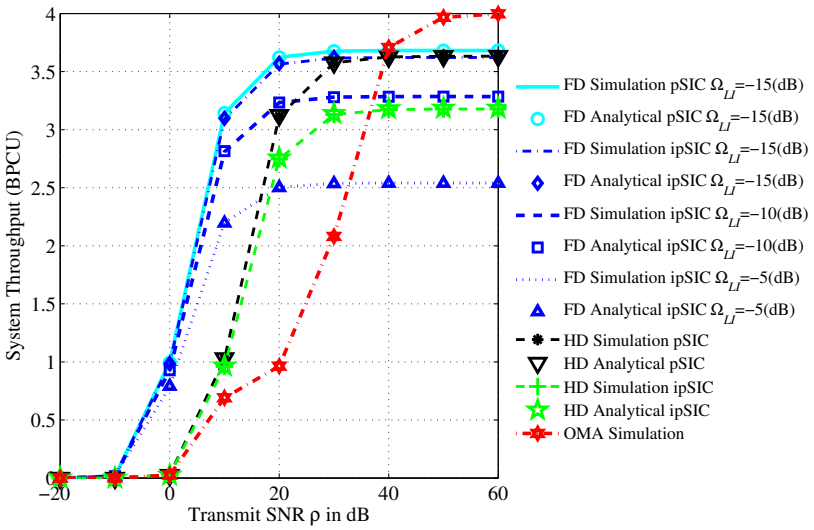

Figure 5.6: System throughput in the delay-limited transmission mode versus the transmit SNR.

FD CNOMA, the mean values of LI channel power gains are assumed as $\Omega_{LI} = -5, -10$ and -15 dB. The theoretical throughput values of the FD CNOMA system and HD CNOMA system with pSIC and ipSIC are calculated based on (5.24) and (5.25). We can observe that the analytical results closely match the simulation results. Moreover, as SNR gradually increases from a small value, the system throughput values for FD CNOMA, HD CNOMA and COMA systems increase as well. In the low SNR region (below 40 dB), FD CNOMA under both pSIC and ipSIC situations with $\Omega_{LI} = -15$ dB outperforms HD CNOMA and COMA systems due to its better outage performance as illustrated in Fig. 5.4. All of the throughput values in the high SNR region reach their steady states, which means they become constants and achieve individual throughput ceilings. The final throughput of FD CNOMA is smaller than that of COMA due to the outage probability floors as illustrated in Fig. 5.3. With smaller Ω_{LI} and hence lower interference, higher ultimate throughput will be achieved in the high SNR region just as expected. Therefore, it is important to design effective SIS techniques for FD CNOMA. Finally, similarly with outage performance, pSIC will further improve the system throughput compared with ipSIC.

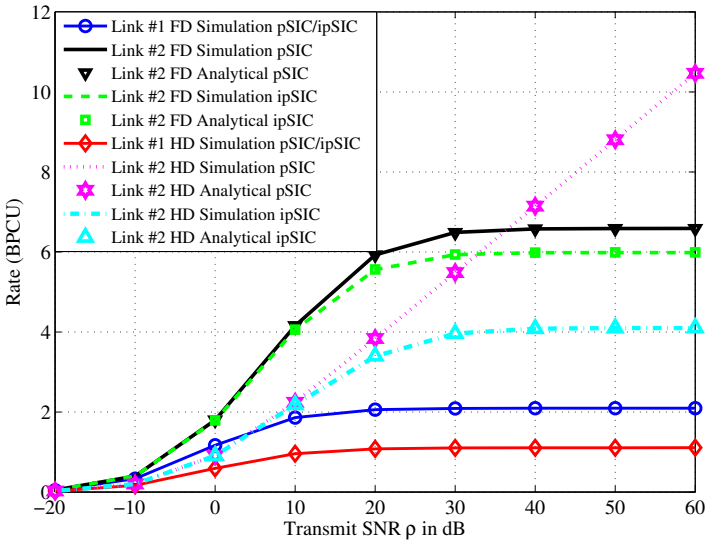

Figure 5.7: Analytical and simulated ergodic achievable rate versus transmit SNR with pSIC/ipSIC.

5.4.3 Ergodic Rate

Figure 5.7 plots the analytical and simulated ergodic achievable rates of the two transmission links with both pSIC and ipSIC for our proposed FD CNOMA system and HD CNOMA. The analytical ergodic rates of Link #2 for FD CNOMA and HD CNOMA with pSIC and ipSIC are plotted based on (5.33), (5.34), (5.35) and (5.36), respectively. The analytical ergodic rates of Link #1 have not been derived and hence they are not plotted. It can be observed that all of the analytical and simulated results match each other very closely. Also, the FD CNOMA scheme outperforms HD CNOMA in any SNR region due to FD CNOMA's less information exchange duration, except Link #2 under the situation of pSIC in the very high SNR region (beyond 36 dB). In such case, the impacts of interference in the FD CNOMA system dominate and thus HD CNOMA achieves the highest rate. It is noted that under the situation of ipSIC which is actually more practical in real-world systems, the proposed FD CNOMA always achieves larger ergodic rates for both links than HD CNOMA, regardless of the SNR value. As expected, pSIC still brings larger ergodic rates for both schemes compared with ipSIC.

Figure 5.8 plots the asymptotic and simulated ergodic achievable rates of the two

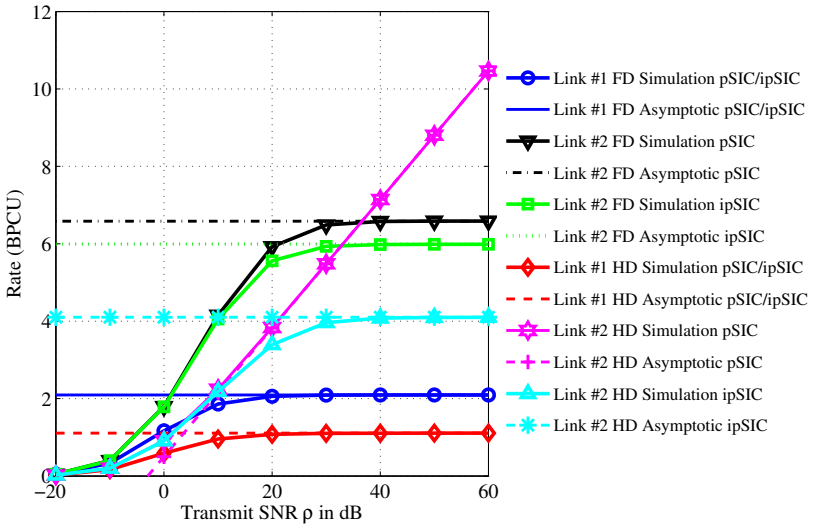

Figure 5.8: Asymptotic and simulated ergodic achievable rate versus transmit SNR with pSIC/ipSIC.

transmission links. The asymptotic ergodic rates of the two links for FD CNOMA with pSIC and ipSIC are plotted based on (5.30), (5.38) and (5.40). Those for HD CNOMA with pSIC and ipSIC are plotted based on (5.31), (5.42) and (5.43). We can observe that corresponding ergodic rates converge to their upper ceilings (asymptotic values) in the following cases, namely Link #1 and Link #2 in the FD CNOMA scheme with both pSIC and ipSIC, Link #1 in the HD CNOMA scheme with pSIC and ipSIC, and Link #2 in the HD CNOMA scheme with ipSIC. The slopes of these curves in the high SNR region are zeros. For Link #2 in the HD CNOMA scheme with pSIC, the ergodic achievable rate keeps increasing in the high SNR region. That is to say pSIC is capable of overcoming the issue of ergodic rate ceiling for Link #2 in the HD CNOMA scheme. The reason is that both $\gamma_{D_2 \to r}$ and γ_{D_1, x_2} are linear with ρ (see Remark 13). Considering the two points (30, 5.48) and (60, 10.46) on the curve in the high SNR region, the slope equals $4.98/30 = 0.166$. This result matches the calculation result in (5.45). The factor 10 appears between these two values because the denominator in (5.45) is in $\log 10(\cdot)$ but the x-axis in Fig. 5.8 is in dB, i.e., $10_{10} \log(\cdot)$.

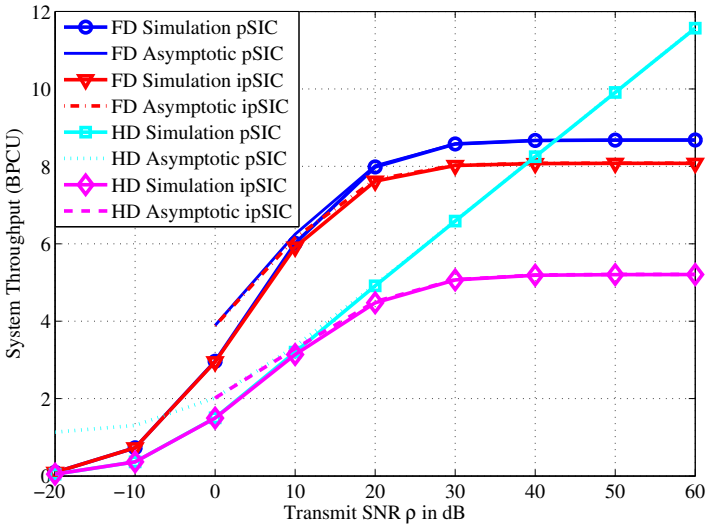

Figure 5.9: System throughput in the delay-tolerant transmission mode versus the transmit SNR.

5.4.4 System Throughput in Delay-Tolerant Transmission Mode

Figure 5.9 plots the system throughput with both pSIC and ipSIC under the delay-tolerant transmission mode for FD CNOMA and HD CNOMA. The asymptotic throughput values of the FD CNOMA and HD CNOMA systems with pSIC and ipSIC are worked out based on (5.46) and (5.47), respectively. We can observe that the simulation results closely approximate the asymptotic results in the high SNR region. As expected, pSIC brings larger system throughput for both FD CNOMA and HD CNOMA compared with ipSIC. Basically speaking, the proposed FD CNOMA scheme always achieves larger throughput except in the high SNR region (beyond 42 dB) with pSIC. The system throughput is in fact the summation of ergodic rates for Link #1 and Link #2, and thus the explanation and analysis can be found in Fig. 5.7 and Fig. 5.8.

FD CNOMA and HD CNOMA have been well compared hereinbefore. The major target of Fig. 5.10 is to compare FD CNOMA with another benchmark, i.e., COMA, in terms of ergodic rates for two transmission links and system throughput in the delay-tolerant transmission mode. Simulation parameters are listed in Table 5.1. It can be observed that the proposed FD CNOMA scheme achieves larger ergodic rates

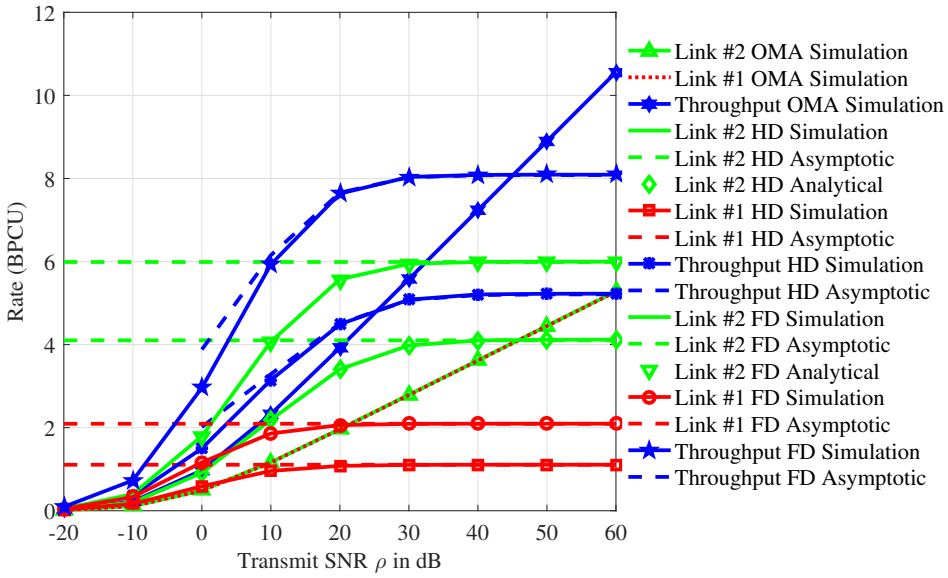

Figure 5.10: Ergodic rates and system throughput in the delay-tolerant transmission mode versus the transmit SNR for FD CNOMA, HD CNOMA and COMA with ipSIC.

for both Link #1 and Link #2 and larger system throughput than COMA in the low SNR region. However, the performance of FD CNOMA will be exceeded in the high SNR region. As we know, LI signal can be suppressed to the same level with the noise floor according to [92, 93] and [96]. Current self-interference suppression techniques are capable of reducing the LI's power $\Omega_{LI}P_r$ to N_0, which means $\Omega_{LI} = \frac{1}{\rho}$. In Fig. 5.10, (15 dB, 6.9 BPCU), (15 dB, 4.9 BPCU) and (15 dB, 2 BPCU) meet the above-mentioned relationship between Ω_{LI} and ρ in real-world scenarios and they belong to the FD CNOMA curves corresponding to $\Omega_{LI} = -15$ dB. In this experiment, FD CNOMA performs the best and has the largest system throughput and largest ergodic rates at these points. Therefore, by comparison, we conclude that FD CNOMA is superior to COMA in real-world scenarios with practical self-interference suppression capabilities in terms of ergodic rates and system throughput.

5.5 Summary

This chapter has proposed a CNOMA system in which both the relay and the two users (D_1 and D_2) operate in the FD mode. The users intend to exchange information with the assistance of the relay. The performance of the proposed FD CNOMA system with both pSIC and ipSIC has been investigated comprehensively. The closed-form outage probability expressions of the two transmission links $D_1 \rightarrow$relay$\rightarrow D_2$ and $D_2 \rightarrow$relay$\rightarrow D_1$, and the expressions of the system throughput in the delay-limited transmission mode have been derived. Based on these derivation results, we have further pointed out that the diversity orders achieved by the two links are zeros due to the inter-user interference among superimposed NOMA signals and the residual LI caused by imperfect self-interference cancellation. Moreover, the closed-form ergodic rate expressions of these links as well as the system throughput in delay-tolerant transmission mode have been derived. By analyzing these ergodic rates with large SNR, we have further pointed out that the rates will converge to upper bounds in the high SNR region. In other words, the slopes of these rate curves are zeros in the high SNR region. Our analytical results have been validated by computer simulations, and the proposed FD CNOMA system is verified to outperform the benchmark systems in the low SNR region. Finally, for FD CNOMA, our results indicate that pSIC is capable of improving its system performance compared with ipSIC, but pSIC cannot overcome the issues of outage probability floors or ergodic rate ceilings.

Appendix 5

Proof of Theorem 6

Denote J_1 as $\Pr\left(\gamma_{D_1\rightarrow r} > T_2,\ \gamma_{D_2\rightarrow r} > T_1\right)$ and J_2 as $\Pr\left(\gamma_{D_1,x_1} > T_2,\ \gamma_{D_1,x_2} > T_1\right)$. Then (5.12) is written as $P_{D_1}^{FD,ipSIC} = 1 - J_1 J_2$. Let x, y and z respectively represent $|h_{r1}|^2$, $\left|h_{LI_1}\right|^2$ and $|g_D|^2$. We have $J_2 = \Pr\left(\frac{\rho a_1 x}{\rho a_2 x+\rho y+1} > T_2, \frac{\rho a_2 x}{\rho z+\rho y+1} > T_1\right)$. When $a_1 > a_2 T_2$, J_2 is

equivalent to

$$\begin{aligned}
J_2 &= \Pr\left(x > \tfrac{1}{\rho(a_1-a_2T_2)}\left(\rho T_2 y + T_2\right), x > \tfrac{T_1}{a_2}z + \tfrac{T_1}{a_2}y + \tfrac{T_1}{\rho a_2}\right) \\
&= U\left(Q_2-Q_1\right)\int_0^\infty\left(\int_0^\infty e^{-\frac{1}{\Omega_1}\left(\rho Q_2 z+\rho Q_2 y+Q_2\right)} f_Y(y)\,dy\right) f_Z(z)\,dz \\
&+ U\left(Q_1-Q_2\right)\int_{\frac{1}{\rho}}^{\frac{Q_1-Q_2}{Q_2}}\left(\int_{\frac{Q_2}{Q_1-Q_2}z-\frac{1}{\rho}}^\infty\left(\int_{Q_1(\rho y+1)}^\infty f_X(x)\,dx\right) f_Y(y)\,dy\right) f_Z(z)\,dz \\
&+ U\left(Q_1-Q_2\right)\int_0^{\frac{1}{\rho}\frac{Q_1-Q_2}{Q_2}}\left(\int_0^\infty\left(\int_{Q_1(\rho y+1)}^\infty f_X(x)\,dx\right) f_Y(y)\,dy\right) f_Z(z)\,dz \\
&+ U\left(Q_1-Q_2\right)\int_{\frac{1}{\rho}\frac{Q_1-Q_2}{Q_2}}^\infty\left(\int_0^{\frac{Q_2}{Q_1-Q_2}z-\frac{1}{\rho}}\left(\int_{\rho Q_2 z+\rho Q_2 y+Q_2}^\infty f_X(x)\,dx\right) f_Y(y)\,dy\right) f_Z(z)\,dz \\
&= U\left(Q_2-Q_1\right)\frac{1}{\Omega_{LI}Q_4}\frac{\Omega_1}{\Omega_1+\Omega_g\rho Q_2}e^{-\frac{1}{\Omega_1}Q_2} \\
&+ U\left(Q_1-Q_2\right)\frac{1}{\Omega_{LI}Q_3}\frac{Q_5}{\Omega_5+\Omega_g Q_3}e^{-\frac{1}{\Omega_1}Q_1-\frac{Q_5}{\rho\Omega_g}} + U\left(Q_1-Q_2\right)\frac{1}{\Omega_{LI}Q_3}e^{-\frac{Q_1}{\Omega_1}}\left(1-e^{-\frac{Q_5}{\rho\Omega_g}}\right) \\
&+ U\left(Q_1-Q_2\right)\left(\frac{1}{\Omega_{LI}\Omega_g Q_4 Q_{11}}e^{-\frac{Q_2}{\Omega_1}-\frac{1}{\rho}Q_5Q_{11}} - \frac{1}{\Omega_{LI}\Omega_g Q_4 Q_6}e^{-\frac{Q_2}{\Omega_1}-\frac{1}{\rho}Q_5Q_6+\frac{1}{\rho}Q_4}\right).
\end{aligned} \tag{5.48}$$

Otherwise, $J_2 = 0$. Let x, y, z and x_g respectively represent $|h_{1r}|^2$, $|h_{2r}|^2$, $\left|h_{LI_r}\right|^2$ and $|g_r|^2$. Then

$$\begin{aligned}
J_1 &= \int_0^\infty\left(\int_0^\infty\left(\int_{T_1T_2x_g+Q_7z+\frac{1}{\rho}Q_7}^\infty\left(\int_{T_1x_g+T_1z+\frac{T_1}{\rho}}^{\frac{1}{T_2}x-z-\frac{1}{\rho}} f_Y(y)\,dy\right) f_X(x)\,dx\right) f_Z(z)\,dz\right) f_{X_g}\left(x_g\right)dx_g \\
&= \frac{1}{Q_8\Omega_{LI}}\frac{\Omega_1\Omega_2}{\Omega_g\Omega_1T_1+\Omega_g\Omega_2T_1T_2+\Omega_1\Omega_2}e^{-\frac{T_1}{\rho\Omega_2}-\frac{Q_7}{\rho\Omega_1}} - \frac{1}{\Omega_{LI}\Omega_1Q_9Q_{10}}\frac{1}{Q_9\Omega_gT_1T_2+1}e^{\frac{1}{\Omega_2\rho}-\frac{Q_7Q_9}{\rho}}.
\end{aligned} \tag{5.49}$$

After substituting (5.48) and (5.49) into $P_{D_1}^{FD,ipSIC} = 1 - J_1J_2$, the proof is completed.

Proof of Theorem 7

Let $z_1 = |h_{r2}|^2$ and $z_2 = \left|h_{LI_2}\right|^2$. Then we have

$$\begin{aligned}
&\Pr\left(\frac{|h_{r2}|^2a_1}{|h_{r2}|^2a_2+\left|h_{LI_2}\right|^2} > y\right) = \Pr\left(z_1 > \frac{yz_2}{a_1-a_2y}\right) \\
&= \left(\int_0^\infty\left(\int_{\frac{yz_2}{a_1-a_2y}}^\infty f_{Z_1}(z_1)\,dz_1\right) f_{Z_2}(z_2)\,dz_2\right) U\left(\frac{a_1}{a_2}-y\right) \\
&= U\left(\frac{a_1}{a_2}-y\right)\frac{(a_1-a_2y)\Omega_2}{\Omega_{LI}y+(a_1-a_2y)\Omega_2}.
\end{aligned} \tag{5.50}$$

We also let z_1, z_2 and z_3 respectively represent $|h_{1r}|^2$, $|h_{2r}|^2$ and $\left|h_{LI_r}\right|^2$. Then we have

$$\begin{aligned}
&\Pr\left(\frac{|h_{1r}|^2}{|h_{2r}|^2+\left|h_{LI_r}\right|^2} > y\right) = \Pr\left(z_1 > yz_2 + yz_3\right) = \\
&\int_0^\infty\left(\int_0^\infty\left(\int_{yz_2+yz_3}^\infty f_{Z_1}(z_1)\,dz_1\right) f_{Z_2}(z_2)\,dz_2\right) f_{Z_3}(z_3)\,dz_3 \\
&= \frac{\Omega_1^2}{(\Omega_2y+\Omega_1)(y\Omega_{LI}+\Omega_1)}.
\end{aligned} \tag{5.51}$$

After substituting (5.51) and (5.50) into (5.29), we obtain the following CDF of Y.

$$\begin{aligned} F_Y(y) = 1 - U\left(\tfrac{a_1}{a_2} - y\right) \tfrac{(a_1 - a_2 y)\Omega_2}{\Omega_{LI} y + (a_1 - a_2 y)\Omega_2} \\ \times \tfrac{\Omega_1^2}{(\Omega_2 y + \Omega_1)(y\Omega_{LI} + \Omega_1)}. \end{aligned} \tag{5.52}$$

After combining (5.27) and (5.52), the ergodic rate with ipSIC/pSIC in the high SNR region is

$$\begin{aligned} & E\left[R_{D_2}^{FD,pSIC,\infty}\right] = E\left[R_{D_2}^{FD,ipSIC,\infty}\right] \\ & = \tfrac{1}{\ln 2}\int_0^{\infty} \tfrac{1-F_Y(y)}{1+y} dy = \tfrac{1}{\ln 2} \times \\ & \int_0^{\frac{a_1}{a_2}} \left(\tfrac{A_1}{1+y} + \tfrac{B_1}{(\Omega_{LI} - a_2\Omega_2)y + a_1\Omega_2} + \tfrac{N_1}{\Omega_2 y + \Omega_1} + \tfrac{M_1}{y\Omega_{LI} + \Omega_1}\right) dy. \end{aligned} \tag{5.53}$$

Moreover, we further obtain the following calculation results. $\frac{1}{\ln 2}\int_0^{\frac{a_1}{a_2}} \frac{A_1}{1+y} dy = \frac{A_1}{\ln 2}\ln\left(1 + \frac{a_1}{a_2}\right)$, $\frac{1}{\ln 2}\int_0^{\frac{a_1}{a_2}} \frac{B_1}{(\Omega_{LI} - a_2\Omega_2)y + a_1\Omega_2} dy = \frac{1}{\ln 2}\frac{B_1}{\Omega_{LI} - a_2\Omega_2}\ln\left(1 + \frac{\Omega_{LI} - a_2\Omega_2}{a_2\Omega_2}\right)$, and $\frac{1}{\ln 2}\int_0^{\frac{a_1}{a_2}} \frac{N_1}{\Omega_2 y + \Omega_1} dy = \frac{1}{\ln 2}\frac{N_1}{\Omega_2} \times \ln\left(1 + \frac{a_1\Omega_2}{a_2\Omega_1}\right)$, $\frac{1}{\ln 2}\int_0^{\frac{a_1}{a_2}} \frac{M_1}{y\Omega_{LI} + \Omega_1} dy = \frac{1}{\ln 2}\frac{M_1}{\Omega_{LI}}\ln\left(1 + \frac{a_1\Omega_{LI}}{a_2\Omega_1}\right)$. Finally, by substituting the above results into (5.53), we complete the proof.

Proof of Theorem 8

$$\begin{aligned} E\left[R_{D_1}^{FD,ipSIC}\right] &= E\left[\log\left(1 + \underbrace{\min\left(\gamma_{D_2 \to r}, \gamma_{D_1, x_2}\right)}_{Y}\right)\right] \\ &= \tfrac{1}{\ln 2}\int_0^{\infty} \tfrac{1-F_Y(y)}{1+y} dy. \end{aligned} \tag{5.54}$$

After applying (5.2) and (5.5) to Y, we have

$$\begin{aligned} F_Y(y) = 1 - \underbrace{\Pr\left(\frac{|h_{2r}|^2\rho}{|g_r|^2\rho + \left|h_{LI_r}\right|^2\rho + 1} > y\right)}_{\Theta_1} \\ \times \underbrace{\Pr\left(\frac{|h_{r1}|^2\rho a_2}{|g_D|^2\rho + \left|h_{LI_1}\right|^2\rho + 1} > y\right)}_{\Theta_2}. \end{aligned} \tag{5.55}$$

Let $x = |h_{r1}|^2$, $z = \left|h_{LI_1}\right|^2$ and $x_g = |g_D|^2$. We have

$$\begin{aligned}\Theta_2 &= \Pr\left(\tfrac{\rho a_2 x}{\rho x_g+\rho z+1} > y\right) = \Pr\left(x > \tfrac{y}{a_2}x_g + \tfrac{y}{a_2}z + \tfrac{y}{\rho a_2}\right) = \\ &\int_0^\infty \left(\int_0^\infty \left(\int_{\frac{y}{a_2}x_g+\frac{y}{a_2}z+\frac{y}{\rho a_2}}^\infty f_X(x)\,dx\right) f_Z(z)\,dz\right) f_{X_g}\left(x_g\right) dx_g \\ &= \tfrac{\Omega_1 a_2}{\Omega_{LI}y+\Omega_1 a_2}\tfrac{\Omega_1 a_2}{\Omega_g y+\Omega_1 a_2} e^{-\frac{y}{\rho\Omega_1 a_2}}.\end{aligned} \tag{5.56}$$

$$\Theta_1 = \frac{\Omega_2}{\Omega_{LI}y+\Omega_2}\frac{\Omega_2}{\Omega_g y+\Omega_2}e^{-\frac{1}{\Omega_2}\frac{y}{\rho}}. \tag{5.57}$$

Combining (5.54), (5.55), (5.56) and (5.57), we obtain

$$\begin{aligned}E\left[R_{D_1}^{FD,ipSIC}\right] = \tfrac{1}{\ln 2}\int_0^\infty \Big(&\tfrac{F_1}{1+y} + \tfrac{\Omega_{LI}F_2}{\Omega_{LI}y+\Omega_2} + \tfrac{\Omega_g F_3}{\Omega_g y+\Omega_2} \\ &+ \tfrac{\Omega_{LI}F_4}{\Omega_{LI}y+\Omega_1 a_2} + \tfrac{\Omega_g F_5}{\Omega_g y+\Omega_1 a_2}\Big) e^{-\mu y}dy.\end{aligned} \tag{5.58}$$

Based on [132], we learn that $\frac{1}{\ln 2}\int_0^\infty \frac{F_1}{1+y}e^{-\mu y}dy = -\frac{F_1}{\ln 2}e^{\mu}\mathrm{Ei}(-\mu)$, $\frac{1}{\ln 2}\int_0^\infty \frac{F_2}{y+\frac{\Omega_2}{\Omega_{LI}}}e^{-\mu y}dy = -\frac{F_2}{\ln 2}e^{\frac{\Omega_2}{\Omega_{LI}}\mu}\mathrm{Ei}\left(-\frac{\Omega_2}{\Omega_{LI}}\mu\right)$, $\frac{1}{\ln 2}\int_0^\infty \frac{F_3}{y+\frac{\Omega_2}{\Omega_g}}e^{-\mu y}dy = -\frac{F_3}{\ln 2}e^{\frac{\Omega_2}{\Omega_g}\mu}\mathrm{Ei}\left(-\frac{\Omega_2}{\Omega_g}\mu\right)$, $\frac{1}{\ln 2}\int_0^\infty \frac{F_4}{y+\frac{\Omega_1 a_2}{\Omega_{LI}}}e^{-\mu y}dy = -\frac{F_4}{\ln 2}e^{\frac{\Omega_1 a_2}{\Omega_{LI}}\mu}\mathrm{Ei}\left(-\frac{\Omega_1 a_2}{\Omega_{LI}}\mu\right)$ and $\frac{1}{\ln 2}\int_0^\infty \frac{F_5}{y+\frac{\Omega_1 a_2}{\Omega_g}}e^{-\mu y}dy = -\frac{F_5}{\ln 2}e^{\frac{\Omega_1 a_2}{\Omega_g}\mu}\mathrm{Ei}\left(-\frac{\Omega_1 a_2}{\Omega_g}\mu\right)$. After substituting the above results into (5.58), we complete the proof.

Chapter 6

Conclusions and Future Work

6.1 Conclusions

As a potential key technology for future wireless networks, non-orthogonal multiple access (NOMA) offers a higher data rate, a higher capacity and more device connections compared with orthogonal multiple access (OMA). Considering the inherent advantages of cooperative communication, including extending coverage and improving the communication reliability, we study cooperative NOMA (CNOMA) schemes, i.e., half-duplex (HD) CNOMA and full-duplex (FD) CNOMA schemes in this thesis.

Firstly, we have proposed a HD CNOMA scheme based on spectrum sensing. The proposed collaborative scheme provides the following benefits: i) it adopts spectrum sensing to identify the spectrum holes for effective data transmission and accordingly to avoid the waste of spectrum hole resources; ii) it enables primary user (PU) and secondary user (SU) to share the licensed spectrum band by NOMA, which further increases the spectrum efficiency. Closed-form expressions of outage probability, ergodic rate and system throughput in delay-limited and delay-tolerant transmission modes have been derived under the practical assumption of imperfect spectrum sensing. Based on the simulation results, we have validated these closed-form expressions, verified the effectiveness of employing spectrum sensing for better system per-

formance, and demonstrated that the proposed HD CNOMA scheme achieving larger throughput than benchmarks. Furthermore, all the schemes are shown to have obtained larger system throughputs with direct link than without the direct link. It is because the direct link is able to provide spatial diversity by offering additional opportunity for signal transmission.

Secondly, we have proposed a FD CNOMA scheme based on spectrum sensing. This proposed scheme not only possesses of the benefits of the aforementioned HD CNOMA scheme, but also gains the advantages of employing the FD mode such as larger capacity. Ergodic rates have been derived under the practical assumptions of imperfect spectrum sensing and imperfect self-interference (SI) cancellation. High signal-to-noise ratio (SNR) slopes of these ergodic rates are then worked out. The high-SNR slope of SU is found to be unity while the high-SNR slope of PU equals the miss detection probability and is much smaller than that of SU. We also derive the system throughput based on the obtained ergodic rate expressions. Simulation results have verified the theoretical derivations. They also demonstrate that the proposed scheme always outperforms benchmarks in terms of ergodic rates and system throughput when the residual SI is at the same level with the noise floor.

Thirdly, we have investigated a three-stage relay selection strategy with dynamic power allocation (TRSPA) for the proposed FD CNOMA scheme based on spectrum sensing. This strategy maximizes the ergodic rate of selected SU relay on the condition of guaranteeing successful transmissions of the PU's signal. In other words, it improves the transmission effectiveness for SU on the condition that the PU's signal is transmitted reliably. Thus the overall spectrum efficiency is increased. To evaluate the performance of TRSPA for the FD CNOMA scheme, we have derived the closed-form expressions of outage probability and ergodic rate. Accordingly, the diversity order is found to be zero, which means imperfectly cancelled loop self-interference (LI) severely restricts the outage performance. The spatial multiplexing gain is found to be unity, which is the maximum achievable value. We have also compared the re-

sults of TRSPA-FD, TRSPA-HD and TRSPA-OMA under reasonable SI suppression scenarios, especially in the high SNR region. It is concluded that FD relaying mode is both outage optimal and ergodic-rate optimal for a practical TRSPA system. Finally, simulation results have been used to verify our derivations and to show the superiority of TRSPA over other relay selection strategies.

Fourthly, we have evaluated the performance of a two-way relaying FD CNOMA scheme. The realistic assumption of imperfect self-interference cancellation and the situations of both perfect successive interference cancellation (pSIC) and imperfect successive interference cancellation (ipSIC) have been considered. The outage probabilities of the two transmission links have been derived. Accordingly, we have shown that the diversity orders achieved by the two links are zero due to the inter-user interference among superimposed NOMA signals and the residual LI caused by imperfect self-interference cancellation. Moreover, the closed-form ergodic rate expressions of these links as well as the system throughput in delay-tolerant transmission mode have been derived. By analysing these ergodic rates at high SNR, we have shown that the rates will converge to upper bounds in the high SNR region. In other words, the slopes of these rate curves are zero at high SNR. Simulation results have been used to validate the theoretical results and to compare the performance of the proposed FD CNOMA system with benchmarks. We conclude that FD CNOMA outperforms the benchmarks in terms of outage probability, ergodic achievable rate and system throughput in low SNR region. The pSIC scheme is capable of improving the performance of FD CNOMA compared to ipSIC, but pSIC cannot overcome the issues of outage probability floors or ergodic rate ceilings.

6.2 Future Work

First, successive interference cancellation (SIC) has been assumed to be perfect throughout our study in the CNOMA schemes in the thesis. In a practical scenario, implemen-

tation issues of SIC such as complexity scaling and error propagation exist. These unfavourable factors will lead to errors in SIC decoding. One future research direction is to evaluate the impact of imperfect SIC to the HD CNOMA and FD CNOMA schemes.

Second, this thesis mainly assumes a two-user system in the study. It would be interesting and probably challenging to extend the work to multiple users in future studies.

Third, this thesis focuses on simple single-antenna NOMA systems. When multiple antennas are employed together with the beamforming technology, resource utilization efficiency can be further improved. This would be another future research direction.

Fourth, this thesis assumes that optimal coding, decoding, modulation and demodulation technologies are adopted. In such an ideal situation, the derived system performance parameters are the achievable best performance our proposed scheme could ever obtain. The main contribution of this thesis is to analyze and derive the theoretical upper boundary of our proposed scheme. Then compare it with existing schemes to illustrate the potential advantages of our scheme and to indicate its research significance and applicable value. From perfect to imperfect but practical scenarios, to consider detailed technologies is definitely an important research topic in the future, so that in such case our proposed scheme will become more complete and realizable with more applicable significance. One of the most important scenarios of the next generation Beyond 5G or 6G cellular systems is the extremely high mobility. In such case, orthogonal time frequency space and orthogonal delay-Doppler division multiplexing are applicable. So in the future when we plan to study NOMA schemes in high mobility scenarios, these two modulation methods can be incorporated.

Bibliography

[1] X. Chen, D. W. K. Ng, W. Yu, E. G. Larsson, N. Al-Dhahir, and R. Schober, "Massive access for 5g and beyond," *IEEE Journal on Selected Areas in Communications*, vol. 39, no. 3, pp. 615–637, 2021.

[2] Cisco, *Visual Networking Index*, Available: White Paper, Cisco.com.

[3] M. Agiwal, A. Roy, and N. Saxena, "Next generation 5g wireless networks: A comprehensive survey," *IEEE Communications Surveys & Tutorials*, vol. 18, no. 3, pp. 1617–1655, 2016.

[4] Z. Ding, Y. Liu, J. Choi, Q. Sun, M. Elkashlan, I. Chih-Lin, and H. V. Poor, "Application of non-orthogonal multiple access in lte and 5g networks," *IEEE Communications Magazine*, vol. 55, no. 2, pp. 185–191, 2017.

[5] *Proposed Solutions for New Radio Access*, Mobile and Wireless Communications Enablers for the Twenty-Twenty Information Society (METIS), 2015.

[6] Y. Liu, Z. Qin, M. Elkashlan, Y. Gao, and L. Hanzo, "Enhancing the physical layer security of non-orthogonal multiple access in large-scale networks," *IEEE Transactions on Wireless Communications*, vol. 16, no. 3, pp. 1656–1672, 2017.

[7] L. Zhang, Y.-C. Liang, and M. Xiao, "Spectrum sharing for internet of things: A survey," *IEEE Wireless Communications*, vol. 26, no. 3, pp. 132–139, 2019.

[8] T. Cover, "Broadcast channels," *IEEE Transactions on Information Theory*, vol. 18, no. 1, pp. 2–14, 1972.

[9] N. Zhang, J. Wang, G. Kang, and Y. Liu, "Uplink nonorthogonal multiple access in 5g systems," *IEEE Communications Letters*, vol. 20, no. 3, pp. 458–461, 2016.

[10] Z. Ding, Z. Yang, P. Fan, and H. V. Poor, "On the performance of non-orthogonal multiple access in 5g systems with randomly deployed users," *IEEE Signal Processing Letters*, vol. 21, no. 12, pp. 1501–1505, 2014.

[11] Y. Xu, C. Shen, Z. Ding, X. Sun, S. Yan, G. Zhu, and Z. Zhong, "Joint beamforming and power-splitting control in downlink cooperative swipt noma systems," *IEEE Transactions on Signal Processing*, vol. 65, no. 18, pp. 4874–4886, 2017.

[12] A. S. Ibrahim, A. K. Sadek, W. Su, and K. R. Liu, "Cooperative communications with relay-selection: when to cooperate and whom to cooperate with?" *IEEE Transactions on Wireless Communications*, vol. 7, no. 7, pp. 2814–2827, 2008.

[13] F. Gao, T. Cui, and A. Nallanathan, "On channel estimation and optimal training design for amplify and forward relay networks," *IEEE Transactions on Wireless Communications*, vol. 7, no. 5, pp. 1907–1916, 2008.

[14] C. Zhong and Z. Zhang, "Non-orthogonal multiple access with cooperative full-duplex relaying," *IEEE Communications Letters*, vol. 20, no. 12, pp. 2478–2481, 2016.

[15] L. Zhang, J. Liu, M. Xiao, G. Wu, Y.-C. Liang, and S. Li, "Performance analysis and optimization in downlink noma systems with cooperative full-duplex relaying," *IEEE Journal on Selected Areas in Communications*, vol. 35, no. 10, pp. 2398–2412, 2017.

[16] Y. Liu, Z. Ding, M. Eïkashlan, and H. V. Poor, "Cooperative non-orthogonal multiple access in 5g systems with swipt," in *2015 23rd European Signal Processing Conference (EUSIPCO)*, 2015, pp. 1999–2003.

[17] Z. Ding, M. Peng, and H. V. Poor, "Cooperative non-orthogonal multiple access in 5g systems," *IEEE Communications Letters*, vol. 19, no. 8, pp. 1462–1465, 2015.

[18] Z. Yang, Z. Ding, Y. Wu, and P. Fan, "Novel relay selection strategies for cooperative noma," *IEEE Transactions on Vehicular Technology*, vol. 66, no. 11, pp. 10 114–10 123, 2017.

[19] L. Lv, J. Chen, and Q. Ni, "Cooperative non-orthogonal multiple access in cognitive radio," *IEEE Communications Letters*, vol. 20, no. 10, pp. 2059–2062, 2016.

[20] L. Lv, J. Chen, Q. Ni, and Z. Ding, "Design of cooperative non-orthogonal multicast cognitive multiple access for 5g systems: User scheduling and performance analysis," *IEEE Transactions on Communications*, vol. 65, no. 6, pp. 2641–2656, 2017.

[21] Y. Chen, L. Wang, and B. Jiao, "Cooperative multicast non-orthogonal multiple access in cognitive radio," in *2017 IEEE International Conference on Communications (ICC)*, 2017, pp. 1–6.

[22] M. Liaqat, K. A. Noordin, T. A. Latef, and K. Dimyati, "Power-domain non orthogonal multiple access (pd-noma) in cooperative networks: An overview," *Wireless Network*, vol. 26, pp. 1–23, 2018.

[23] J. Men and J. Ge, "Non-orthogonal multiple access for multiple-antenna relaying networks," *IEEE Communications Letters*, vol. 19, no. 10, pp. 1686–1689, 2015.

[24] J. Men, J. Ge, and C. Zhang, "Performance analysis of non-orthogonal multiple access for relaying networks over nakagami-m fading channels," *IEEE Transactions on Vehicular Technology*, vol. 66, no. 2, pp. 1200–1208, 2017.

[25] ——, "Performance analysis for downlink relaying aided non-orthogonal multiple access networks with imperfect csi over nakagami-m fading," *IEEE Access*, vol. 5, pp. 998–1004, 2016.

[26] S. Lee, D. B. da Costa, and T. Q. Duong, "Outage probability of nonorthogonal multiple access schemes with partial relay selection," in *2016 IEEE 27th Annual International Symposium on Personal, Indoor, and Mobile Radio Communications (PIMRC)*, 2016, pp. 1–6.

[27] Z. Yang, Z. Ding, Y. Wu, and P. Fan, "Novel relay selection strategies for cooperative noma," *IEEE Transactions on Vehicular Technology*, vol. 66, no. 11, pp. 10 114–10 123, 2017.

[28] Z. Ding, H. Dai, and H. V. Poor, "Relay selection for cooperative noma," *IEEE Wireless Communications Letters*, vol. 5, no. 4, pp. 416–419, 2016.

[29] X. Liu and X. Wang, "Outage probability and capacity analysis of the collaborative noma assisted relaying system in 5g," in *2016 IEEE/CIC International Conference on Communications in China (ICCC)*, 2016, pp. 1–5.

[30] C. Zhong and Z. Zhang, "Non-orthogonal multiple access with cooperative full-duplex relaying," *IEEE Communications Letters*, vol. 20, no. 12, pp. 2478–2481, 2016.

[31] Z. Zhang, Z. Ma, M. Xiao, Z. Ding, and P. Fan, "Full-duplex device-to-device aided cooperative non-orthogonal multiple access," *IEEE Transactions on Vehicular Technology*, vol. 66, no. 5, pp. 4467–4471, 2017.

[32] X. Yue, Y. Liu, S. Kang, A. Nallanathan, and Z. Ding, "Outage performance of full/half-duplex user relaying in noma systems," in *2017 IEEE International Conference on Communications (ICC)*, 2017, pp. 1–6.

[33] L. Zhang, J. Liu, M. Xiao, G. Wu, Y.-C. Liang, and S. Li, "Performance analysis and optimization in downlink noma systems with cooperative full-duplex relaying," *IEEE Journal on Selected Areas in Communications*, vol. 35, no. 10, pp. 2398–2412, 2017.

[34] Y. Liu, Z. Ding, M. Elkashlan, and H. V. Poor, "Cooperative nonorthogonal multiple access with simultaneous wireless information and power transfer," *IEEE Journal on Selected Areas in Communications*, vol. 34, no. 4, pp. 938–953, 2016.

[35] N. T. Do, D. B. da Costa, T. Q. Duong, and B. An, "A bnbf user selection scheme for noma-based cooperative relaying systems with swipt," *IEEE Communications Letters*, vol. 21, no. 3, pp. 664–667, 2017.

[36] J. So and Y. Sung, "Improving non-orthogonal multiple access by forming relaying broadcast channels," *IEEE Communications Letters*, vol. 20, no. 9, pp. 1816–1819, 2016.

[37] N. Li, M. Xiao, and L. K. Rasmussen, "Optimized cooperative multiple access in industrial cognitive networks," *IEEE Transactions on Industrial Informatics*, vol. 14, no. 6, pp. 2666–2676, 2018.

[38] L. Lv, H. Jiang, Z. Ding, L. Yang, and J. Chen, "Secrecy-enhancing design for cooperative downlink and uplink noma with an untrusted relay," *IEEE Transactions on Communications*, vol. 68, no. 3, pp. 1698–1715, 2020.

[39] A. Arafa, W. Shin, M. Vaezi, and H. V. Poor, "Secure relaying in non-orthogonal multiple access: Trusted and untrusted scenarios," *IEEE Transactions on Information Forensics and Security*, vol. 15, no. 1, pp. 210–222, 2020.

[40] I. Kakalou, K. E. Psannis, P. Krawiec, and R. Badea, "Cognitive radio network and network service chaining toward 5g: Challenges and requirements," *IEEE Communications Magazine*, vol. 55, no. 11, pp. 145–151, 2017.

[41] J. So and Y. Sung, "Improving non-orthogonal multiple access by forming relaying broadcast channels," *IEEE Communications Letters*, vol. 20, no. 9, pp. 1816–1819, 2016.

[42] Z. Zhang, Z. Ma, M. Xiao, Z. Ding, and P. Fan, "Full-duplex device-to-device-aided cooperative nonorthogonal multiple access," *IEEE Transactions on Vehicular Technology*, vol. 66, no. 5, pp. 4467–4471, 2017.

[43] C. Zhong and Z. Zhang, "Non-orthogonal multiple access with cooperative full-duplex relaying," *IEEE Communications Letters*, vol. 20, no. 12, pp. 2478–2481, 2016.

[44] L. Zhang, J. Liu, M. Xiao, G. Wu, Y.-C. Liang, and S. Li, "Performance analysis and optimization in downlink noma systems with cooperative full-duplex relaying," *IEEE Journal on Selected Areas in Communications*, vol. 35, no. 10, pp. 2398–2412, 2017.

[45] X. Yue, Y. Liu, S. Kang, A. Nallanathan, and Z. Ding, "Exploiting full/half-duplex user relaying in noma systems," *IEEE Transactions on Communications*, vol. 66, no. 2, pp. 560–575, 2018.

[46] ——, "Outage performance of full/half-duplex user relaying in noma systems," in *2017 IEEE International Conference on Communications (ICC)*, 2017, pp. 1–6.

[47] Z. Ding, H. Dai, and H. V. Poor, "Relay selection for cooperative noma," *IEEE Wireless Communications Letters*, vol. 5, no. 4, pp. 416–419, 2016.

[48] Z. Yang, Z. Ding, Y. Wu, and P. Fan, "Novel relay selection strategies for cooperative noma," *IEEE Transactions on Vehicular Technology*, vol. 66, no. 11, pp. 10 114–10 123, 2017.

[49] L. Lv, J. Chen, Q. Ni, and Z. Ding, "Design of cooperative non-orthogonal multicast cognitive multiple access for 5g systems: User scheduling and performance analysis," *IEEE Transactions on Communications*, vol. 65, no. 6, pp. 2641–2656, 2017.

[50] P. Xu, Z. Yang, Z. Ding, and Z. Zhang, "Optimal relay selection schemes for cooperative noma," *IEEE Transactions on Vehicular Technology*, vol. 67, no. 8, pp. 7851–7855, 2018.

[51] L. Zhang, M. Xiao, G. Wu, M. Alam, Y.-C. Liang, and S. Li, "A survey of advanced techniques for spectrum sharing in 5g networks," *IEEE Wireless Communications*, vol. 24, no. 5, pp. 44–51, 2017.

[52] Y.-S. Choi and H. Shirani-Mehr, "Simultaneous transmission and reception: Algorithm, design and system level performance," *IEEE Transactions on Wireless Communications*, vol. 12, no. 12, pp. 5992–6010, 2013.

[53] U. Siddique, H. Tabassum, and E. Hossain, "Downlink spectrum allocation for in-band and out-band wireless backhauling of full-duplex small cells," *IEEE Transactions on Communications*, vol. 65, no. 8, pp. 3538–3554, 2017.

[54] X. Yue, Y. Liu, S. Kang, A. Nallanathan, and Z. Ding, "Spatially random relay selection for full/half-duplex cooperative noma networks," *IEEE Transactions on Communications*, vol. 66, no. 8, pp. 3294–3308, 2018.

[55] C. E. Shannon, "Two-way communication channels," in *Berkeley Symposium Mathematical Statistics and Probability*, 1961, pp. 611–644.

[56] S. Zhang, S. C. Liew, and P. P. Lam, "Hot topic: Physical-layer network coding," in *2006 ACM Annual International Conference on Mobile Computing and Networking (MobiCom)*, 2006, pp. 358–365.

[57] P. Popovski and H. Yomo, "The anti-packets can increase the achievable throughput of a wireless multi-hop network," in *2006 IEEE International Conference on Communications (ICC)*, vol. 9, 2006, pp. 3885–3890.

[58] S. Katti, S. Gollakota, and D. Katabi, "Embracing wireless interference: Analog network coding," in *2007 ACM SIGCOMM Computer Communication Review*, vol. 37, no. 4, 2007, pp. 397–408.

[59] E. D. N. Ndih and S. Cherkaoui, "Reliable broadcasting in vanets using physical-layer network coding," in *2012 International Conference on Communications and Information Technology (ICCIT)*, 2012, pp. 363–368.

[60] ——, "Mac for physical-layer network coding in vanets," *International Journal of Business Data Communications and Networking*, vol. 8, no. 4, pp. 84–106, 2012.

[61] I. W.-H. Ho, S. C. Liew, and L. Lu, "Feasibility study of physical-layer network coding in 802.11 p vanets," in *2014 IEEE International Symposium on Information Theory*, 2014, pp. 646–650.

[62] F. Rossetto and M. Zorzi, "On the design of practical asynchronous physical layer network coding," in *2009 IEEE 10th Workshop on Signal Processing Advances in Wireless Communications*, 2009, pp. 469–473.

[63] H. Yan and H. H. Nguyen, "Adaptive physical-layer network coding in two-way relaying with ofdm," in *2013 IEEE Global Communications Conference (GLOBECOM)*, 2013, pp. 4244–4249.

[64] L. Lu and S. C. Liew, "Asynchronous physical-layer network coding," *IEEE Transactions on Wireless Communications*, vol. 11, no. 2, pp. 819–831, 2011.

[65] L. Lv, Q. Ni, Z. Ding, and J. Chen, "Application of non-orthogonal multiple access in cooperative spectrum-sharing networks over nakagami-m fading channels," *IEEE Transactions on Vehicular Technology*, vol. 66, no. 6, pp. 5506–5511, 2017.

[66] X. Yue, Y. Liu, S. Kang, A. Nallanathan, and Y. Chen, "Modeling and analysis of two-way relay non-orthogonal multiple access systems," *IEEE Transactions on Communications*, vol. 66, no. 9, pp. 3784–3796, 2018.

[67] N. Ayir and P. Ubaidulla, "Transceiver design for mimo full-duplex two-way relay network," *IEEE Wireless Communications Letters*, vol. 7, no. 5, pp. 772–775, 2018.

[68] J.-M. Kang, I.-M. Kim, and H.-M. Kim, "Estimation of time-varying channels in mimo two-way multi-relay systems," *IEEE Transactions on Wireless Communications*, vol. 17, no. 6, pp. 4002–4016, 2018.

[69] B. Zheng, X. Wang, M. Wen, and F. Chen, "Noma-based multi-pair two-way relay networks with rate splitting and group decoding," *IEEE Journal on Selected Areas in Communications*, vol. 35, no. 10, pp. 2328–2341, 2017.

[70] B. Zheng, M. Wen, C.-X. Wang, X. Wang, F. Chen, J. Tang, and F. Ji, "Secure noma based two-way relay networks using artificial noise and full duplex," *IEEE Journal on Selected Areas in Communications*, vol. 36, no. 7, pp. 1426–1440, 2018.

[71] M. Ali and H. Nam, "Effect of spectrum sensing and transmission duration on spectrum hole utilisation in cognitive radio networks," *IET Communications*, vol. 11, no. 16, pp. 2539–2543, 2017.

[72] P. Goyal, A. S. Buttar, and M. Goyal, "An efficient spectrum hole utilization for transmission in cognitive radio networks," in *2016 3rd International Conference on Signal Processing and Integrated Networks (SPIN)*, 2016, pp. 322–327.

[73] Z. Qin, Y. Gao, and C. G. Parini, "Data-assisted low complexity compressive spectrum sensing on real-time signals under sub-nyquist rate," *IEEE Transactions on Wireless Communications*, vol. 15, no. 2, pp. 1174–1185, 2016.

[74] Z. Qin, Y. Gao, M. D. Plumbley, and C. G. Parini, "Wideband spectrum sensing on real-time signals at sub-nyquist sampling rates in single and cooperative multiple nodes," *IEEE Transactions on Signal Processing*, vol. 64, no. 12, pp. 3106–3117, 2016.

[75] Y. Ma, Y. Gao, Y.-C. Liang, and S. Cui, "Reliable and efficient sub-nyquist wideband spectrum sensing in cooperative cognitive radio networks," *IEEE Journal on Selected Areas in Communications*, vol. 34, no. 10, pp. 2750–2762, 2016.

[76] I. S. Gradshteyn and I. M. Ryzhik, *Table of Integrals, Series and Products*. New York, USA: Academic Press, 2000.

[77] Z. Ding, X. Lei, G. K. Karagiannidis, R. Schober, J. Yuan, and V. K. Bhargava, "A survey on non-orthogonal multiple access for 5g networks: Research challenges and future trends," *IEEE Journal on Selected Areas in Communications*, vol. 35, no. 10, pp. 2181–2195, 2017.

[78] M. Amjad, F. Akhtar, M. H. Rehmani, M. Reisslein, and T. Umer, "Full-duplex communication in cognitive radio networks: A survey," *IEEE Communications Surveys & Tutorials*, vol. 19, no. 4, pp. 2158–2191, 2017.

[79] X. Yue, Y. Liu, S. Kang, A. Nallanathan, and Z. Ding, "Exploiting full/half-duplex user relaying in noma systems," *IEEE Transactions on Communications*, vol. 66, no. 2, pp. 560–575, 2018.

[80] X. Wang, M. Jia, I. W.-H. Ho, Q. Guo, and F. C. M. Lau, "Exploiting full-duplex two-way relay cooperative non-orthogonal multiple access," *IEEE Transactions on Communications*, vol. 67, no. 4, pp. 2716–2729, 2019.

[81] X. Yue, Y. Liu, S. Kang, A. Nallanathan, and Z. Ding, "Outage performance of full/half-duplex user relaying in noma systems," in *2017 IEEE International Conference on Communications (ICC)*, 2017, pp. 1–6.

[82] L. Zhang, Y.-C. Liang, and M. Xiao, "Spectrum sharing for internet of things: A survey," *IEEE Wireless Communications*, vol. 26, no. 3, pp. 132–139, 2019.

[83] M. A. Mehaseb, Y. Gadallah, A. Elhamy, and H. Elhennawy, "Classification of lte uplink scheduling techniques: An m2m perspective," *IEEE Communications Surveys & Tutorials*, vol. 18, no. 2, pp. 1310–1335, 2016.

[84] X. Yue, Y. Liu, S. Kang, A. Nallanathan, and Z. Ding, "Exploiting full/half-duplex user relaying in noma systems," *IEEE Transactions on Communications*, vol. 66, no. 2, pp. 560–575, 2018.

[85] ——, "Spatially random relay selection for full/half-duplex cooperative noma networks," *IEEE Transactions on Communications*, vol. 66, no. 8, pp. 3294–3308, 2018.

[86] H. Xing, Y. Liu, A. Nallanathan, Z. Ding, and H. V. Poor, "Optimal throughput fairness tradeoffs for downlink non-orthogonal multiple access over fading channels," *IEEE Transactions on Wireless Communications*, vol. 17, no. 6, pp. 3556–3571, 2018.

[87] X. Wang, M. Jia, I. W.-H. Ho, Q. Guo, and F. C. M. Lau, "Exploiting full-duplex two-way relay cooperative non-orthogonal multiple access," *IEEE Transactions on Communications*, vol. 67, no. 4, pp. 2716–2729, 2019.

[88] I. S. Gradshteyn and I. M. Ryzhik, *Table of Integrals, Series and Products*. New York, USA: Academic Press, 2000.

[89] S. Wang, Z.-H. Zhou, M. Ge, and C. Wang, "Resource allocation for heterogeneous multiuser ofdm-based cognitive radio networks with imperfect spectrum sensing," in *2012 Proceedings IEEE INFOCOM*, 2012, pp. 2264–2272.

[90] Y. Liao, T. Wang, L. Song, and Z. Han, "Listen-and-talk: Protocol design and analysis for full-duplex cognitive radio networks," *IEEE Transactions on Vehicular Technology*, vol. 66, no. 1, pp. 656–667, 2017.

[91] M. Duarte, A. Sabharwal, V. Aggarwal, R. Jana, K. K. Ramakrishnan, C. W. Rice, and N. K. Shankaranarayanan, "Design and characterization of a full-duplex multiantenna system for wifi networks," *IEEE Transactions on Vehicular Technology*, vol. 63, no. 3, pp. 1160–1177, 2014.

[92] P. Tehrani, F. Lahouti, and M. Zorzi, "Resource allocation in ofdma networks with half-duplex and imperfect full-duplex users," in *2016 IEEE International Conference on Communications (ICC)*, 2016, pp. 1–6.

[93] D. Bharadia, E. McMilin, and S. Katti, "Full duplex radios," in *2013 ACM Special Insterest Group on Data Communication (SIGCOMM)*, 2013, pp. 375–386.

[94] L. Jiménez Rodríguez, N. H. Tran, and T. Le-Ngoc, "Performance of full-duplex af relaying in the presence of residual self-interference," *IEEE Journal on Selected Areas in Communications*, vol. 32, no. 9, pp. 1752–1764, 2014.

[95] L. Zhang, M. Xiao, G. Wu, G. Zhao, Y.-C. Liang, and S. Li, "Proactive cross-channel gain estimation for spectrum sharing in cognitive radio," *IEEE Journal on Selected Areas in Communications*, vol. 34, no. 10, pp. 2776–2790, 2016.

[96] H. Tabassum, A. H. Sakr, and E. Hossain, "Analysis of massive mimo-enabled downlink wireless backhauling for full-duplex small cells," *IEEE Transactions on Communications*, vol. 64, no. 6, pp. 2354–2369, 2016.

[97] Y. Liao, T. Wang, L. Song, and Z. Han, "Listen-and-talk: Protocol design and analysis for full-duplex cognitive radio networks," *IEEE Transactions on Vehicular Technology*, vol. 66, no. 1, pp. 656–667, 2017.

[98] X. Wang, M. Jia, and Q. Guo, "Full-duplex cooperative non-orthogonal multiple access with spectrum sensing," in *2020 15th IEEE International Conference on Signal Processing (ICSP)*, vol. 1, 2020, pp. 411–416.

[99] X. Wang, M. Jia, I. W.-H. Ho, Q. Guo, and F. C. M. Lau, "Exploiting full-duplex two-way relay cooperative non-orthogonal multiple access," *IEEE Transactions on Communications*, vol. 67, no. 4, pp. 2716–2729, 2019.

[100] L. Zheng and D. Tse, "Diversity and multiplexing: a fundamental tradeoff in multiple-antenna channels," *IEEE Transactions on Information Theory*, vol. 49, no. 5, pp. 1073–1096, 2003.

[101] M. Abramowitz and I. A. Stegun, *Handbook of Mathematical Functions With Formulas, Graphs, and Mathematical Tables*. Washington D. C., USA: Dover Publications, 1964.

[102] J. Lee and N. Jindal, "High snr analysis for mimo broadcast channels: Dirty paper coding versus linear precoding," *IEEE Transactions on Information Theory*, vol. 53, no. 12, pp. 4787–4792, 2007.

[103] A. Kuhestani, A. Mohammadi, and M. Mohammadi, "Joint relay selection and power allocation in large-scale mimo systems with untrusted relays and passive eavesdroppers," *IEEE Transactions on Information Forensics and Security*, vol. 13, no. 2, pp. 341–355, 2018.

[104] L. Wang, M. Elkashlan, J. Huang, R. Schober, and R. K. Mallik, "Secure transmission with antenna selection in mimo nakagami- *m* fading channels," *IEEE Transactions on Wireless Communications*, vol. 13, no. 11, pp. 6054–6067, 2014.

[105] S. Wang, Z.-H. Zhou, M. Ge, and C. Wang, "Resource allocation for heterogeneous multiuser ofdm-based cognitive radio networks with imperfect spectrum sensing," in *2012 Proceedings IEEE INFOCOM*, 2012, pp. 2264–2272.

[106] L. Zhang, J. Liu, M. Xiao, G. Wu, Y.-C. Liang, and S. Li, "Performance analysis and optimization in downlink noma systems with cooperative full-duplex relaying," *IEEE Journal on Selected Areas in Communications*, vol. 35, no. 10, pp. 2398–2412, 2017.

[107] Y. Zhou, V. W. Wong, and R. Schober, "Stable throughput regions of opportunistic noma and cooperative noma with full-duplex relaying," *IEEE Transactions on Wireless Communications*, vol. 17, no. 8, pp. 5059–5075, 2018.

[108] B. Xu, Z. Xiang, P. Ren, and X. Guo, "Outage performance of downlink full-duplex network-coded cooperative noma," *IEEE Wireless Communications Letters*, vol. 10, no. 1, pp. 26–29, 2021.

[109] A. Tregancini, E. E. B. Olivo, D. P. M. Osorio, C. H. M. de Lima, and H. Alves, "Performance analysis of full-duplex relay-aided noma systems using partial relay selection," *IEEE Transactions on Vehicular Technology*, vol. 69, no. 1, pp. 622–635, 2020.

[110] C. Guo, L. Zhao, C. Feng, Z. Ding, and H.-H. Chen, "Energy harvesting enabled noma systems with full-duplex relaying," *IEEE Transactions on Vehicular Technology*, vol. 68, no. 7, pp. 7179–7183, 2019.

[111] B. K. S. Lima, D. B. da Costa, L. Yang, F. R. M. Lima, R. Oliveira, and U. S. Dias, "Adaptive power factor allocation for cooperative full-duplex noma systems with imperfect sic and rate fairness," *IEEE Transactions on Vehicular Technology*, vol. 69, no. 11, pp. 14 061–14 066, 2020.

[112] M. Ahmed, A. Baz, and C. Tsimenidis, "Performance analysis of noma systems over rayleigh fading channels with successive-interference cancellation," *IET Communications*, vol. 14, no. 6, pp. 1065–1–72, 2020.

[113] X. Wang, M. Jia, Q. Guo, I. W.-H. Ho, and F. C.-M. Lau, "Full-duplex relaying cognitive radio network with cooperative nonorthogonal multiple access," *IEEE Systems Journal*, vol. 13, no. 4, pp. 3897–3908, 2019.

[114] L. Jiménez Rodríguez, N. H. Tran, and T. Le-Ngoc, "Performance of full-duplex af relaying in the presence of residual self-interference," *IEEE Journal on Selected Areas in Communications*, vol. 32, no. 9, pp. 1752–1764, 2014.

[115] P. Tehrani, F. Lahouti, and M. Zorzi, "Resource allocation in ofdma networks with half-duplex and imperfect full-duplex users," in *2016 IEEE International Conference on Communications (ICC)*, 2016, pp. 1–6.

[116] H. Tabassum, A. H. Sakr, and E. Hossain, "Analysis of massive mimo-enabled downlink wireless backhauling for full-duplex small cells," *IEEE Transactions on Communications*, vol. 64, no. 6, pp. 2354–2369, 2016.

[117] T. Cover, "Broadcast channels," *IEEE Transactions on Information Theory*, vol. 18, no. 1, pp. 2–14, 1972.

[118] Y. Jing and H. Jafarkhani, "Single and multiple relay selection schemes and their achievable diversity orders," *IEEE Transactions on Wireless Communications*, vol. 8, no. 3, pp. 1414–1423, 2009.

[119] J. Hossain, M.-s. Alouini, and V. K. Bhargava, "Multi-user opportunistic scheduling using power controlled hierarchical constellations," *IEEE Transactions on Wireless Communications*, vol. 6, no. 5, pp. 1581–1586, 2007.

[120] I. S. Gradshteyn and I. M. Ryzhik, *Table of Integrals, Series and Products*. New York, USA: Academic Press, 2000.

[121] J. Lee and N. Jindal, "High snr analysis for mimo broadcast channels: Dirty paper coding versus linear precoding," *IEEE Transactions on Information Theory*, vol. 53, no. 12, pp. 4787–4792, 2007.

[122] L. Wang, M. Elkashlan, J. Huang, R. Schober, and R. K. Mallik, "Secure transmission with antenna selection in mimo nakagami- *m* fading channels," *IEEE Transactions on Wireless Communications*, vol. 13, no. 11, pp. 6054–6067, 2014.

[123] M. Jia, X. Wang, Q. Guo, I. W.-H. Ho, X. Gu, and F. C.-M. Lau, "Performance analysis of cooperative non-orthogonal multiple access based on spectrum sensing," *IEEE Transactions on Vehicular Technology*, vol. 68, no. 7, pp. 6855–6866, 2019.

[124] M. Abramowitz and I. A. Stegun, *Handbook of Mathematical Functions With Formulas, Graphs, and Mathematical Tables*. Washington D. C., USA: Dover Publications, 1964.

[125] L. Zhang, J. Liu, M. Xiao, G. Wu, Y.-C. Liang, and S. Li, "Performance analysis and optimization in downlink noma systems with cooperative full-duplex

relaying," *IEEE Journal on Selected Areas in Communications*, vol. 35, no. 10, pp. 2398–2412, 2017.

[126] P. Li, T. Zhang, C. Huang, X. Chen, and B. Fu, "Rsu-assisted geocast in vehicular ad hoc networks," *IEEE Wireless Communications*, vol. 24, no. 1, pp. 53–59, 2017.

[127] X. Yue, Y. Liu, S. Kang, A. Nallanathan, and Z. Ding, "Outage performance of full/half-duplex user relaying in noma systems," in *2017 IEEE International Conference on Communications (ICC)*, 2017, pp. 1–6.

[128] Z. Ding, X. Lei, G. K. Karagiannidis, R. Schober, J. Yuan, and V. K. Bhargava, "A survey on non-orthogonal multiple access for 5g networks: Research challenges and future trends," *IEEE Journal on Selected Areas in Communications*, vol. 35, no. 10, pp. 2181–2195, 2017.

[129] X. Yue, Y. Liu, S. Kang, A. Nallanathan, and Z. Ding, "Exploiting full/half-duplex user relaying in noma systems," *IEEE Transactions on Communications*, vol. 66, no. 2, pp. 560–575, 2018.

[130] T. Kwon, S. Lim, S. Choi, and D. Hong, "Optimal duplex mode for df relay in terms of the outage probability," *IEEE Transactions on Vehicular Technology*, vol. 59, no. 7, pp. 3628–3634, 2010.

[131] H. Xing, Y. Liu, A. Nallanathan, Z. Ding, and H. V. Poor, "Optimal throughput fairness tradeoffs for downlink non-orthogonal multiple access over fading channels," *IEEE Transactions on Wireless Communications*, vol. 17, no. 6, pp. 3556–3571, 2018.

[132] I. S. Gradshteyn and I. M. Ryzhik, *Table of Integrals, Series and Products*. New York, USA: Academic Press, 2000.

[133] H. Tabassum, A. H. Sakr, and E. Hossain, "Analysis of massive mimo-enabled downlink wireless backhauling for full-duplex small cells," *IEEE Transactions on Communications*, vol. 64, no. 6, pp. 2354–2369, 2016.